Operating Limits and Dynamic Average-Value Modelling of VSC-HVDC Systems

By

Mohamed M. Zakaria Moustafa

A Thesis submitted to the Faculty of Graduate Studies of

The University of Manitoba

in partial fulfilment of the requirements of the degree of

DOCTOR OF PHILOSOPHY

Department of Electrical and Computer Engineering

University of Manitoba

Winnipeg

Abstract

This thesis deals with modeling, simulation and operating limits of high-voltage direct-current (HVDC) transmission systems that employ voltage-source converters (VSCs) as their building blocks. This scheme is commonly known as the VSC-HVDC transmission.

A simulation-based study is undertaken in which detailed electromagnetic transient (EMT) models are developed for a back-to-back VSC-HVDC transmission system. Different control strategies are implemented and their dynamic performances are investigated in the PSCAD/EMTDC EMT simulator.

The research presented in this thesis firstly specifies the factors that limit the operating points of a VSC-HVDC system with particular emphasis on the strength of the terminating ac system. Although the EMT model shows these limits it provides little analytical reason for their presence and extent. A phasor-based quasi-steady state model of the system including the phase-locked loop firing control mechanism is proposed to determine and characterize the factors contributing to these operating limits. Stability margins and limits on the maximum available power are calculated, taking into consideration the maximum voltage rating of the VSC. The variations of ac system short-circuit ratio (SCR) and transformer impedance are proven to significantly impact the operating limits of the VSC-HVDC system. The results show how the power transfer capability reduces as the SCR decreases. The analysis shows that VSC-HVDC converters can operate into much weaker networks, and with less sensitivity, than the conventional line commutated converters (LCC-HVDC). Also for a given SCR the VSC-HVDC

system has a significantly larger maximum available power in comparison with LCC-HVDC.

A second research thrust of the thesis is introduction of a simplified converter model to reduce the computational intensity of its simulation. This is associated with the admittance matrix inversions required to simulate high-frequency switching of the converter valves. This simplified model is based on the concept of dynamic average-value modelling and provides the ability to generate either the full spectrum or the fundamental-frequency component of the VSC voltage. The model is validated against the detailed VSC-HVDC circuit and shows accurate matching during steady state and transient operation. Major reductions of 50-70% in CPU-time in repetitive simulation studies such as multiple runs and optimization-based controller tuning are achieved.

Acknowledgements

The author wishes to express his deepest gratitude, appreciation and very special thanks to his advisor ***Dr. Shaahin Filizadeh*** for his consistent guidance, assistance, advice and encouragement throughout the research period. His valuable suggestions, advice and moral supports were helpful for the achievement of this thesis and are gratefully acknowledged.

The author wishes also to thank and express his deepest gratitude to the help, advice and encouragement of ***Prof. Dr. Ani Gole***. Throughout my doctoral program Prof. Gole provided guidance, encouragement, good teaching and good company. Working with him is a great opportunity to gain experience in science and life.

The author would like also to thank ***Prof. Dr. Hassan Soliman*** for accepting to be part of the advisory committee and for his valuable discussions throughout the research period.

The financial support for this research by Natural Sciences and Engineering Research Council (NSERC) of Canada, Manitoba Hydro Company and Mathematics of Information Technology and Complex Systems (MITACS) is greatly appreciated.

The author is very thankful to Prof. Ani Gole and Mr. Udana Gnanarathna for their useful contribution to the research work presented in Chapter six.

Special thanks and gratitude are due to everyone that helped in the realization of this work.

Mohamed Moustafa

Dedication

To my loving parents and my two sisters Dina and Dalia

Table of Contents

List of Tables

List of Figures

List of Abbreviations

AC	Alternating Current
DC	Direct Current
ESCR	Equivalent Short Circuit Ratio
EMT	Electromagnetic Transient
FACTS	Flexible AC Transmission System
GTO	Gate Turn Off Thyristors
HVAC	High Voltage Alternating Current
HVDC	High Voltage Direct Current
IGBT	Isolated Gate Bipolar Transistor
KCL	Kirchhoff's Current Law
KVL	Kirchhoff's Voltage Law
MMC	Modular Multilevel Converter
MTDC	Multi-Terminal Direct Current
OHTL	Over-Head Transmission Line
PAM	Pulse Amplitude Modulation
PCC	Point of Common Coupling
PI	Proportional Integral
PLL	Phase Locked Loop
PWM	Pulse Width Modulation
RI	Radio Interference

RMS	Root Mean Square
ROW	Right Of Way
SCR	Short Circuit Ratio
SHE	Selective Harmonic Elimination
SPWM	Sinusoidal Pulse Width Modulation
THD	Total Harmonic Distortion
UHVDC	Ultra High Voltage Direct Current
VA	Voltages Ampères
VCO	Voltage Controlled Oscillator
VSC	Voltage Source Converter

Chapter 1: Introduction

1.1 Historical Background of HVDC Systems

High Voltage Direct Current (HVDC) transmission is a means for transmitting electric power over long distances [1]. Unlike ac transmission networks [1-3], which face numerous stability problems over long distances and require extensive reactive power compensation and voltage support along the transmission line, HVDC systems require no reactive compensation, except at the two converter ends, and eliminate stability issues inherent in ac systems. Rapid controllability of HVDC links has made them ideal for connecting large ac systems in a stable manner [1-4]. Moreover they are used for connecting ac systems with different frequencies at many installations all over the globe [2, 4]. The ability of an HVDC system in connecting systems with different frequencies is due to the intermediate steps of conversion to and from dc, which eliminates the need for the ac system to be synchronous.

One of the first HVDC systems similar to the ones existing nowadays was implemented using mercury arc valves. In 1941[5] a 60MW, ±200kV, 115km buried-cable link was designed for the city of Berlin (Elbe-Project); however due to the collapse of the German government in 1945 the project was never completed. The main motivation for the project was that during war time a buried cable would be less conspicuous as a bombing target and hence offered higher reliability service. The equipment was removed to the Soviet Union and was put into service there.

The mercury arc valves introduced to commercial service in 1954 marked the beginning of the modern era of HVDC transmission [2, 5]. They were common in systems designed up to 1975 but since then HVDC systems only use solid-state devices. A significant improvement in HVDC technology came around 1970 when thyristor valves were introduced to replace mercury arc valves. This reduced the size and complexity of HVDC converter stations significantly.

Later in the 1990's [6, 7], a combination of the drawbacks of the conventional dc systems with the recent advances in semiconductor technology prompted the use of a new generation of static switches for high power dc transmission. In the new scheme, high-speed self-commutated switches, e.g., IGBTs and GTOs, previously used for motor drive and other similar applications, replace less rapid thyristors in an arrangement known as a voltage-source converter (VSC). The VSC-based HVDC (VSC-HVDC) system came in service for the first time in Sweden in 1997 as a trial 3 MW scheme [8]. Since then, more VSC transmission schemes have been built and several are currently in commercial operation.

In the province of Manitoba, the HVDC transmission technology has been used as a way of electric power transmission since early 1970's using mercury arc valves as the switching elements, which have recently been upgraded to thyristor valves [9, 10]. Two HVDC transmission lines exist in Manitoba under the names of Bipole 1 and Bipole 2 [9, 10]. Moreover, a major HVDC project (Bipole 3) is planned to be placed in service by 2017.

1.2 Research path, motivation and problem statement

The research presented in this thesis began with the aim to explore several aspects of using the voltage-source converter technology in bulk dc power transmission, including power supply to electrically weak (in an extreme case even without local generation) ac systems, as well as an investigation of the computational aspects of their simulation and simulation-based controller tuning.

The most accurate simulation platform for study of complex power systems with high-frequency power-electronic converters is an electromagnetic transient simulator. A detailed computer simulation model for HVDC transmission systems using VSCs was firstly developed in the PSCAD/EMTDC transient simulator. This model represents both transient and steady state behaviour of the system and is valid for a wide range of frequencies from dc to a few kilo-Hertz. This model was then used to design proper control strategies and structures in order to fully utilize the capability of a VSC in transmitting power by applying nonlinear optimization to determine optimal control settings.

The detailed transient model revealed that the VSC-HVDC system was unable to reach and operate certain operating regions, despite the wide-spread belief that the degrees of freedom offered by a VSC allow a wide region of operation. A thorough investigation of the operating limits of VSC-HVDC systems, with particular emphasis on the strength of the terminating ac system, was then launched. The aim of this portion of the research was to determine the underlying factors that limit the range of operating points of VSC-HVDC systems and assess the sensitivity of the feasible range to inevitable variations of these factors.

Another research thrust that was initiated as a result of experiments with the detailed simulation model of the VSC-HVDC transmission system (particularly when repetitive simulations were conducted in the course of controller tuning) was to reduce the computational intensity of the simulation of the electromagnetic transient model. Due to the presence of high-frequency switching elements, the underlying admittance matrix of the circuit changes when a switch is turned on or off, and hence the new matrix needs to be inverted. This is a time-consuming and frequently needed task, which leads to lengthy and resource demanding simulations. Development of low-cost (from a computational point-of-view) simulation models while preserving the accuracy of results was therefore undertaken.

1.3 Review of related research

To fully understand the extent of application of VSC-HVDC systems, it is important to note the operating characteristics and limitations under different operating conditions [11]. The strength of an ac network is a major contributor to the operating constraints of dc transmission systems terminating thereto. The ac system strength is measured in terms of the short-circuit ratio (SCR), defined as the ratio of the ac system short circuit capacity over the rated power of the VSC-HVDC system [12]. A weak ac system is normally characterized by its large impedance value [11, 12]. As the impedance of the ac system increases, the AC voltage becomes more sensitive to power variations of the HVDC system [12, 13]. In [13] it is stated that if the SCR decreases, the ac filter and the phase locked loop (PLL) have larger contributions in the system dynamics. Research presented in [14-16] showed that the PLL dynamics might have a negative impact on the

performance of weak VSC-HVDC systems. In [11], the operating limits were analyzed for VSC-HVDC systems using a primitive model that presented the AC system as an inductance neglecting the resistance effect. In [14] the range of SCR considered was from 1.0 to 20.0 and it was shown that for weak systems the maximum power transmittable reduces with SCR (e.g. SCR of 1.0, the maximum transmitted power considered is 0.4 pu). A control methodology based on power synchronization concept was proposed in [17] to overcome the negative impact of the PLL dynamics. Investigating this concept in the interconnection of two very weak ac systems and island systems was presented in [18] and [19], respectively. The above research materials [11-19] did not specify accurately the reasons behind the limited capabilities of VSC-HVDC transmission systems at different operating conditions. Moreover the effect of ac system strength and other VSC scheme components, e.g. converter transformer, on the stable operating limits as well as the maximum available power have not been investigated. Furthermore, the relation between the maximum operating limit and the maximum available power limit has not been identified.

Modelling and simulation of VSC-HVDC systems is another complicated task that requires a compromise between level of detail, simulation speed and the required data. A model of the VSC-HVDC was analyzed and presented in [20-22]. In [16] a model intended for analytical studies in the frequency domain above 5Hz was introduced. The model was developed by linearizing converter state space equations around the nominal operating point. A VSC-HVDC phasor model for stability studies based on coupled current injectors is presented in [23]. Dynamic average value modeling techniques for representing static switching converters for system-level studies are presented in an IEEE

Task Force paper [24]. This paper also included different approaches used to develop such models for dc-dc and ac-dc converters. The dynamic model and control for the VSC-HVDC is presented in [25-27]. A generalized dynamic model for multi-terminal application of VSC-HVDC is presented in [28] including the model of the converter and its controllers, DC circuit equations and coupling equations. Despite the intensive modelling effort presented in the previous research materials [20-28], the possibility of modeling the VSC based on dependent current and voltage sources components and its relation with the transmitted dc power has not been discussed. In particular the CPU-time consumption associated with the proposed models has not been addressed as well. This has profound impact on repetitive simulation studies such as multiple run and optimization-based controller tuning.

1.4 Thesis Layout

This thesis is subdivided into seven chapters. Following the introduction given in this chapter, a survey of the two main configurations of HVDC transmission systems and their technical advantages are presented in Chapter two. The constituent building blocks of each configuration are reviewed and their roles are described. The environmental advantages of HVDC transmission systems are also illustrated.

Chapter three discusses the principles of operation of VSC-HVDC systems including different converter topologies, converter control using sinusoidal pulse width modulation, switching frequency selection and ac filter requirements. In addition, different VSC-HVDC systems modes of operation and their practical coordination are also described. VSC control topologies are also presented including a new control technique for passive load applications.

Chapter four focuses on the simulation and analysis of a detailed back to back VSC-HVDC transmission system model. Active and passive receiving ends are implemented to demonstrate the flexibility of VSC-HVDC transmission systems in supplying different load types. The control topologies illustrated in Chapter three are implemented and detailed comparison between the direct and decoupled control is presented. Additionally, the optimization concept and its effect are introduced as the basis of controller' gains tuning.

The VSC-HVDC systems operating limits are investigated in Chapter five. A phasor base steady state model for the converter system including the phase locked loop is proposed. Verification of the proposed model is conducted against simulation results from the PSCAD/EMTDC. A mathematical equation is derived to accurately specify the maximum stable operating limits of the VSC-HVDC systems. Parametric analyses of the factors affecting the operating limits are also presented.

Chapter six proposes a model of the three level VSC relying on dependent current and voltage sources concepts with an ability to produce the fundamental as well as the full spectrum of the converter voltage. The proposed model is intended to reduce the complexity and time consumption of the detailed three level model. The proposed model is validated versus the detailed model using PSCAD/EMTDC under normal and faulty operating conditions.

The thesis is concluded in Chapter seven, which presents the conclusions of the thesis and the author's suggestions for future work.

Chapter 2: High-Voltage DC (HVDC) Transmission

2.1 Introduction

This chapter discusses the two main types of the HVDC transmission, namely the line-commutated converter (LCC) and VSC-based HVDC schemes. Main components, merits and disadvantages of each configuration are also discussed. Moreover, the environmental aspect of the HVDC transmission is also addressed; this is also accompanied by describing some of the VSC-HVDC projects that are either currently in service or planned for future operation.

The material in this chapter lays a foundation for understanding the studies presented in the next chapters. It also shows the progression from the conventional LCC-HVDC to the modern VSC-HVDC technology.

2.2 LCC HVDC Transmission Schemes

Line-commutated HVDC schemes, which may be referred to as conventional HVDC in the context of this thesis, are presently the most widely-used dc transmission systems [5, 29]. The semi-conductor valve used in the converter blocks of LCC HVDC systems is a thyristor, which is a naturally commutated device capable of blocking high voltages (up to 10kV) and carrying high currents (4kA) [30, 31]. LCC-HVDC schemes offer a solution for interconnecting ac networks with different nominal frequencies of operation (for

example 50Hz to 60Hz) depending on the design requirements [2, 29, 32]. The main elements of a conventional HVDC scheme, as shown in Figure 2.1, are the converters, converter transformers, harmonic filters, dc reactors and HVDC transmission lines.

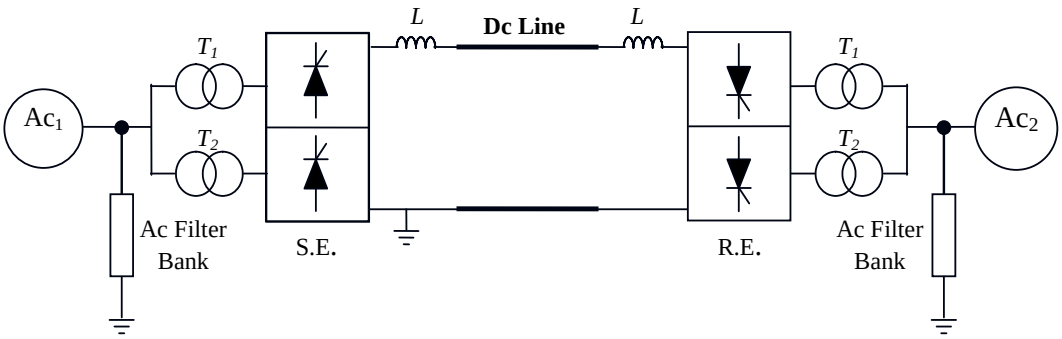

Figure 2.1 Schematic diagram of an LCC-HVDC transmission scheme

2.2.1 Line commutated Converters

The HVDC converters used in LCC-HVDC systems are current source converters [33]. They perform the conversion from ac to dc (also referred to as rectification) at the sending end and dc to ac (known as inversion) at the receiving end [2, 29, 33]. The central component in the converter station is the thyristor valve [5, 29, 31]. Thyristor valves can be built-up in different ways depending on the manufacturer and the application [2, 31]. Since a single device is incapable of withstanding voltages and carrying currents required in large dc transmission, the thyristor valves with their auxiliary circuits are usually stacked in series or parallel depending on the level of voltages and currents required to be achieved [34-36].

Most of the HVDC converter stations use a three-phase converter bridge with 12-pulse configuration as shown in Figure 2.2 [1, 2]. The 12-pulse configuration is achieved by connecting two three-phase 6-pulse converters in series on the dc side. The converters are connected to the ac side by two converter transformers with two different winding configurations (Y-Y and Y-Δ) [1, 2, 29]. This results in the cancellation of ac side current harmonics of orders $6n\pm1$ and dc side $6n$ harmonics leading to a significant reduction in ac filter size and cost [2, 37, 38]. Elimination of harmonics in a 12-pulse arrangement is due to the phase shifting introduced by Y-Y and Y-Δ windings. The ac and dc side harmonics will be of orders $12n\pm1$ and $12n$, respectively. The higher order harmonics are more easily damped than low order ones due to the mostly inductive nature of ac networks [2, 37, 38]. Figure 2.3 presents the three phase ac voltage, dc current and the dc link voltage of a back to back twelve-pulse conventional HVDC scheme.

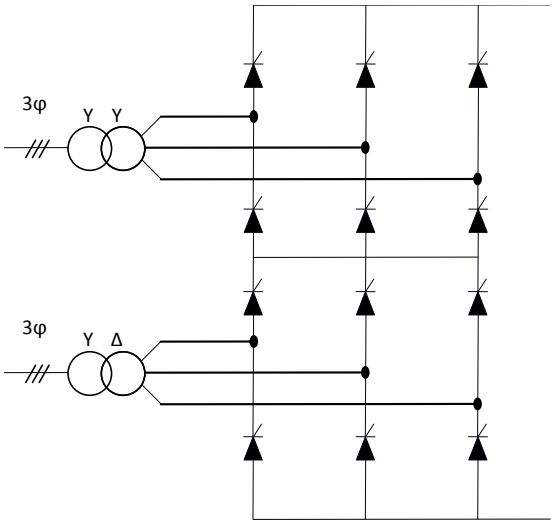

Figure 2.2 Three phase twelve-pulse converter bridge

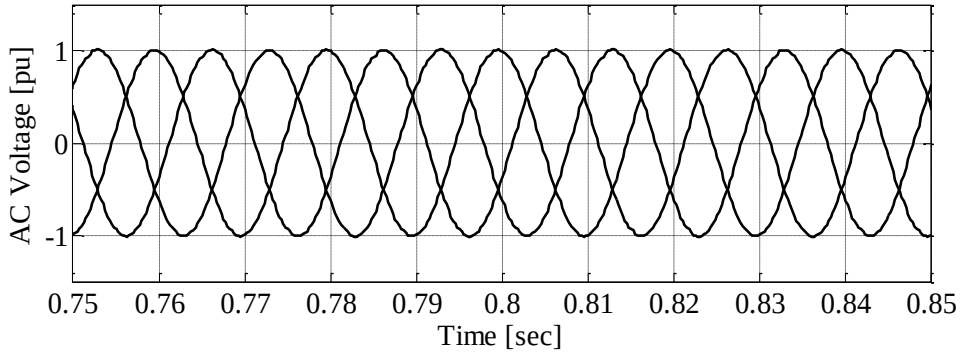

(a) HVDC scheme - Three phase ac voltage

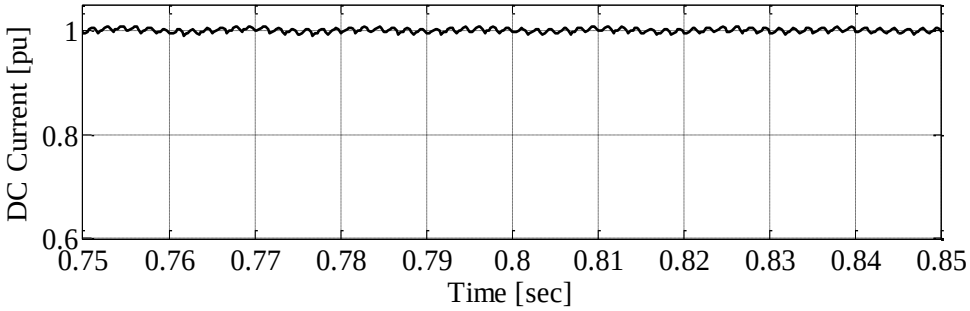

(b) HVDC scheme - dc current

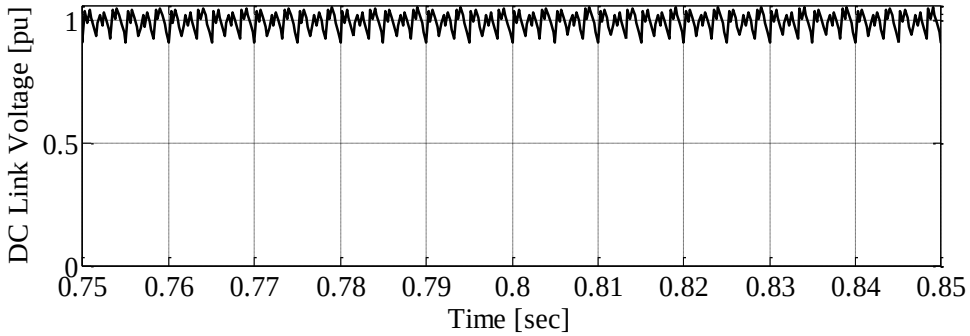

(c) HVDC scheme - DC link voltage

Figure 2.3: Conventional HVDC scheme performance

2.2.2 Transformers

The converter transformers are considered as one of the essential equipments in an HVDC substation. The key role of the transformers is to adjust the ac voltage value at the converter ac terminals to be suitable to the dc voltage on the converter dc side. Converter transformers are usually connected in star connection for the primary side (ac network side) [1, 2]. For the secondary side (converter side) of the two converter transformers, two connections are used Y and Δ resulting in smoother current waveforms on both the ac and dc side [1, 2]. This is due to the phase shift introduced by the connection that eliminates certain low-order harmonics. The other role of the transformer is in its contribution to the commutation reactance.

The converter transformers are equipped with a large tap changer (25-30%) with a primarily role of compensating the ac network voltage variation without affecting the system efficiency [2, 39, 40]. A small tap step is also added to serve the secondary role of the converter transformer, which is compensating for the reactive power. The small tap change allows voltage variation that compensates for the reactive voltage drop in the conversion between ac and dc [2, 41, 42]. The converter transformers are designed with high value of reactance usually between 15%-18% [2, 43]. The high reactance value serves in limiting the short circuit current during the faults. In addition it has a major contribution in reducing the rate of rise of valve currents during commutation between valves, thus protecting the valves against large *di/dt* rates, which may lead to the early failure of the valves [2, 40, 43].

2.2.3 Harmonic Filters

Harmonic filters (ac and dc) are installed to eliminate characteristic harmonics produced by the 12-pulse converter bridge on both the ac side of the converter transformer and dc side of the converter, respectively. The ac filter banks are one of the essential parts of any conventional scheme and serve two main purposes [38, 44-46]:

(i) Eliminating $12n\pm1$characterstic harmonic: ac filters are typically tuned to eliminate 11^{th}, 13^{th}, 23^{rd} and 25^{th} for a 12-pulse converter.

(ii) Partially compensating for the reactive power consumed by the converter (which is in the range of 50% to 60% of the total real power transmitted). Capacitor banks on the ac side of the transformers provide the rest of reactive power compensation required. These also provide further filtering for high-frequency harmonics.

The rating of the ac filter banks is within the range of 20% to 30% of the converter rating leading to an increase in the cost and the complexity of the HVDC scheme.

DC harmonic filters are used to eliminate the $12n$ characteristic harmonics introduced by the converter bridge [47]. This results in reduction of dc current ripple and leads to minimization of coupling and interference in telecommunication circuits [44, 45, 47]. DC filters are not required to be installed in case of back to back and underground cables configurations as there is no overhead transmission line (OHTL) [44, 47]. The dc filters are considerably smaller in size and less expensive in comparison to the ac filters. Nowadays, active filters are used in a wide range using power electronics in order to provide effective filtering [48-50].

2.2.4 DC Reactors

The dc reactors are used on the dc side of the converter bridge. It serves in minimizing the ripples of the dc current so that continuous dc current flow is maintained during system operation especially during high load operation mode, as shown in Figure 2.3(b). In addition, the reactor contributes with the converter transformer reactance in the total value of commutation reactance [2, 5, 29]. This result in reduction of commutation failure incidents caused by dips in ac voltage at the converter bus. The reactor also serves in limiting the crest value of the fault current in the rectifier side in case of a fault in dc line.

2.2.5 HVDC Transmission Lines

The HVDC transmission lines are available in different forms; submarine cables are used when crossing large bodies of water. OHTL and underground cables are also available depending on the environmental consideration and the right of way (ROW). In case of back to back systems, no transmission lines are required [2, 5, 29, 33].

2.3 Advantages of LCC-HVDC systems

The LCC-HVDC transmission systems offer many advantages over the conventional HVAC transmission systems in the forms of technical and environmental merits. The technical benefits offered by the conventional HVDC systems present non-costly solutions to some of the technical problems raised by using the HVAC transmission systems. Some of these merits are:

- HVDC transmission cables do not require compensation due to their minimum capacitance [2, 29]. HVAC transmission cables are not suitable for underwater transmission due the intermediate compensation required for their high capacitance [5, 29, 32, 33].

- HVDC transmission lines can carry more power per conductor, leading to a reduction of insulation thickness and conductor spacing [29, 30, 51]. This allows existing transmission lines to carry more power into an area of high power consumption, resulting in lower costs [2, 52, 53].

- HVDC allows interconnection of unsynchronized ac networks [29, 52], i.e. networks with unequal fundamental frequencies. With the strong international trend to connect different countries and continents with the purpose of trading electric power at different peak hours, this option becomes highly appealing as many of these networks are unsynchronized.

- HVDC increases the stability of power systems [41, 52, 53]. HVDC systems offer fast and accurate power flow control [53]. It should however be noted that the ability of an HVDC system in rapidly controlling the power depends on the strength of ac system in which it is terminated. Moreover, HVDC can help increase system stability by preventing cascading failures, which is a common effect seen in ac high voltage systems, from propagating from one part to another in a wide power transmission grid, whilst still allowing power to be imported or exported in the event of smaller failures. This has caused many power system operators to contemplate wider use of HVDC technology for its stability benefits alone [41, 52, 53].

- HVDC transmission lines do not require series/shunt compensation as in the case of HVAC lines in order to reduce the total reactance and maintain the voltage profile [2, 29].

2.4 VSC based HVDC Transmission

Voltage source converters (VSCs) have undergone major technological innovations in the last few decades in the rating as well as the design and control methodologies [1, 33]. This has led to a greater role for VSC application in power system engineering area. One of their rising applications is in HVDC transmission. The VSC-HVDC offers numerous technical and environmental advantages as it will be shown in the following sections.

A simplified schematic diagram of a VSC transmission system is shown in Figure 2.4. It consists of two voltage-source converters (VSC_1 and VSC_2) interconnected on the dc side via a dc transmission line (OHTL or under-ground/water cable). The dc system connects two ac grids (same grid or different grids) [1, 54]. DC capacitors on the dc side of the VSC provide the dc voltage support required for the stable operation of the VSC scheme. One of the basic features of a VSC configuration is that the dc voltage polarity is always the same [1, 54, 55]. Therefore, the direction of power flow on the dc line is determined by the direction of the dc current, which always flows from a higher dc voltage level to a lower dc voltage level; this is unlike conventional HVDC schemes where the power reversal is achieved by changing the voltage polarity [7, 56, 57].

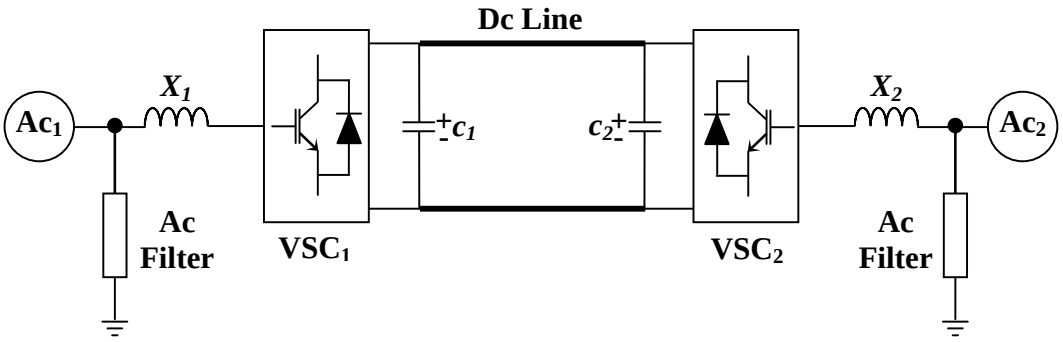

Figure 2.4: VSC-HVDC Transmission Scheme

2.4.1 Force-Commutated Converters

The converters in the VSC-HVDC use insulated gate bipolar transistors (IGBT) valves as their semi-conductor switching element. Similar to a thyristor, an IGBT can be turned on using a user-supplied gate signal; however they offer the added benefit that a similar gate signal can turn the device off as well, which leads to a fully-controlled force-commutated operation [6, 54, 58]. Different converter topologies, such as two-level and multi-level converters, can be used to construct the converter blocks. Pulse-width modulation (PWM) control techniques are used in order to craft the output voltage of the converter and to obtain voltages of desired magnitude and harmonic spectrum [59, 60]. More details about the converter topologies and PWM controls will be described in the next chapter.

2.4.2 DC capacitors (C_1 and C_2) [1,13-15]

The dc capacitors are connected across the terminals of each VSC to provide the dc voltage source and the energy storage needed for the proper operation of the system and

the control of power flow [1, 55, 57]. The capacitors serve also in providing a low inductive path for the valves' turn-off currents. Moreover, they serve in the control of the voltage ripple on the dc line with a rating that depends on the required dc voltage level [56, 61]. The size of the capacitors depends on the dc voltage level required for transmission and the voltage variations during disturbances in the ac system such as faults and valves switching action [1, 6, 8, 33].

2.4.3 Converter reactor or interface transformer (T_1 and T_2)

The interface transformer is connected between the ac network and the ac terminal on the VSC side. The transformer has several beneficial features; it serves as isolation and acts as a filter between the ac grid voltage and the VSC ac terminal voltage [1, 56, 57]. Moreover, the transformer provides suitable ac voltage to permit the use of an optimum converter voltage rating. Additionally, the reactance permits the VSC output to shift in phase and amplitude with respect to the ac system, which enables stable control of converter power output. In VSC transmission application the reactance of the transformer is usually in the range of 0.1 to 0.2p.u [1, 8, 56, 61].

2.4.4 AC filters

Filters can be tuned to lower or higher order harmonics depending on the pulse width modulation (PWM) method employed or converter topology used [59, 60]. However, filters with higher tuned frequency are less expensive and more compact than lower order filters. These harmonics can affect the performance of the VSC-HVDC transmission

system in terms of increasing losses in ac system equipments and affect the telecommunication systems close to the lines [1]. The compensation of the reactive power is not required as in other scheme leading to an additional positive effect in reducing the ac filter size. Filter design will be discussed in more detail in Chapter 3.

2.4.5 HVDC Transmission Lines

The HVDC transmission lines used in the VSC-HVDC schemes are available in different forms such as OHTL, underground and submarine cables. The cables use a new developed insulation made of an extruded polymer that is resistant to dc voltage in addition of their low weight and flexibility features [1, 62]. Additionally, the cables are not designed for voltage polarity reversal as in the case of the conventional schemes [1, 62].

2.5 Unique Features of VSC-HVDC Transmission

Voltage source converter-based HVDC transmission schemes were placed in service for the first time in Sweden in 1997 as a trial 3MW system [8]. Despite the fact that the VSC-HVDC transmission is a new technology and the numbers of the installed schemes is limited in comparison to the conventional HVDC schemes; the VSC-HVDC transmission has a number of appealing technical features over the conventional line commutated converter HVDC transmission scheme [1, 2, 29, 41, 53, 56, 57, 61, 63, 64], including:

- Independent real and reactive power control: The VSC-HVDC transmission system offers a unique advantage in its ability to be controlled to either absorb or

generate reactive power in an independent and rapid mode. Additional controllable parameters (ac voltage, dc link voltage, frequency control) can be regulated in an independent manner as it will be discussed later in more details in Chapter 3.

- Greater independence from ac network strength: The VSC-HVDC transmission can be used to connect to a weak ac network or a passive ac network with no local power generation. Unlike conventional HVDC, the short circuit capacity of the ac system is widely believed not to present a critical issue. However the results presented in this thesis show that the strength of the ac system has a significant effect.
- Limited requirements to filters and reactive power compensation resulting in a cheaper and smaller size filters.
- Pulse-width modulation (PWM): Sophisticated PWM methods allow eliminating critical harmonics employing special optimized pulse patterns.
- No risk of commutation failure: One of the problems existing in the conventional HVDC systems is the risk of commutation failure resulting in disturbances of the ac system. The VSC-HVDC transmission schemes use IGBT valves with PWM technology, the IGBT valves are semi-conductor switches with an inherent self commutating capability; which eliminate any risk of commutation failure.
- Minimum telecommunication requirements: as the control systems on the sending and receiving ends operate independently, this can lead to the improvement of system reliability and stability.

- Possible multi-terminal connection: VSC transmission can be the best choice in order to realize the multi-terminal HVDC grid as minimum coordination is required between the interconnected converters.
- Specific features: Black-start capability, Harmonic and flicker reduction, phase unbalance compensation.

However there are some drawbacks that face VSC transmission such as [1, 56, 63, 64]:

- Higher cost;
- Lower rating compared to conventional HVDC;
- High power loss due to the high switching frequency of the valves; i.e. the semi-conductor valves are switched on and off several times each power frequency cycle, leading to appreciably higher losses than conventionally HVDC converters.

2.6 Environmental Aspects of VSC-HVDC Transmission

In any specific power transmission applications, technical specifications are the main measure in selecting the type of transmission whether it is ac or dc (conventional or VSC based). At the same time, environmental characteristics of the type of transmission are also of high importance. The laws ruling and regulating the environmental concerns of the society enforce heavy restrictions on building new power transmission systems. The possible influences on the environment can include right of ways, effect of electric and magnetic field, radio interference and audible noise.

2.6.1 The right of way (ROW)

VSC-HVDC transmission offers a great environmental advantage due to its compact design and small footprint of the substation and transmission towers when compared to other forms of transmission [1, 65]. It is becoming difficult and complicated to build new OHTL schemes due to the associated change in the landscape which makes the process of obtaining permission time consuming and more expensive [1, 65, 66]. On the other side, the ROW of the HVDC OHTL towers is less than its ac equivalent which facilitates suitable routes in populated areas and in regions with difficult terrains. The full potential of the VSC-HVDC schemes is reached when using the extruded cable. The cables do not require a wide ROW and there is no visual impact in the landscape. From the political and public sides, the cables are always accepted as environmentally friendly solution.

2.6.2 The effect of electromagnetic field

The ac power lines produce a varying electromagnetic field; in the case of the dc OHTL they emit a constant electromagnetic field reducing the health concerns. In the case of dc cables the electric field produced is very small and reduced to almost zero when shielding the converter station and the cables. Moreover, since the VSC-HVDC schemes are bipolar, no current will be injected to the ground reducing the possibility of pipelines corrosion [1, 67, 68].

2.6.3 Radio interference

Radio interference (RI) is associated with the harmonics and noise frequency of the range of 50 kHz to hundreds of MHz. The RI is a result of corona discharge at positive voltage around the conductors [1, 65, 67, 68]. The HVDC line produces RI only from the positive pole conductors, however in the case of AC transmission the RI is produced by the three-phase conductors. In case of similar conditions, the RI measurements show that HVDC transmission is lower by 6-8dB than of ac scheme [1, 67].

2.6.4 Audible noise

The main source of audible noise in VSC transmission scheme is the converter transformer as the use of filters on the converter side results in very low level of harmonics in the transformer [1, 67]. Other sources of audible noise include VSC valves, harmonic filters and dc capacitors. The VSC-HVDC scheme elements have noise component at higher frequency than conventional scheme. As a rule, the audible noise in residential areas should not exceed 40dB at night and 50dB during the day [1, 67].

2.7 Existing VSC Transmission Projects

The first VSC transmission test system, as mentioned earlier, was built in Sweden as a link between Hällsjön and Grängesberg in central Sweden with a limited capacity of 3MW with a dc link voltage of ±10kV. Since that time, a great progress in the VSC transmission systems area has been performed leading to an increase of the capacity of the systems up to 350 MW, that are currently in commercial operation [69]. The most

recent project, with the highest level of power transmission, is between England and Ireland with 500MW capacity and dc transmission voltage of ±200kV [69]. Table 2.1 shows some of the VSC transmission installations with part of their technical features depending on what is available from the manufacturer.

Table 2.1 VSC Transmission Projects

Installation	In service year	Converter topology	Switching pattern	Switching frequency [Hz]	Installed Capacity [MW]
Gotland	1999	2-level	SPWM	1950	50
Murraylink	2002	3-level	SPWM	1350	220
Estlink	2006	2-level	Optimum PWM	1150	350
East west Interconnector	2012	N/A	N/A	N/A	500

2.8 Summary

This chapter presented the two main configurations of HVDC-transmission systems, conventional and VSC-HVDC schemes. The beneficial of using HVDC transmission was also presented in terms of its superiority over HVAC transmission and its advantage of using VSC-HVDC configuration over the conventional scheme. In this chapter, the main

building blocks of each configuration were described including its technical role. The advantages of HVDC transmission was extended to another level by presenting its environmental advantages.

Chapter 3: Principles of Operation of Voltage-Source Converter HVDC Systems

3.1 Introduction

This chapter describes the principles of operation of VSC-HVDC transmission system. Converter topologies such as two-level and multi-level are discussed. VSC control using PWM is also presented with an emphasis on sinusoidal PWM. Moreover the chapter will discuss the details of various modes of operation of the scheme as well as the combination of the different modes depending on the application. Different control strategies such as direct, decoupled and hybrid control are demonstrated.

3.2 Converter topology and voltage synthesis

At the heart of every VSC-HVDC scheme is a voltage-source converter (VSC). VSCs are designed in various topologies but they ultimately serve to generate an ac voltage with controlled magnitude, phase shift and frequency. In the next few subsections, different circuit topologies that have been used in practice are discussed. A well established voltage synthesis PWM technique is also presented.

3.2.1 Voltage Source Converter (VSC) Topologies

A VSC consists of an array of fully-controlled semi-conductor switches (e.g. IGBT) that are switched ON and OFF in a controlled manner to craft an output voltage waveform with desired fundamental frequency component and harmonic spectrum [1, 56, 61]. A voltage-source converter is supported, on its dc side, by either dc voltage sources or a number of equally-charged capacitors [1, 56, 61].

Several circuit topologies with varying levels of complexity exist for VSCs. Circuit topologies with more complexity generally allow crafting voltage waveforms of higher quality (e.g. improved harmonic spectrum) with fewer switching events and hence less switching losses. This however is achieved at the expense of converter cost and control system complexity. The VSCs topologies can be classified broadly into two categories of two-level and multi-level VSCs [1, 70-72]. These two categories of topologies are described in the following sections.

3.2.1.1 Two Level VSC

A three-phase two-level VSC is shown in Figure 3.1. The bridge consists of six valves and each valve consists of an insulated-gate bipolar transistor (IGBT) and an anti-parallel diode. A series connection of such semi-conductor valves may be necessary in order to support the required high voltage used for the transmission (in the range of hundreds of kilovolts) and then each valve will be built up of a number of series connected IGBT devices and anti-parallel diodes [6]. Each phase is capable of generating a voltage of $+E$ (when the top switch is ON) or $-E$ (when the bottom one is ON), and hence the name two-level converter. The PWM techniques (discussed later) are commonly used to

generate a symmetric sequence of such ±*E* pulses at the converter outputs. The desired fundamental and harmonic spectrums are obtained by manipulating the width of those pulses [56, 61, 73]. A sample waveform for the output phase-to-neutral voltage is shown in Figure 3.2.

The commutation circuit and the associated problems experienced in conventional HVDC converter blocks do not exist in self-commutated inverters, which use IGBTs in this case, and therefore weight, efficiency, and voltage control range are improved [1, 6, 73]. In power systems applications, the VSC switches are typically switched at a frequency of 1-2 kHz as it will be explained in section 3.2.4. Higher switching rates are possible and are deployed in lower power applications such as motor drives, but they are avoided in bulk power converters to limit the amount of switching losses generated.

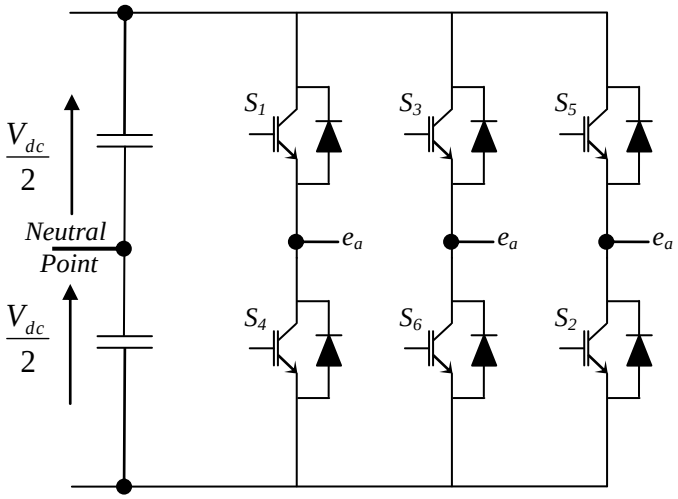

Figure 3.1: Topology of a three-phase two-level VSC

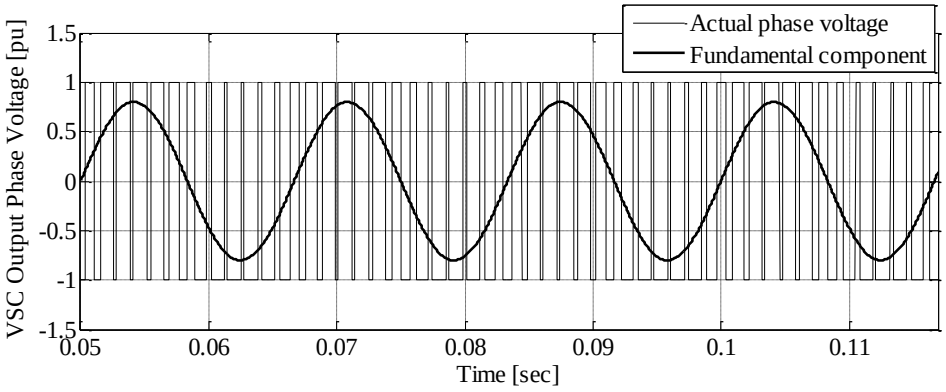

Figure 3.2: Two level VSC output voltage

3.2.1.2 Multi-level Converters - Three Level VSC

The three level VSC is a member of the broad category of multi-level converters [1, 70, 71]. The three-level VSC structure offers an advantage over the two level one in HVDC applications in its ability to modulate the phase voltages between three levels of voltage instead of two. The general structure of the multi-level converters uses an array of switches to select the output voltage from a number of available dc voltage levels. The dc voltage sources are typically implemented using capacitors with a charge-balancing scheme used to maintain equal voltage across all capacitors [73, 74].

The number of voltage levels to which the ac bus voltage can be switched will depend on the complexity of the switch array and the number of dc capacitor subdivisions [1, 71, 74]. As the number of attainable voltage levels increases, the converter becomes able to generate a closer approximation of a sine wave and hence offer superior harmonic spectrum and require less filtering to remove harmonics [1, 75, 76]. The unique structure of multi-level VSCs allows them to reach high voltages with low harmonics without the

use of transformers or series connected synchronized-switching devices [1, 6]. For the purpose of this thesis only the three-level arrangement will be discussed

Three level VSCs can be classified into two main types:

- Diode-clamped converter.
- Nested cell converter.

3.2.1.2.1 Three-level neutral point diode-clamped converter

The key components that distinguish this topology from the two-level converter are the two clamping diodes in each phase, as shown in Figure 3.3. These two diodes clamp the switch voltage to half of the dc voltage [73, 75]. The three-level VSC with its three ac input terminals is used to connect to a split or centre-tapped DC source, as shown in Figure 3.4. Thus, each phase of the VSC can switch to three different voltage levels, i.e., the positive DC terminal (+*E*), the negative dc terminal (-*E*) and the mid-point voltage of zero. The relative duration of the positive and negative output voltage with respect to the duration of the zero output defines the conduction interval of the top most, and the bottom most switches which is useful in setting the amplitude of one of the harmonics to zero [71, 74].

The additional degree of freedom offered by the zero output-voltage level provides flexibility in crafting voltage waveform with a closer match to the reference ac sinusoidal voltage and leads to less harmonic content while avoiding increased switching frequencies. Compared to two-level VSCs, three-level neutral point clamped (NPC) VSCs require more diodes for neutral-point clamping. However, the total number of switching components does not necessarily have to be higher when the converter block is

considered [1, 71, 74]. The reason is that for HVDC applications, a valve consists of many series-connected switches. In the two-level case a valve has to withstand twice as high voltage than in the three-level case. Accordingly, the total number of switches is approximately equal. This leads to a lower switching losses in case of the three-level NPC converter [6, 70, 75].

Despite their merit in producing waveforms of higher quality with less harmonic distortion, multi-level converters are reported to have complications with the insulation and cooling design of the converter valve [1, 71, 73]. Therefore, an NPC concept with a number of voltage levels higher than three has never been considered for HVDC applications.

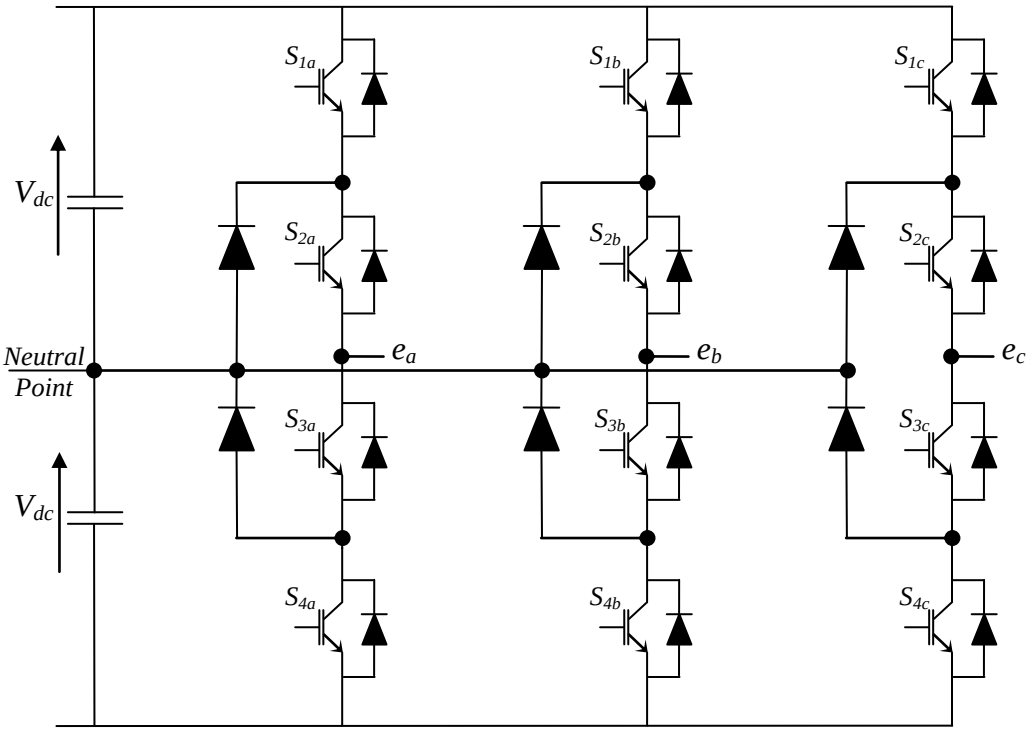

Figure 3.3: Topology of a three-phase three-level NPC VSC

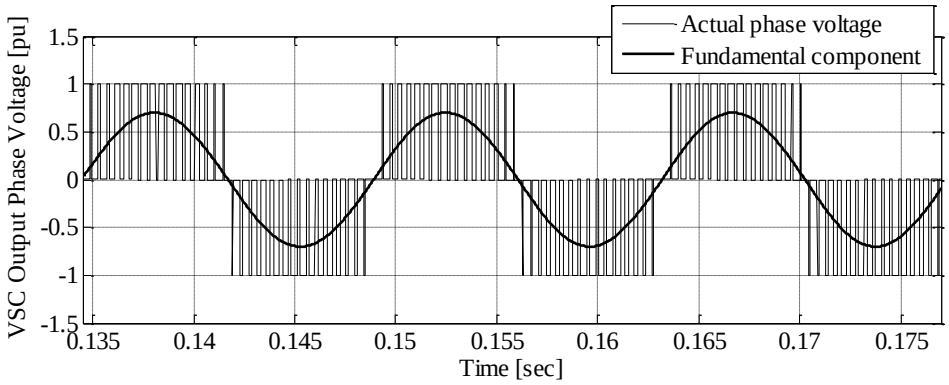

Figure 3.4: Three level VSC output voltage

3.2.1.2.2 Three-level nested cell converter

The nested cell converter is also known as the floating capacitor converter. As shown in Figure 3.5 each cell consists of a pair of switches, one upper and one lower operated as complements, and a capacitor that is not referenced to the dc bus [1, 6]. The semi-conductor valves are mainly used to direct the current through the dc capacitors, adding and subtracting the voltage of dc capacitors as desired, by which different voltage levels can be obtained [1, 71]. A large number of storage capacitors are required leading to high voltage amperes (VA) dc capacitor rating due to two main reasons: the need for separate capacitors for each phase and the requirements to minimize the ripple current carried by the dc capacitors to improve the overall performance of the scheme [1, 6, 71]. The large dc capacitor in each phase unit has a great advantage regarding that the unbalanced loading can easily be maintained by the converter. An additional advantage is achieved in the form of better performance in terms of active power exchange and stability of capacitor voltages.

However, the cost of the nested cell capacitor is relatively high due to the high cost associated with the storage capacitor [56, 75]. Also, the switching frequency and the switching losses are high for real power transmission compared to the NPC topology and the converter control is complicated. This type of VSCs is outside the scope of the thesis.

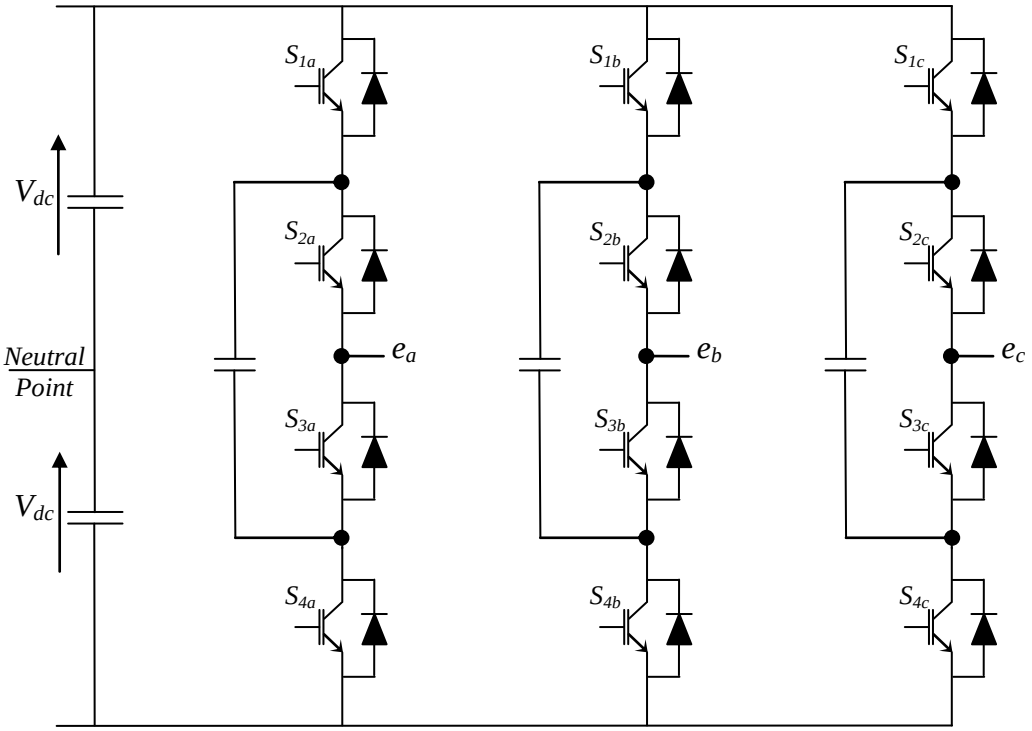

Figure 3.5: Three level nested cell converter circuit diagram

3.2.1.2.3 Modular multilevel converter (MMC)

A new type of multilevel converter technology is described as Modular Multilevel Converter (MMC). It consists of an arbitrary number of series submodules with the purpose of generating single-phase or three-phase output voltage as shown in Figure 3.6. The submodule is generally a bidirectional PWM chopper-cell composed of two IGBT

switches and a local dc storage capacitor, as shown in Figure 3.7 [71, 72, 77]. The independent submodule concept permits the selective control option for each of the individual submodules with a broader participation of each converter leg as a controllable voltage source [78-80]. The total voltage of the two converter legs in one phase unit equals the dc link voltage, and by adjusting the ratio of the converter leg voltages in one phase module, the desired sinusoidal voltage at the ac terminal can be achieved [72, 78]. The scaling to different voltage levels and power levels can be simply done by varying the number of submodules. This adds an advantage to the MMC application that the same hardware with the same mechanical/electrical construction can be used for a wide range of applications [78, 79]. As shown in Figure 3.8, a highly smooth and nearly sinusoidal waveform can then be generated with MMC converters; therefore the requirements to filter circuits are less than the other multilevel topologies. Additionally, the submodules can be switched at a significantly lower frequency which leads to lower operational losses of the converter [72, 78, 79]. The VSC design in newer VSC-HVDC transmission schemes tends to use the MMC technology as their option. The MMC is outside the scope of the thesis.

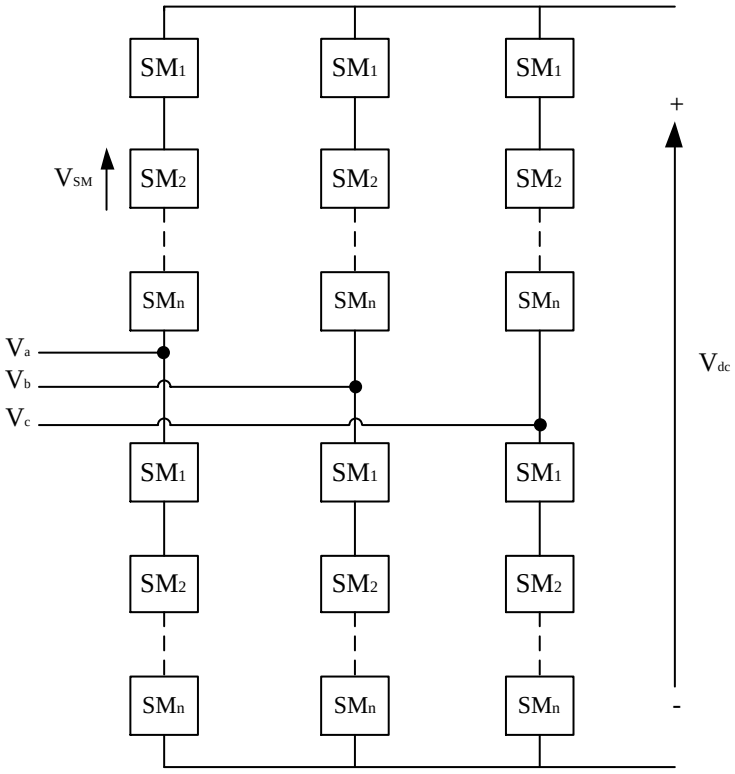

Figure 3.6: Three phase diagram of MMC

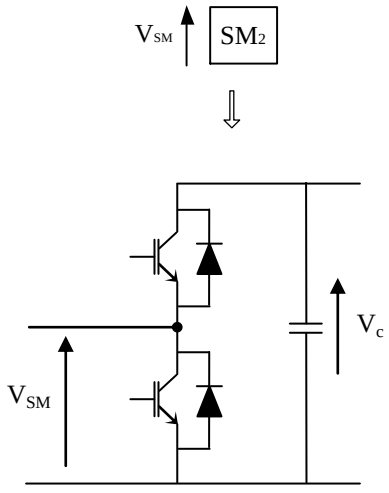

Figure 3.7: Configuration of submodule of MMC

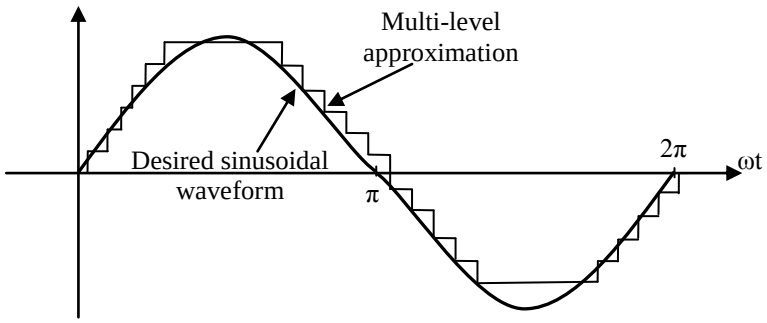

Figure 3.8: MMC output phase voltage

3.2.2 Pulse Width Modulation Techniques for Voltage Source Converters

VSC applications require a means of output voltage control. In most of these applications this control is required in order to provide step-less adjustment of the VSC output voltage [81]. The methods of control are grouped into two broad categories; control of the dc voltage supplied to the VSC input also called Pulse Amplitude Modulation (PAM) and Control of the AC output voltage delivered by the VSC know as Pulse Width Modulation (PWM).

The method of PAM involves a number of well-known methods of controlling the dc voltage supplied to a VSC or the ac voltage delivered by a VSC. These include the use of dc choppers, magnetic amplifiers, induction regulators, phase-controlled rectifiers and transistor series or shunt regulators[73]. The principal disadvantage of these methods is that the power delivered by the VSC is handled twice as shown in Figure 3.9, once by the dc or ac input voltage control and once by the VSC [73]. Moreover, with a phase-controlled rectifier, the AC line-side harmonics are high and the power factor deteriorates

at reduced voltage. In the other case of a chopper controller, the power is converted twice but has the advantage of high line-side power factor with near unity displacement factor [1, 73]. If the primary power is dc, a chopper can also be used to control the VSC dc voltage. This process generally involves more equipment than is required if the voltage control function can be within the VSC itself.

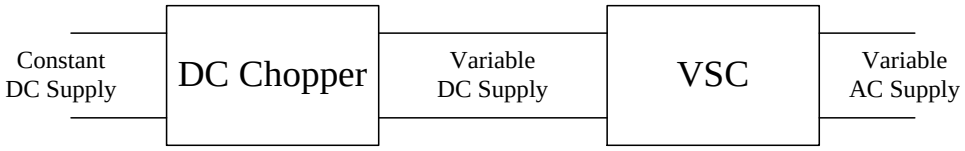

Figure 3.9: Pulse Amplitude Modulation using DC Chopper

Control of the VSC output voltage may be achieved by incorporating time-ratio controls within the VSC circuit. This method is known as voltage control by pulse width modulation (PWM) [82, 83].

The most efficient method of controlling the output voltage is to use PWM control, which is also called variable duty cycle regulation [73, 82, 83]. There are various schemes to pulse width modulate converter switches in order to shape the output ac voltages to be as close to a sinusoidal wave as possible; such as sinusoidal pulse width modulation (SPWM), Selected Harmonic Elimination (SHE) PWM, Trapezoidal PWM, Adaptive hysteresis band current control PWM and Space vector PWM [59, 60, 73, 81-83]. These modulation techniques have an additional advantage in suppressing and minimizing specific low-order harmonics or minimize the total harmonic content and have been implemented successfully in practical systems. Out of the various schemes, SPWM is

discussed here for its simplicity, suitability and ease of implementation in HVDC applications as it will be presented later in this chapter.

In the majority of PWM techniques, the concept of modulation relies on comparing a carrier signal with a modulating signal (reference signal) and the output of comparison is used to switch the valves ON/OFF to shape the output voltage [59, 73, 79]. The output frequency of the VSC is determined by the frequency of the modulating signal and the amplitude of the modulating signal determines the amplitude of the fundamental component of the output voltage.

3.2.2.1 Sinusoidal Pulse Width Modulation

SPWM also known as the triangulation, sub harmonic, or suboscillation method, is popular in industrial applications and is extensively reviewed in the literature [1, 59, 60, 73, 81-83]. For realizing SPWM, a high-frequency triangular carrier (f_s) signal is compared with a sinusoidal reference V_{sine} of the desired frequency. The intersection of the two signals determines the switching instants and commutation of the modulated pulse, as shown in Figure 3.10. The switching devices are switched ON and OFF many times within a half cycle to generate a variable voltage output which is normally low in harmonic contents. In order to fully understand and demonstrate the concept of SPWM, some important factors should be defined:

The amplitude modulation ratio: $m_a = \frac{A_m}{A_c}$ (3.1)

where A_m is the peak amplitude of the sinusoidal modulating signal.

and A_c is the peak of the triangular carrier signal.

Frequency modulation ratio: $m_f = \frac{f_c}{f_m}$ (3.2)

The output voltage switches between $+V_s$ and $-V_s$. The peak value of fundamental frequency component of the output voltage is:

$$V_{ac1}(t) = m_a V_{dc} \sin(\omega_1 t) \quad (3.3)$$

The above equation is valid when the sinusoidal modulating signal frequency is much smaller than the switching frequency corresponding to linear modulation range $0<m_a<1.0$. In this case, the amplitude of the fundamental frequency voltage varies linearly with m_a as shown in Figure 3.11. When m_a is increased beyond 1, amplitude also increases which results in over modulation. The output voltage waveform contains many more harmonics in the side bands as compared with the linear range.

Normalized peak amplitude of the fundamental frequency component $\left(\frac{V_{a01}}{V_s}\right)$ as a function of modulation ratio m_a is shown in Figure 3.11.

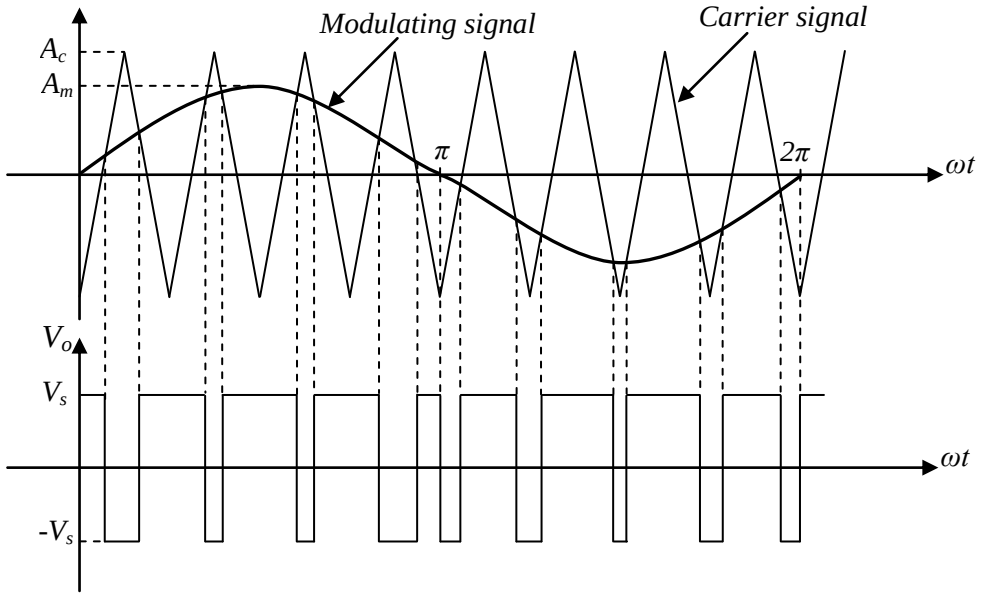

Figure 3.10: Bipolar Sinusoidal Pulse Width Modulation scheme

Harmonics that are dominant in the linear range may not be dominant during over modulation. Amplitude of the fundamental frequency component does not vary linearly with ma. When m_a is sufficiently large, the inverter voltage waveform degenerates from a linear PWM with shifted harmonic content into a square waveform, which has low frequency harmonic content and uncontrollable fundamental.

The selection of the modulation index is a challenging issue as it represents a trade-off between output power and system dynamic response. Higher m_a is preferred from the stand point of harmonics, i.e. high ma for m_a <1 results in low total harmonic distortion (THD) [73, 81-83]. On the other hand, higher m_a will leave a smaller modulation index margin for dynamic response [73, 81-83].

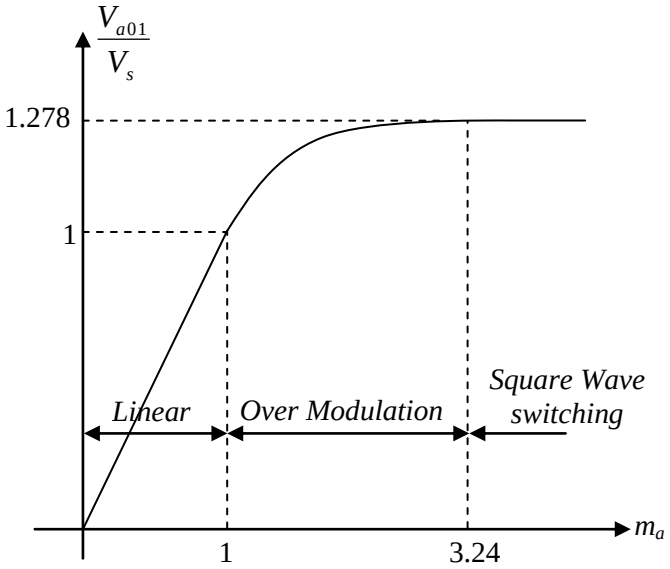

Figure 3.11: Variation of fundamental component of output voltage with m_a

3.2.3 AC Filtering

AC filters, one of the essential parts of VSC transmission configuration, are connected in shunt with the ac grid side of the converter transformer [1, 56, 61]. They are used to reduce the harmonics of the ac output voltage caused by the switching of the IGBT valves [1, 7, 54]. These harmonics affect the overall performance of both ac system equipment and neighbourhood telecommunication networks. AC Filters in VSC transmission systems have a reduced size compared to the line commutated converters as there is no requirements for reactive power compensation. They can be tuned to lower or higher order harmonics depending on the PWM method or converter topology used [1, 56]. However, filters with higher tuning frequency are less expensive and more compact than lower order filters.

The selection of the value of the frequency modulation depends on the balance between harmonic losses and switching losses [1, 8, 84]. A higher of switching per cycle reduces the overall harmonic losses but increases the switching losses. On the other hand, a lower switching frequency increases the overall harmonic losses but reduces the switching losses [1, 8, 56]. A compromise between the desired harmonic performance and the valves losses should be made to reduce the overall losses and the ac filter size in the system under consideration.

The AC filter design and performance is described in more details in Appendix A.

3.2.4 Switching Frequency Selection

The switching frequency f_s is one of the important governing the VSC behaviour despite the fact that f_s cannot be arbitrarily increased for the following reasons:

a) The switching losses of semiconductor devices increase proportional to the switching frequency [73].

b) Semiconductor switches for high power ratings generally produce higher switching losses. This limits the switching frequency for bipolar transistor modules of higher rating to a few kilohertz; IGBTs are conventionally operated up to 5-20 kHz while the maximum switching frequency for GTOs is only a few hundred Hertz [1, 76].

c) The regulations regarding electromagnetic compatibility are stricter for power conversion equipment operating at switching frequencies higher than 9 kHz. This is primarily a cost problem (from the point of view of filtration of acoustical noise) [1, 76].

The frequency modulation index m_f is always an odd integer number (to ensure quarter cycle symmetry) with a high value that trades off between switching losses increase and harmonic losses decrease.

In some VSC transmission scheme, the switching frequency is chosen to be 1950Hz (for a 50Hz based system) and 1980Hz (for a 60Hz based system). This will result in N=39 for a 50Hz system and N=33 for a 60 Hz system which lead to a better harmonic spectrum.

The choice of the suitable carrier wave shape and carrier frequency enables the design of less expensive and more compact filter as described previously. However, a compromise between the switching frequency and the harmonic performance must be taken into consideration in order to obtain acceptable harmonic spectrum with low harmonic losses.

3.3 VSC Transmission Modes of Operation

The VSC transmission offers a great deal of advantage over the conventional HVDC transmission schemes in terms of presenting two flexible degrees of freedom at each end. These degrees of freedom are reflected into various control functions as it will be discussed in the following subsections. The choice of different control function combinations will mainly depend on the application as well as the available resources offered by the transmission case under study. The current limiting control and capacitor voltage balancing control are present in almost every scheme despite the type of application.

3.3.1 Real and Reactive Power Control

The ac side of a VSC connected to an ac grid via a converter transformer with a reactance X_L, can be represented by two ac sources with different magnitudes and different phase angles, as shown in Figure 3.12.

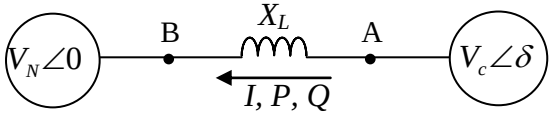

Figure 3.12: Basic VSC connected to a grid equivalent representation

The fundamental apparent power in the connection point of the converter is given by:

$$S = P + jQ = \bar{V}_N \bar{I}^* \tag{3.4}$$

where S is the fundamental apparent power, P is the real power, Q is the reactive power, $\bar{V}_N$ is the ac network voltage and $\bar{I}$ is the current flowing between the converter and the AC grid.

In high power applications, the inductor losses are small and can be neglected when calculating the real and reactive power from the converter [1, 7, 56, 76]. Thus the real and reactive power can be expressed as:

$$P = \frac{|V_N||V_c|}{X_L} \sin\delta \tag{3.5}$$

$$Q = \frac{|V_N||V_c|}{X_L} \cos\delta - \frac{|V_N|^2}{X_L} \tag{3.6}$$

The angle δ is the phase difference between $\bar{V}_N$ and the converter ac side voltage $\bar{V}_c$. From the above expressions, it can be seen that $\bar{V}_N$, $\bar{V}_c$ and δ can control both the real and reactive power.

The real and reactive power control can be described using the *P*-*Q* diagram shown in Figure 3.13; it shows the ability of VSC-HVDC transmission to operate in four quadrants as well as the independent control of both real and reactive power. These features enable the VSC to deliver additional services, such as the possibility to be operated as a power oscillation damper [1, 61, 76, 85].

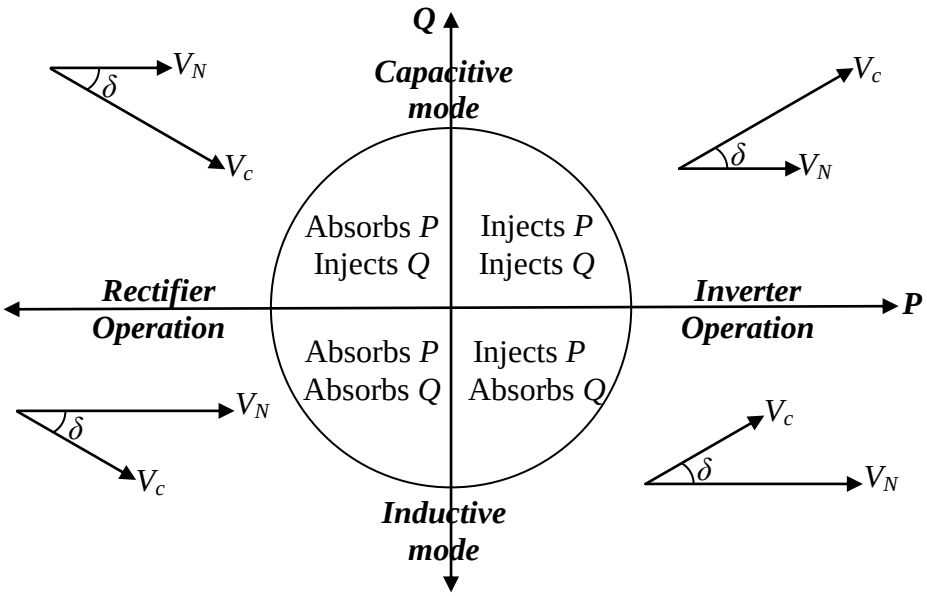

Figure 3.13: The real and reactive power diagram of VSC

3.3.2 AC Voltage Control

AC voltage control is achieved with the aim of providing a constant and stable input ac voltage to the three phase terminals of the VSC.

The voltage across the ac terminal of the VSC is measured, filtered and compared to the ac voltage reference value V_{AC}^*, as shown in Figure 3.14 to obtain the deviation from the reference value by means of a controller.

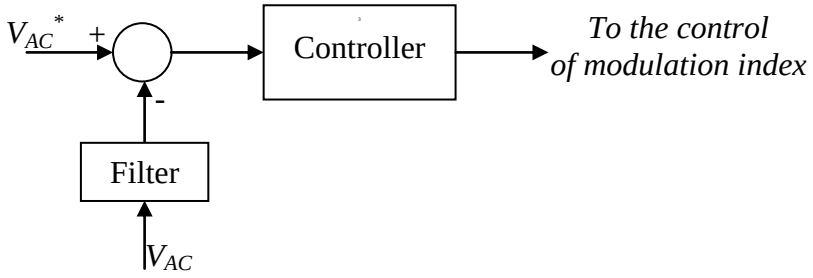

Figure 3.14: AC voltage control

3.3.3 Frequency Control

In most power system applications, it is required to tightly maintain the frequency within the international standard range of 60±0.5%. In case of an active load, this is achieved by using a phase locked loop (PLL) locked to the three-phase terminals of the active load. The frequency control becomes a challenge in the case of dead load or a passive load with no local generation. This situation can be solved by using a device such as the independent voltage controlled oscillator (VCO), shown in Figure 3.15, instead of the phase locked loop (PLL) at the receiving end side. The VCO serves in keeping the load frequency within the standard limits by providing an independent source of frequency stabilization.

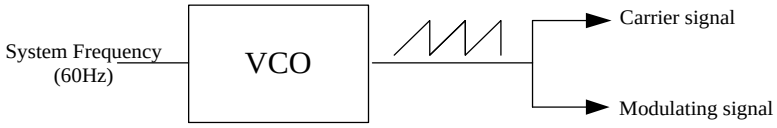

Figure 3.15: Voltage Controlled Oscillator used in case of passive load

3.3.4 DC Link Voltage Control

A dc voltage controller can regulate real power to maintain the required voltage level across the dc capacitor. The voltage across the capacitor is measured, filtered and compared to the dc voltage reference value V_{dc}^{*}, as shown in Figure 3.16 to get the deviation from the reference value by means of PI controller. An alternative control structure is demonstrated in references [86, 87].

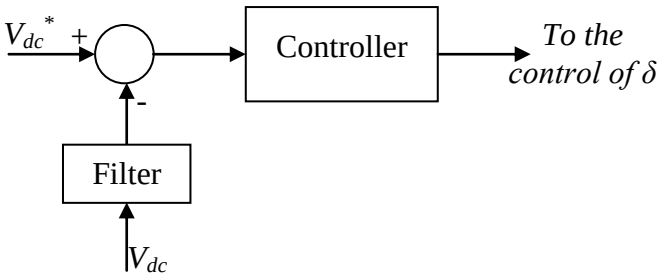

Figure 3.16: DC voltage control

3.3.5 Current limiting and Control

The current control is an important inherent type of control that is usually implemented using a current limiter. The objective of this control is to ensure that the current order requested by the control system does not surpass the maximum current rating of the VSC valves. The current controller keeps the current flowing through the valve within the designed boundaries; represented in Figure 3.17 by the circle. This is achieved by converting the current stationary axes signals to polar form and limiting the magnitude of the output control signal.

In other words, in case the *d* and *q* current orders are outside the circle (point A) the current controller generates new values within the valve currents boundaries (point B). Moreover, and depending on the control structure, it can be used as a backup protection for the valves preventing them from long overload periods causing stress or damage to the valves; as the VSC transmission scheme does not have overload capability as the synchronous generators have for example.

3.3.6 Capacitor Voltage Balancing Control

The capacitor voltage balancing for the two capacitors is one of the challenging issues when using the three-level VSC topology in VSC transmission schemes in order to maintain equal and uniform voltage stress on the valves as well as the dc capacitors. The origin of the capacitor voltage unbalance problem comes from the non-uniform switching of the VSC upper and lower valves. This results in overcharging one of the capacitor and undercharging the other one; unbalanced dc side voltages will add non-characteristic even harmonics to the ac side [88, 89]. Several methods for balancing the capacitors voltages have been introduced in [90-93].

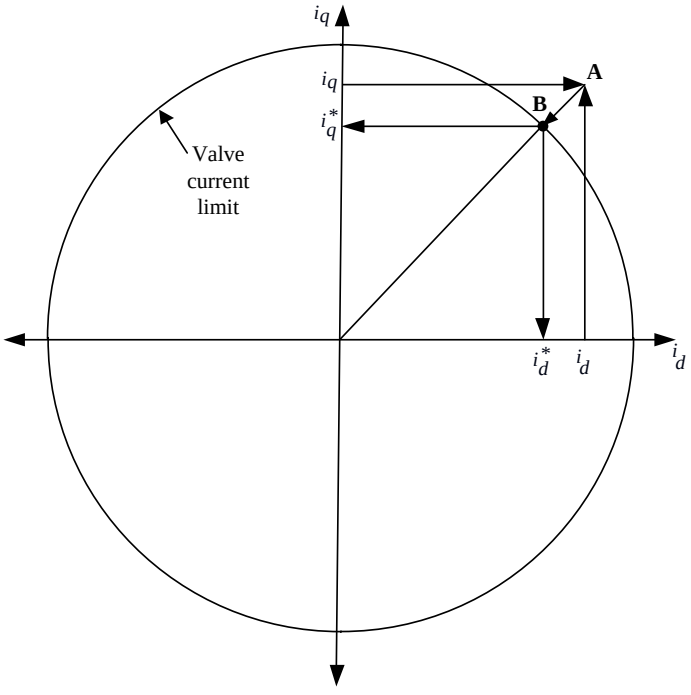

Figure 3.17: Current limiting control concept

The method used in the implemented simulation depends on introducing a phase shift angle to the sinusoidal modulating reference signal of each phase of the three-phase system. The added phase shift is based on the difference between the two capacitors voltages resulting in a zero phase shift when a complete voltage balance is achieved between the two capacitors. Figure 3.18 shows the block diagram of the implemented control scheme.

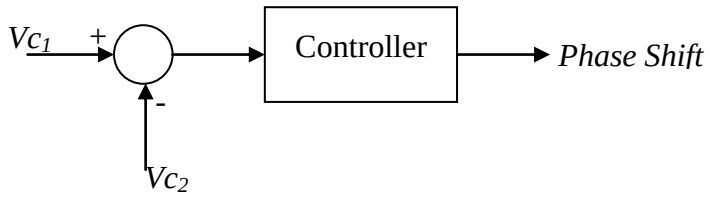

Figure 3.18: Voltage balancing scheme block diagram

3.4 Practical Management of Different Control Modes

The VSC transmission system has great flexibility in terms of its controllable parameters offering two degrees of freedom at each end in order to provide a stable and robust control for the scheme. The controlled parameters vary according to the application used and the type of the load being supplied [1]:

i) Supply to a load with no other source of generation, which is the case implemented in this paper:

- Sending end: dc link voltage control and ac voltage control.
- Receiving end: Frequency control (defining the load frequency) and ac voltage control.

ii) Interconnection of two or more ac networks:

- Sending end: dc link voltage control and ac voltage control.

- Receiving end: Real power control and ac voltage control.

iii) Supply from a wind farm:

- Sending end: ac voltage control, Frequency control and Real power control

- Receiving end: Real power and ac voltage control.

3.5 VSC Control Strategies

As mentioned in section 3.2.7, the VSC offers two degrees of freedom at each end which enable more choices in terms of controlled parameters as well as much more stable and consistent operation. Control of the modulation index m and the phase shift angle δ is implemented using the direct control and decoupled control methods. Another control approach has been implemented in case of a dead load end, which is the hybrid control method. This control method takes advantage of the single controlled parameter at the dead end with the intention of accelerating the control response of the VSC transmission system and eliminating the disadvantages of both direct and decoupled control methods. The three previously mentioned control methods will be described in more details in the following subsections.

3.5.1 Direct Control

Direct control concept is achieved by measuring and comparing the converter controlled parameter, to the corresponding reference parameter value to get the deviation from the reference value by means of PI-controller in order to provide the suitable value of control

function required by adjusting the output voltage and phase shift of the VSC, as it was presented in the previous sections. Figure 3.19 shows a simplified block diagram of the general concept of the direct control method application in VSC-HVDC transmission scheme. In this diagram two electrical quantities are compared representing the required value A_{ref} and the actual value A_{actual}. These values can represent any of the controlled quantities in VSC schemes (ac voltage, dc link voltage, real power, reactive power, load frequency). A PI controller is used to provide the VSC control signals either the modulation index m or the phase shift angle depending on the controlled parameter, i.e. the real power P is more affected by δ and the reactive power Q is controlled by m.

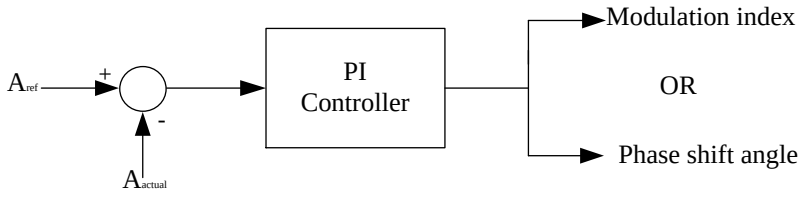

Figure 3.19: Direct control simplified block diagram

3.5.2 Decoupled Control

A three phase view of the VSC ac side is shown in Figure 3.20. Using the rotating reference frame theory [1, 63, 76, 94], the d and q components for voltage and current of the VSC can be calculated using Park's transformation.

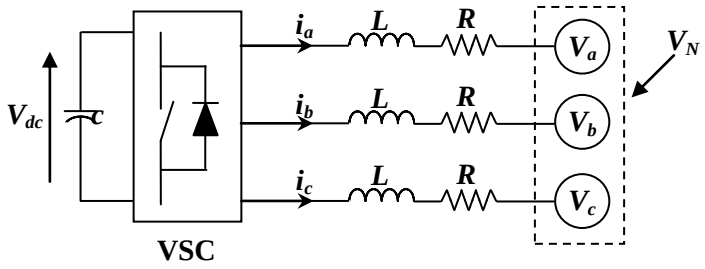

Figure 3.20: VSC connected to a three-phase network

$$\begin{bmatrix} x_d \\ x_q \\ x_0 \end{bmatrix} = \frac{2}{3} \begin{bmatrix} \cos(\omega t) & \cos(\omega t - 120) & \cos(\omega t + 120) \\ -\sin(\omega t) & -\sin(\omega t - 120) & -\sin(\omega t + 120) \\ 1/2 & 1/2 & 1/2 \end{bmatrix} \begin{bmatrix} x_a \\ x_b \\ x_c \end{bmatrix} \tag{3.7}$$

Where the variable *x* represents the instantaneous voltage and current.

From the converter AC side:

$$L\frac{di}{dt} + Ri = V_c - V_N = \Delta V \tag{3.8}$$

This equation can be applied for each phase of the three phase where $i=i_a$, i_b, i_c and V_N represents the network voltage for each phase $V=V_a$, V_b and V_c. Assuming that the zero sequence current is equal to zero which is the case for balanced systems, we obtain:

$$\frac{di_d}{dt} = \omega i_q + \frac{1}{L}\Delta V_d - \frac{R}{L} i_d \tag{3.9}$$

$$\frac{di_q}{dt} = -\omega i_d + \frac{1}{L}\Delta V_q - \frac{R}{L} i_q \tag{3.10}$$

The instantaneous real and reactive power equation based on the *dq* reference frame can be calculated from the following equations:

$$P = \frac{3}{2}\left(V_{Nd}\, i_d + V_{Nq}\, i_q\right) \tag{3.11}$$

$$Q = \frac{3}{2}\left(V_{Nd}\, i_q - V_{Nq}\, i_d\right) \tag{3.12}$$

Using the Park's transformation, one can observe that under balanced steady state conditions, the *d*-axis coincides with the instantaneous network voltage vector, thus:

$V_{Nd} = V_m$ and $V_{Nq} = 0$

This is done by synchronizing the rotating reference frame and the ac network as it will be shown later in more details. Then the real and reactive power equations will be:

$$P = \frac{3}{2} V_{Nd}\, i_d \tag{3.13}$$

$$Q = \frac{3}{2} V_{Nd}\, i_q \tag{3.14}$$

From the above equations, it can be seen that the *d* and *q* axis current components control the instantaneous real and reactive power, respectively.

Decoupled control method is applied in order to decouple all these quantities whether it is real and reactive power case or capacitor voltage and reactive power case. The decoupled control model used in the simulations is shown in Figure 3.21. The model consists of three main parts:

- The decoupled controller: as described before.
- The VSC controller: this part is responsible of producing the control signal required for the VSC in order to generate the required real and reactive power.
- Synchronization & transformation: the PLL is the main building block of this part in order to synchronize the reference frame by locking it to the ac network voltage. Also, the *abc* to *dq* transformation for voltages and currents is implemented in this part.

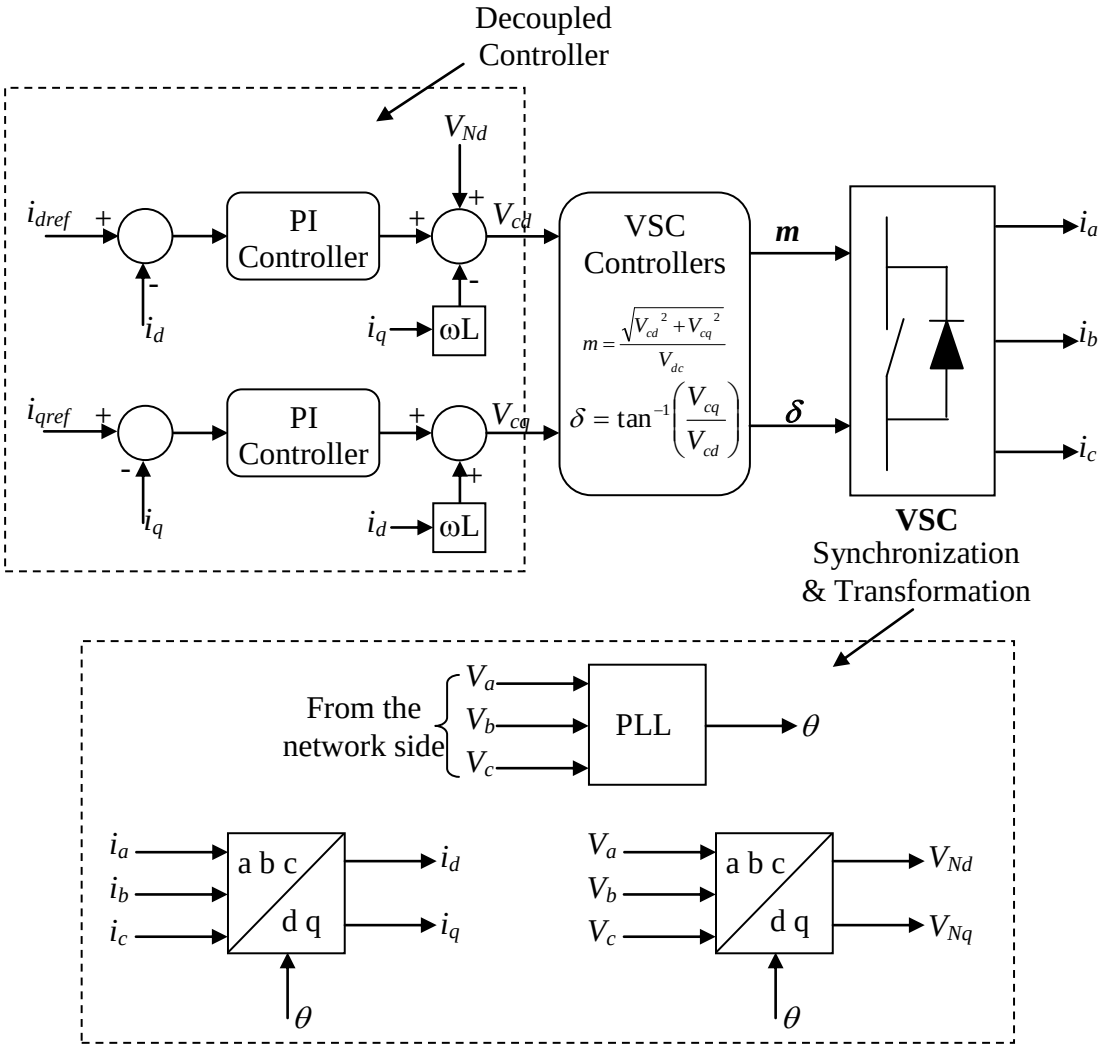

Figure 3.21: decoupled current control model of the d and q axis currents in PSCAD

3.5.3 Hybrid Control

This control method is inspired from both the direct and the decoupled control methods; the idea is based on the combination between the advantages and the prevention of the disadvantages of both control methods. Advantages such as fast dynamic performance of the direct control and the inherent valve protection of the decoupled control method are

retained in this approach. The disadvantages that are aimed to be avoided in this proposed control method are the coupling between the controlled parameters associated with the direct control method and the time delay related to the *abc* to *dq* transformation embedded in the decoupled control concept.

The receiving end rms ac voltage $V_{ACactual}$, is measured and compared to the rms ac voltage reference value V_{ACref}, as shown in Figure 3.22 to obtain the deviation from the reference value by means of PI controller. The output of this PI controller is used to set the reference value of the current limited dictated by the available valve current rating. This reference value is compared with the actual current value through a second PI controller to generate the suitable modulation index value. This control method can be considered as an implementation of decoupled control to achieve the voltage and real power control objectives.

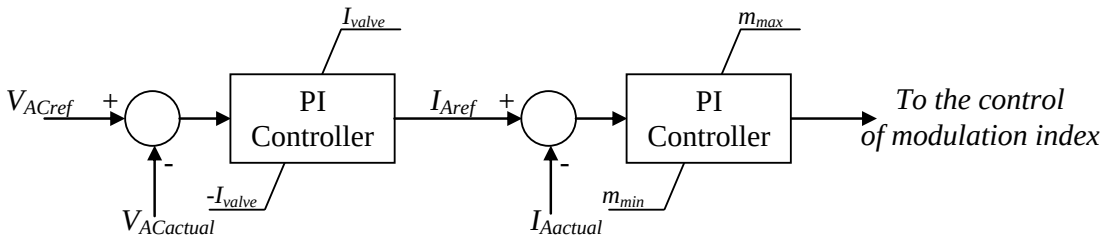

Figure 3.22: Hybrid control of the AC voltage control in case of dead load

3.6 Summary

This chapter presented the principles of operation of VSC-HVDC transmission scheme including different converter topologies with an emphasis on the two-level VSC and three

level neutral point diode clamped converter. Sinusoidal pulse width modulation was also discussed. Different control modes and control methodologies was also described in larger details. Hybrid control technique was also implemented for passive loads based on a combination between direct and decoupled control.

Chapter 4: VSC Transmission Control and Performance

4.1 Introduction

This chapter presents the simulation and analysis of a detailed model of a back to back VSC transmission system, with the implementation of the control topologies discussed in Chapter 3. The receiving end of the system is designed to demonstrate the ability and flexibility of VSC-HVDC transmission in terms of supplying efficiently both active and passive loads. Direct and decoupled control topologies are simulated in two level VSC transmission scheme case supplying active load as well as an analysis of these topologies under different operating conditions. Optimization is also introduced through a simplex optimization procedure in order to refine the controllers' parameters. The effect of the optimization on the system performance is shown in case of three level VSC configuration supplying passive loads using decoupled and hybrid control topologies. Simulation and optimization results are obtained using an electromagnetic transient simulation program (PSCAD/EMTDC).

4.2 Interconnection of Two Active AC Networks

The back-to-back VSC transmission system shown in Figure 4.1 is modelled in PSCAD/EMTDC transient simulation program. Table 4.1 represents the general specifications of the VSC scheme used in the simulation case under study. The VSC_1

represents the sending end converter where the dc link voltage and reactive power through the converter are controlled. On the other end, the real and reactive power flows represent the two control parameters on the receiving end. Dynamic performance results of the VSC based transmission system for both sending and receiving ends are presented in this section using both direct and decoupled control methods. The simulation results show the system dynamic response to step changes applied to the system reference values, such as dc link voltage, and real and reactive power. The simulated step changes represent, in a real system, the change of the system operating conditions whether it is an increase/decrease in the electric power demand or even a change of the power flow direction between two different grids at different peak load hours.

The PSCAD/EMTDC transient simulation program is a widely accepted tool for power system simulation. PSCAD/EMTDC provides a fully modular and visual general purpose power systems simulation environment giving the user online control of input data, and the ability to record and display output data using advanced plotting technique. It is used extensively for many types of ac and dc power simulation studies, including power electronics, sub-synchronous resonance and lightning overvoltages. The PSCAD/EMTDC users include commercial and industrial organizations as well as energy utilities and research labs around the world [95]. Simulation results obtained using PSCAD/EMTDC are generally accepted to be close representations of the actual fact and are often used to as a benchmark to validate results obtained from other simulations.

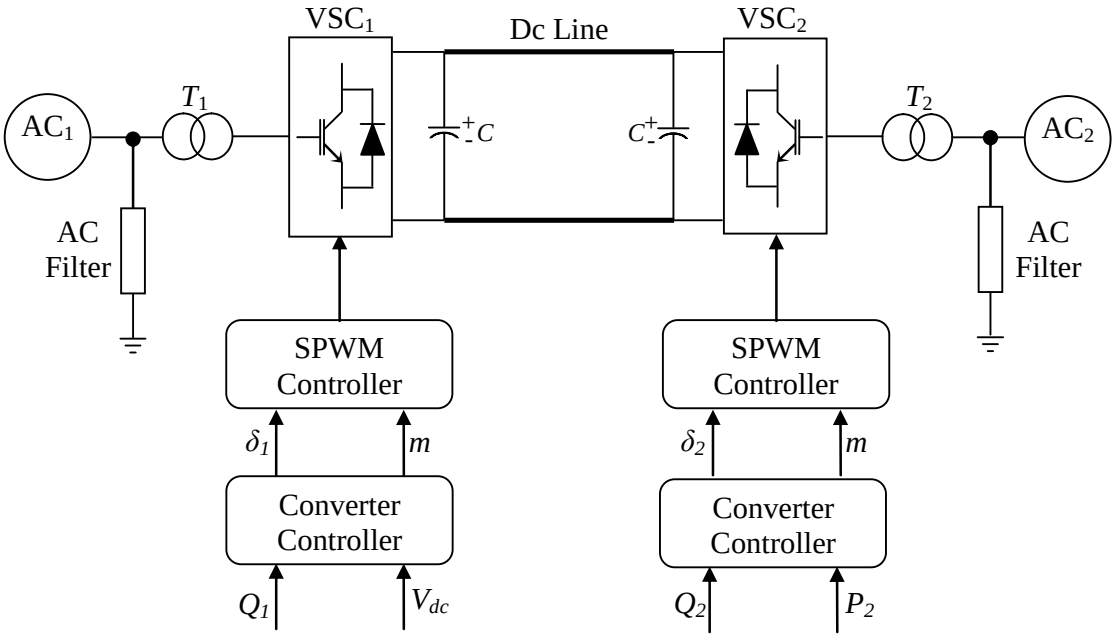

Figure 4.1: Block diagram of the implemented VSC transmission scheme

Table 4.1. Specifications of the VSC-HVDC transmission scheme

Parameters	**Rating**
Power Rating	100MW
DC Link Voltage	100kV
Sending End SCR	5.0∠75°
Receiving End SCR	4.0∠75°

Figure 4.2 represents the simulation results of the sending end converter using direct control method. It is evident that, due to the coupling between the control parameters, change in one parameter strongly affects the other one resulting in large transient

deviation. In some cases, these deviations may even influence the overall system stability and performance.

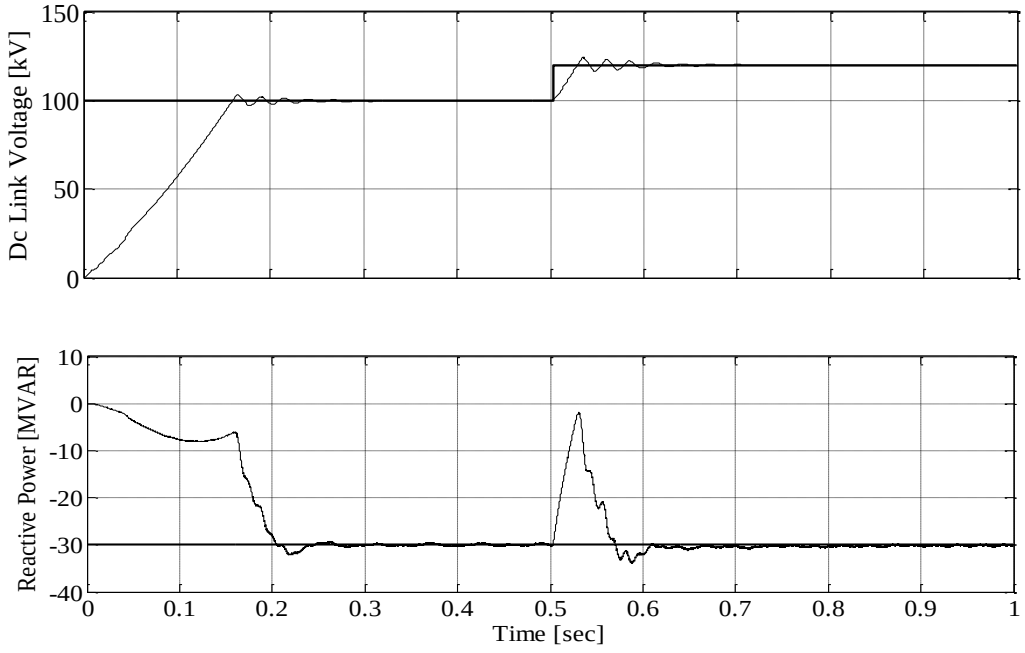

Figure 4.2: VSC transmission system performance - Direct Control

Decoupled control is implemented in order to decouple the interaction between the controlled parameters at each end, as described in details in the previous chapter. The simulation results are shown in Figure 4.3 for both the sending end and receiving end converters. It is noticeable that the system performance has a strong stability at both ends. Any change in the controlled values, dc link voltage and real/reactive power, at one end does not affect the other end whether by increasing or decreasing or even changing direction in case of real and reactive power.

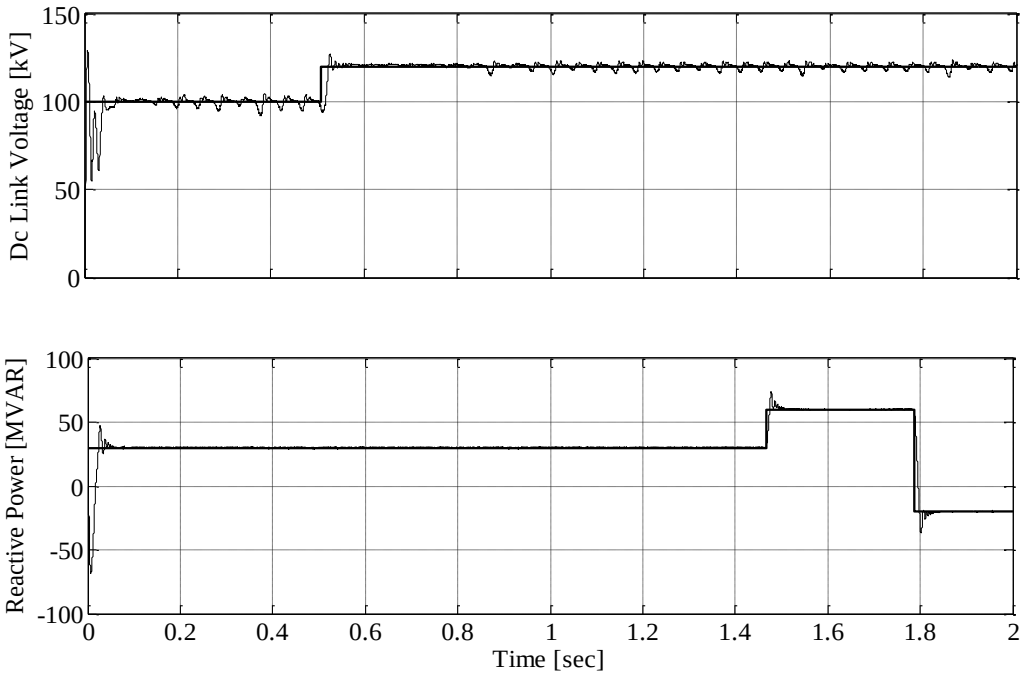

(a) Sending end controller

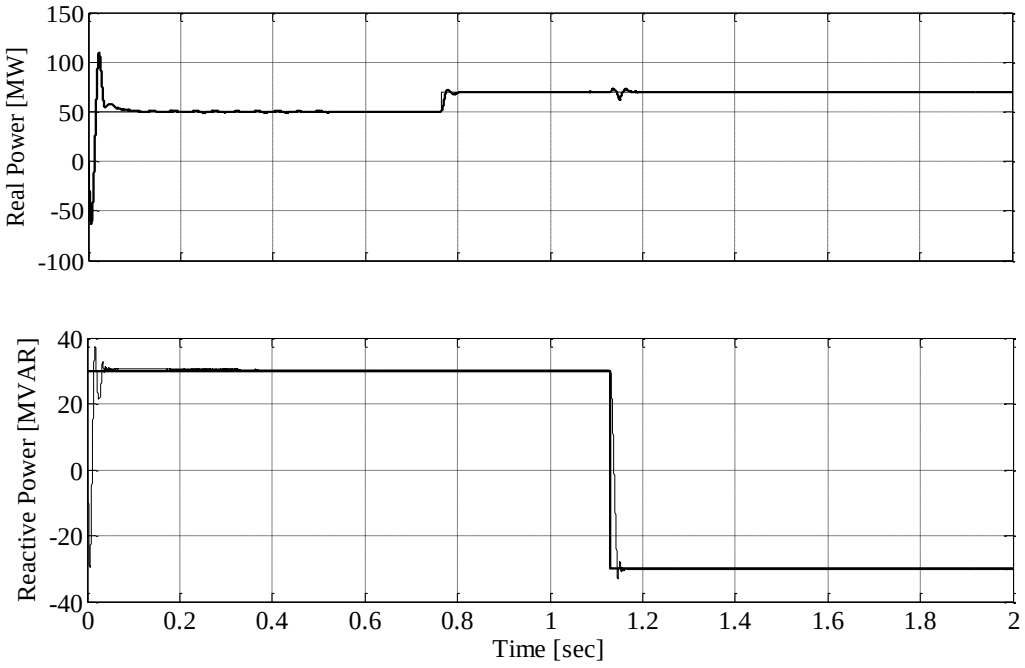

(b) Receiving end controller

Figure 4.3: VSC transmission system performance –Decoupled Control

Based on the previous description of both direct and decoupled control method, it was mentioned that the decoupled control offers an additional advantage regarding its inherent current control ability via its ability to independently regulate the d and q components of the currents. Figure 4.4 shows the receiving end fundamental RMS ac current for the same value of reactive power using both the direct and decoupled control. It can be shown due to the inner current control loop in the decoupled control the current does not go beyond a previously specified value reflecting the rated value of valve current. However, due to the absence of the current control in the direct control method, the current increases to a higher value in order to satisfy the system operator requirements potentially causing the damage of the VSC valves. Figure 4.5 shows the receiving end fundamental RMS ac current waveforms for both the direct and decoupled control methods at the same value of reactive power required within the VSC transmission limits.

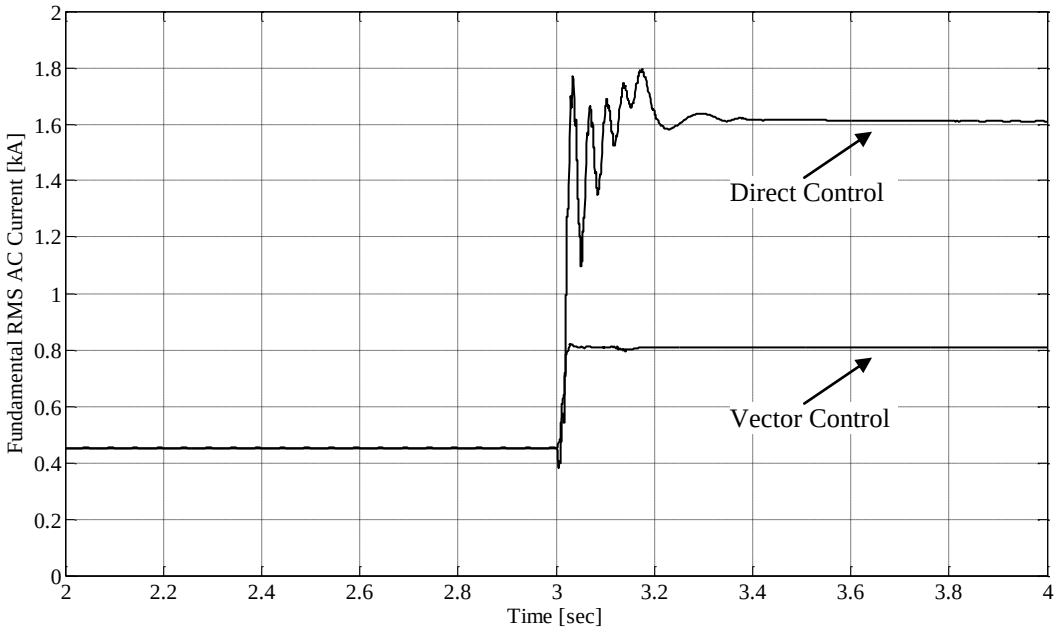

Figure 4.4: The fundamental RMS receiving end current using direct and decoupled control methods: limitation effect

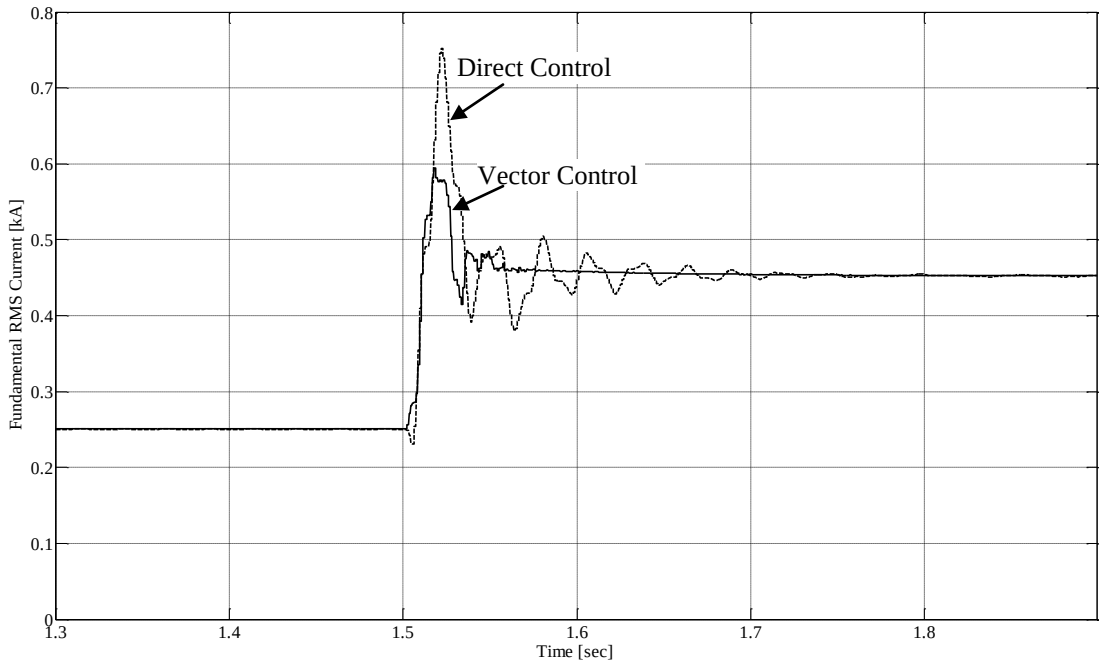

Figure 4.5: The fundamental RMS receiving end AC current using direct and decoupled control methods: steady state operation

4.3 Optimization of Control System Parameters

The design of the control system at both ends of the back-to-back scheme is always a challenging issue in terms of coordination of the controllers at each end in order to prevent controllers' interactions. However, optimization of the controller gains is another challenging step for the system designer due to the large number of controller parameters at each end. The total number of controller gains at both ends is 18 gains (for the case considered herein) distributed equally between proportional and integral gains for various inner and outer control loops. Therefore, the design of the objective function and the optimization procedure are required to be considered in a proper manner with the

intention of preventing any control interaction between different control systems, as mentioned earlier, as well as achieving the desired objective beyond the use of optimization methodology.

Details about the optimization method and algorithm are presented in Appendix B.

4.4 Supply to a Passive Load

One of the major advantages of the VSC transmission scheme, either as a two level or multi-level scheme, over the conventional schemes is its ability to supply dead loads with no local power generations. A back-to-back three level VSC transmission scheme supplying a dead load is shown in Figure 4.6. The sending end converter station controls the dc link voltage and converter ac voltage. On the other end, the ac voltage represents the controlled parameter. The frequency is maintained constant which is achieved by using an independent voltage controlled oscillator (VCO) instead of the phase locked loop (PLL) at the dead end.

One of the challenging issues in three level back to back VSC-HVDC transmission schemes is to maintain the voltage unbalance between different levels requiring capacitor voltage balance control as described and solved in the previous chapter. On the other hand, the three level VSC is preferred in many cases of the VSC transmission systems as the valve design becomes easier than the two level VSC. In three level case, for a given dc voltage level, each valve is designed for half of the terminal to terminal dc voltage; however in two level case a large number of series connected switches are needed in the valves [60, 70, 71, 96].

Two different control methods are used to control the receiving end ac voltage of the three level VSC; as one of the main goals is to keep the load voltages within the limits identified by the customers. The two control methods implemented in the receiving end are decoupled and hybrid control concepts. The control methods methodologies were discussed in the previous chapter.

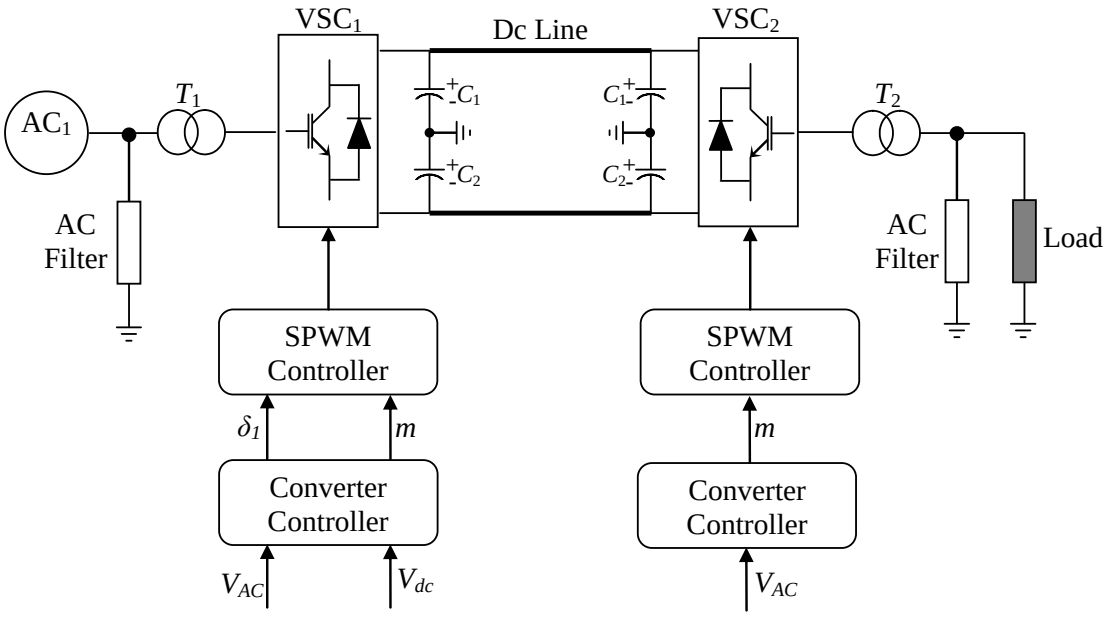

Figure 4.6: Block diagram of the implemented VSC transmission scheme

The rest of this chapter will present the simulation results of a back to back three-level VSC transmission system. The effect of the optimization methodology, introduced in the previous section, is also shown.

4.4.1 Decoupled Control

This section represents the simulation results of the three level back to back VSC transmission system using decoupled control method at both sending and receiving end in order to control the load ac voltage; while using decoupled control method at the sending end.

Figure 4.7 and Figure 4.8 show the unoptimized and optimized performance of the VSC transmission system at both the sending and receiving end for different reference values. Figure 4.9 shows the capacitor voltages for each of the two capacitors.

Table 4.2 and Table 4.3 show the effect of optimization on the gains values for both sending and receiving end, respectively.

The simulation results show the beneficial effect of using optimization techniques in terms of improving the system overall response either in steady state case. This results in reducing system peak overshoot and reducing the controlled parameter settling time and steady state error.

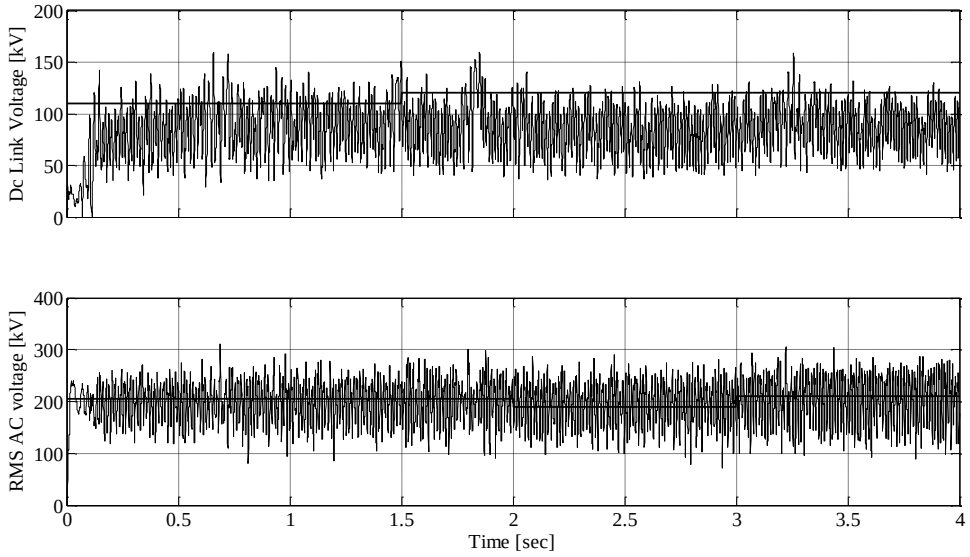

(a**) Sending end controller**

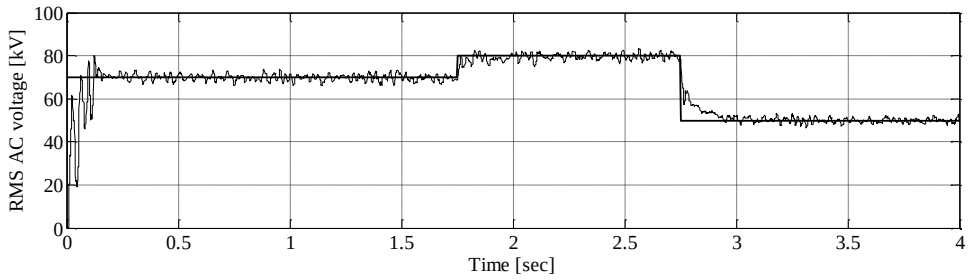

(b) Receiving end controller

Figure 4.7: VSC transmission system performance

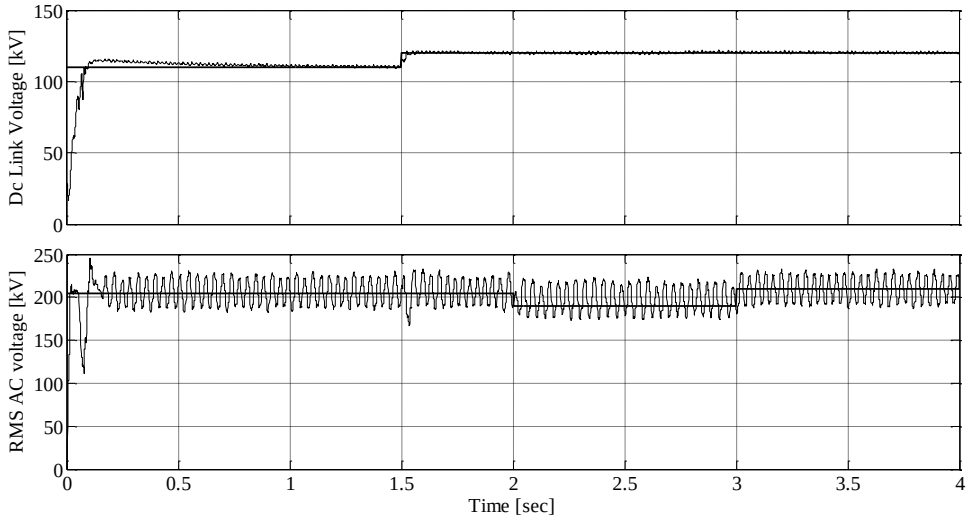

(a) Sending end controller

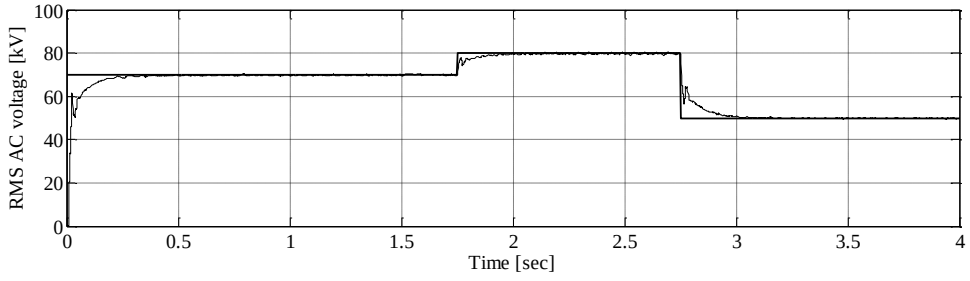

(b) Receiving end controller

Figure 4.8: VSC transmission system optimized performance

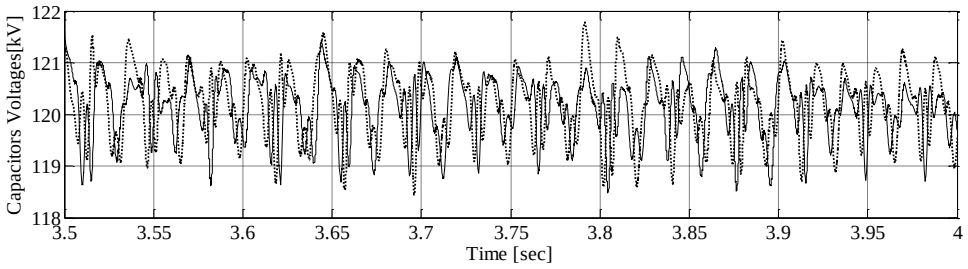

Figure 4.9: VSC transmission system optimized performance: Capacitor voltages

Table 4.2: Sending End gains values

		Gains	**Before Optimization**	**After Optimization**
Inner control loop	Direct axis	Proportional gain	5.6	67.298
		Integral gain	0.001	0.00037
	Quadrature axis	Proportional gain	10	1.63
		Integral gain	0.001	0.0075
Outer Control loop	AC Voltage	Proportional gain	0.1	0.701
		Integral gain	10	80.88
	DC link Voltage	Proportional gain	0.1	0.063
		Integral gain	10	8.548

Table 4.3: Receiving End gains values

		Gains	Before Optimization	After Optimization
Inner control loop	Direct axis	Proportional gain	224	394.15
		Integral gain	0.0035	0.023
Outer Control loop	AC Voltage	Proportional gain	0.01	0.016
		Integral gain	10	2.55

4.4.2 Hybrid control

This section represents the simulation results of the three level back to back VSC transmission system using hybrid control method at the receiving end in order to control the load ac voltage; while using hybrid control method at the sending end. Figure 4.10 and Figure 4.11 show the unoptimized and optimized performance of the VSC transmission system at both the sending and receiving end for different reference values. Table 4.4 and Table 4.5 show the effect of optimization on the gains values for both sending and receiving end, respectively. The simulation results show the beneficial effect of using optimization techniques in terms of improving the system overall response either in startup or steady case. This results in reducing system peak overshoot and reducing the controlled parameter settling time and steady state error.

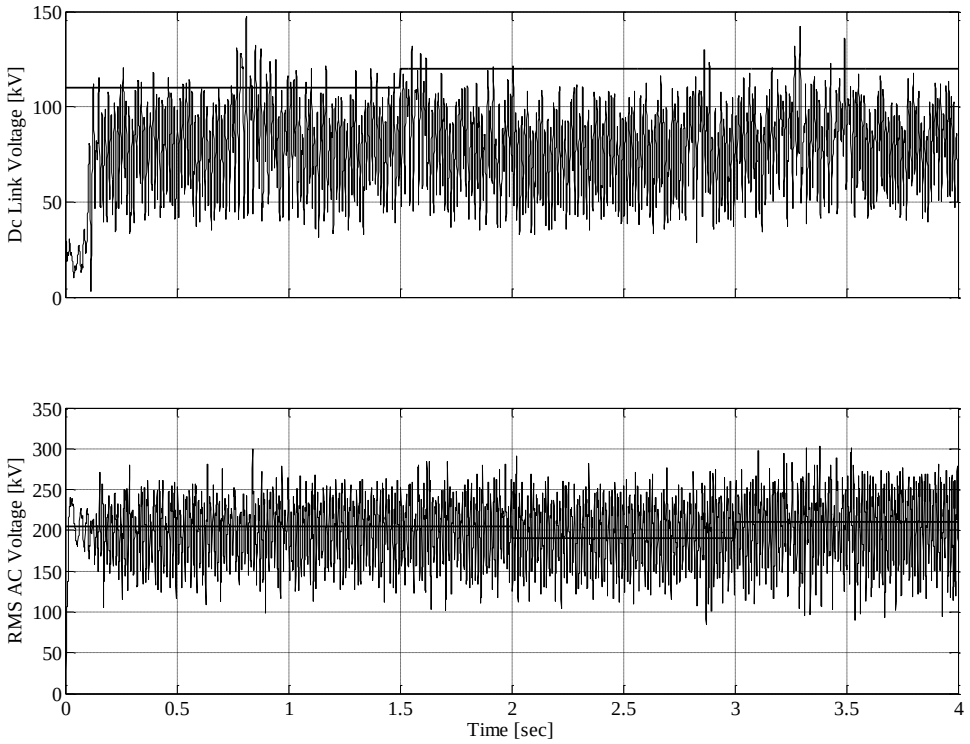

(a) Sending end controller

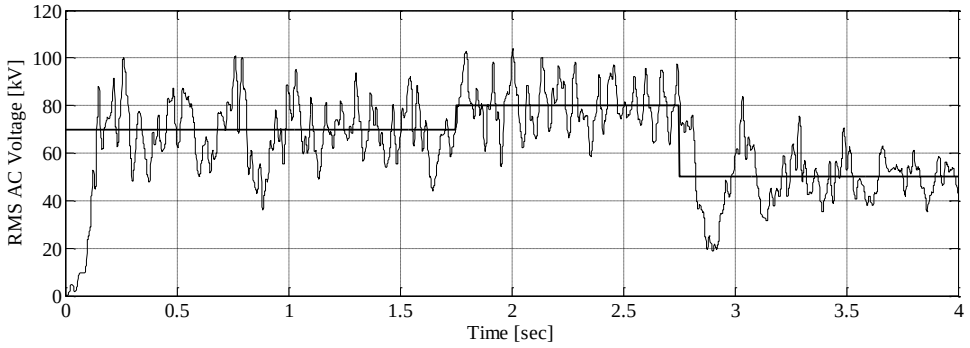

(b) Receiving end controller

Figure 4.10: VSC transmission system performance

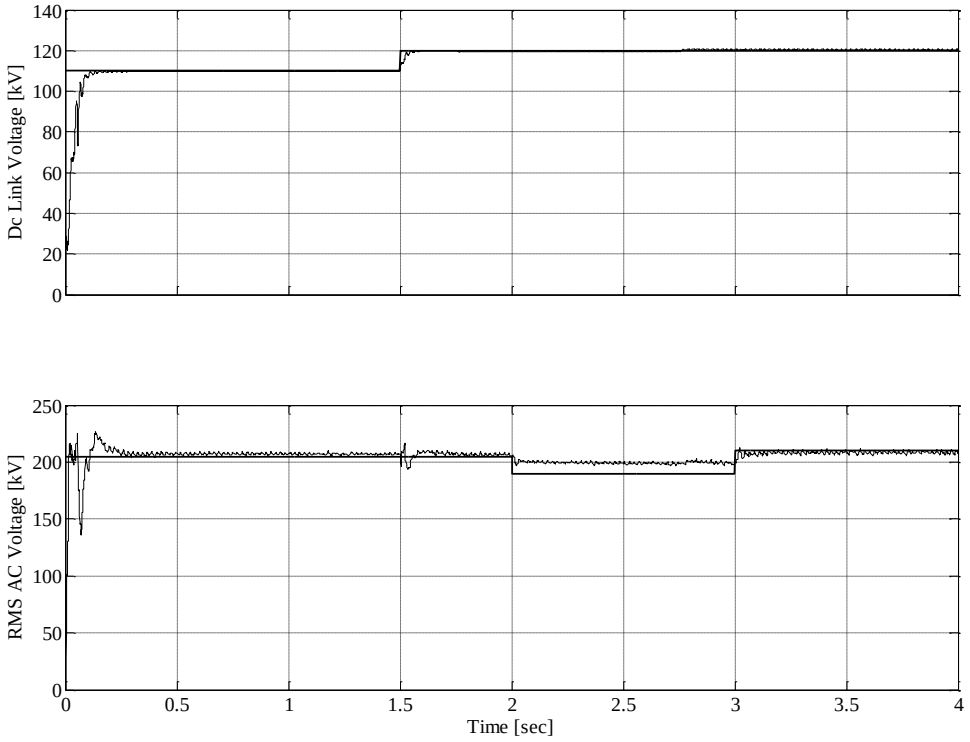

(a) Sending end controller

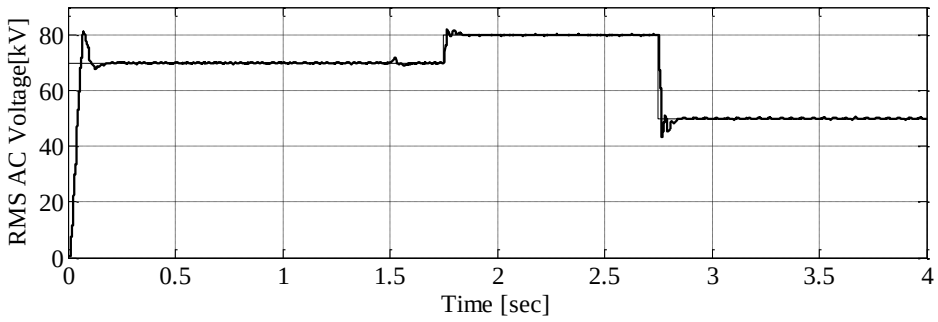

(b) Receiving end controller

Figure 4.11: VSC transmission system optimized performance

Table 4.4: Sending End gains values

		Gains	Before Optimization	After Optimization
Inner control loop	Direct axis	Proportional gain	5.6	102.73
		Integral gain	0.001	0.0141
	Quadrature axis	Proportional gain	10	5.731
		Integral gain	0.001	0.0002
Outer Control loop	AC Voltage	Proportional gain	0.1	0.021
		Integral gain	10	172.24
	DC link Voltage	Proportional gain	0.1	0.054
		Integral gain	10	55.91

Table 4.5: Receiving End gains values

		Gains	Before Optimization	After Optimization
Inner control loop	Direct axis	Proportional gain	1.3	0.35
		Integral gain	0.09	0.04
Outer Control loop	AC Voltage	Proportional gain	1.1	0.35
		Integral gain	0.07	0.04

4.5 Discussion of the Simulation Results

The simulation results of the back to back VSC transmission system supplying either an active or passive load using two and three level VSC topologies have been shown in the previous sections. From these results, the beneficial effect of using optimization techniques in terms of improving the system overall response either in startup or steady case is obvious. This advantageous effect results in reducing system peak overshoot and reducing the controlled parameter settling time and steady state error. The direct control method shows a noticeable acceptable response in terms of steady state response; however, during the transition between different controlled parameters values is accompanied by a perceptible overshoot in the same or the other end. This implies to both two level and three level topologies and either if the back to back system supplies a passive load or active network. This is mainly due to the coupling between the controlled parameter. The decoupled control method with its inherent decoupled current control loop offers a solution for the coupling issue raised up by the use of the direct control method. However, the decoupled control has a disadvantage related to time delay in the transformation between different coordinate systems in order to provide decoupling between the controlled parameters. Serious limitations in supplying power have been noticed in case of low ac system short circuit ratio, which will be the subject of deep analysis in the following chapter to accurately identify the reason behind this phenomenon.

In the passive load case, the hybrid control method, which is mainly a combination between direct and decoupled control, presents a moderate solution of the disadvantages between the previously mentioned control methods in terms of reducing the overshoot

and the time delay. The capacitor voltages, in the case of the three level VSC, has been maintained balance as it was shown in Figure 4.9 due to the introduce of capacitor voltage balancing control scheme described in the previous chapter.

4.6 Power Order Limitation and Simulation Time Step

The extensive simulation performed in the previous sections raises two important concerns. The first is the power order limitations of the VSC-HVDC transmission scheme. The second is the required level of details to be used in the electromagnetic transient simulation program and its reflection on the simulation time length. This section will demonstrate the above concerns in reflection to the previously shown simulation cases.

4.6.1 Power order limitation

The variation of the AC system strength becomes an important issue in determining the operating limit of the VSC-HVDC transmission scheme. Figure 4.12 shows the inability of the VSC-HVDC transmission scheme (modeled in section 4.2) to match an increase of real power order to 175MW in case of a receiving end SCR magnitude equal to 1.3. The optimization algorithm showed a negligible effect in the ability of increasing the power limits at lower value of SCR. This shows that the limited operating range is not due to the settings of the controllers and is a result of a more fundamental contributor pertaining to the system properties. The reasons behind this power limitation at lower SCR will be investigated in details in the next chapter.

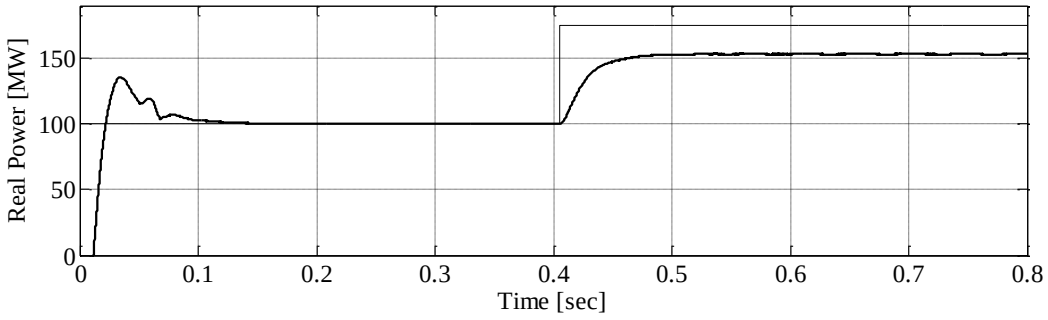

Figure 4.12: Variation of real power at SCR=1.8

4.6.2 Simulation length and time step

The previous simulation scenarios are performed using 5µsec simulation time step for a 4sec simulation run. This small time step for the passive load scenario results in an actual simulation time of 10.2min when using the decoupled control concept and 9.92min in case of hybrid control.

Figure 4.13 to Figure 4.17 represent the receiving end RMS ac voltage of Figure 4.11(b) at different time steps starting from 10µsec to 50µsec. It is noted that using larger time step affects the steady state and transient behaviour of the simulated scheme. It is also clear using a time step >20µsec leads to a further deterioration in the simulated system performance. However, the actual simulation time turns to be reduced significantly as shown in Table 4.6. This time consumption illustrates the need for a simplified model for the VSC as it is the main component for the VSC-HVDC transmission scheme in order to reduce both the complexity of the simulation case and the simulation time length especially in three-level VSC case. The simplified model presented in Chapter 6

introduces a compromise between the level of required details and the actual simulation time. The goal of development of a reduced order simulation model is to relieve the computational intensity of the simulations, while retaining adequate accuracy in the simulated results.

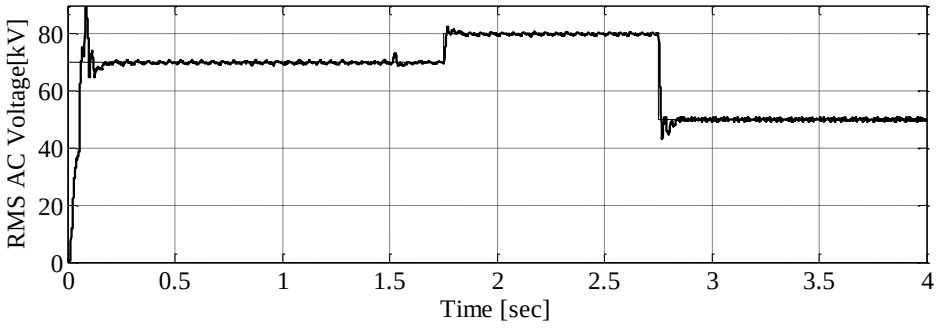

Figure 4.13: RMS ac voltage order change using time step=10µsec

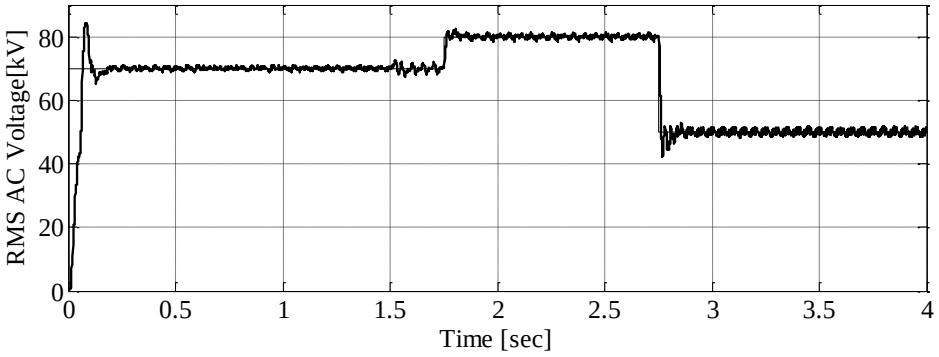

Figure 4.14: RMS ac voltage order change using time step=20µsec

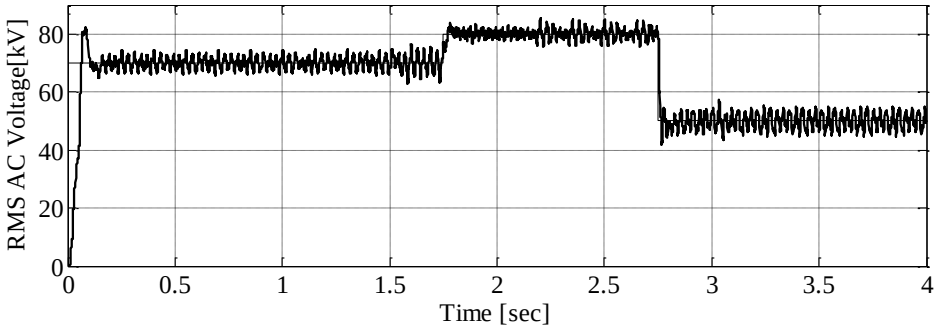

Figure 4.15: RMS ac voltage order change using time step=30µsec

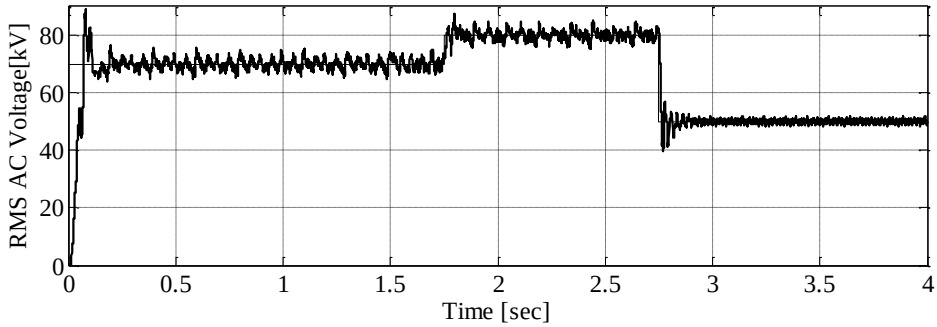

Figure 4.16: RMS ac voltage order change using time step=40µsec

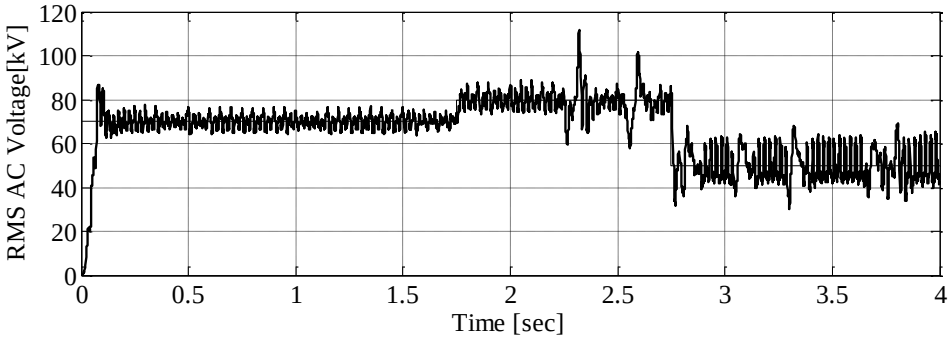

Figure 4.17 : RMS ac voltage order change using time step=50µsec

Table 4.6: Actual simulation time at different simulation time step

Simulation time step [µsec]	Simulation actual time [min]
5	9.92
10	4.38
20	3.1
30	2.41
40	2.18
50	1.48

4.7 Summary

This chapter presented a simulation case of a back to back VSC-HVDC transmission system under two different receiving ends (active and passive). Two and three level VSC topologies had been implemented in the simulation case. Evaluation of the performance of direct, decoupled and hybrid control methodologies was demonstrated. The simplex optimization concept to refine the controllers' gains was introduced. The challenges and limitations resulting from the simulation case were also presented and discussed.

Chapter 5: VSC-HVDC Operating Limits

5.1 Introduction

This chapter presents a phasor-based steady state model for a VSC-HVDC transmission scheme. The VSC is represented using a controlled voltage source whose magnitude and phase angle are determined by a control system using a phase-locked loop (PLL) that tracks the voltage at the point of common connection. The power transfer limits of the scheme under different ac network conditions is determined using mathematical analysis of the developed model and is then verified using a fully-detailed electromagnetic transient model. A parametric analysis is conducted to quantify the effect of the ac network strength and changes in transformer parameters on the power transmission and firing angle limits of the VSC-HVDC transmission scheme.

5.2 Equivalent Circuit of the VSC-HVDC System

An analytical phasor-based steady state model of the converter system is developed. It includes representations of the system strength and the phase-locked loop based firing control system. The developed model is validated using electromagnetic transient simulation.

5.2.1 Development of a Phasor-Based Equivalent Circuit

An ac equivalent circuit of one end of the VSC-HVDC system is shown in Figure 5.1. The terminating ac system is represented using a voltage source ($\mathbf{E}_s = E_s\angle 0$) and a Thevenin equivalent impedance of $\mathbf{Z} = Z\angle\beta$. The strength of terminating ac system depends on this impedance.

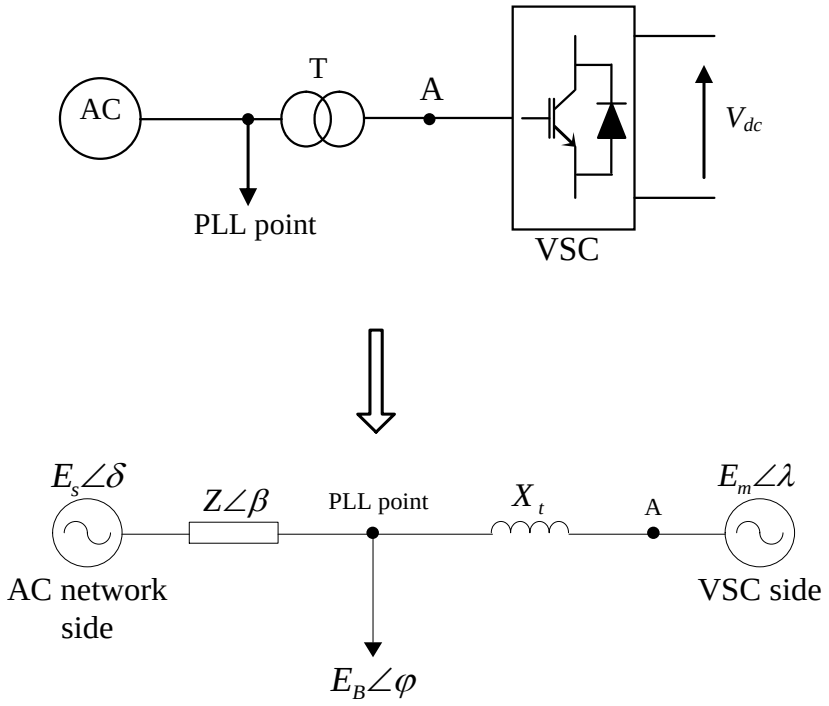

Figure 5.1:. Equivalent circuit of the ac side of the VSC transmission

The VSC is represented as a voltage-source with a fundamental frequency phasor ($\mathbf{E_m} = E_m\angle\lambda$). The amplitude and phase angle of this source are assumed to be controllable through high-frequency PWM switching within allowed limits. The transformer is modelled using its leakage inductance X_t. It is further assumed that a PLL

tracks the voltage at the point of common connection (PCC) and generates a corresponding phasor of the PCC voltage as $\mathbf{E_B} = E_B \angle \varphi$, which requires a model of the PLL to be developed as shown later.

The phase angle of the voltage at the PCC is the reference phase for the generation of suitably sequenced PWM firing pulses for the VSC. In other words, the phase angle of the fundamental component voltage crafted by the VSC, i.e. the angle λ, is generated by the converter control based on the knowledge of φ.

Although the output voltage of the converter is synthesised using the measurements done by the PLL at the point of common connection, the three voltages (E_s, E_m, E_B) shown in Figure 5.1 cannot assume any arbitrary value and are bound to satisfy the KVL and the KCL. A simple analysis of the single-line diagram of Figure 5.1 reveals that the magnitude and phase of the voltage at the PCC are related to those of the terminating ac system and the VSC as follows:

$$\mathbf{E_B} = \mathbf{E_S} - \left(\frac{\mathbf{E_S} - \mathbf{E_m}}{\mathbf{Z_T}} \right) \mathbf{Z} \tag{5.1}$$

where

$$\mathbf{Z_T} = \mathbf{Z} + jX_t = Z_T \angle \beta_T \tag{5.2}$$

This yields the following expression for the phase angle of the voltage at the PCC, i.e. φ.

$$\varphi = \tan^{-1} \left(\frac{A \sin\gamma + B \sin(\lambda + \alpha')}{A \cos\gamma + B \cos(\lambda + \alpha')} \right) \tag{5.3}$$

where $\mathbf{A} = A \angle \gamma = \mathbf{E_s} - \dfrac{\mathbf{E_s Z}}{\mathbf{Z_T}}$, $\mathbf{B} = B \angle \lambda + \alpha' = \dfrac{\mathbf{E_m Z}}{\mathbf{Z_T}}$ and $\alpha' = \beta - \beta_T$.

The angle φ is not readily accessible to the VSC control system; it is rather measured and tracked by a PLL. A simple model of a PLL consists of a proportional-integral (PI) controller to follow and lock onto the PCC phase angle. In steady state the PLL output will be identical to the phase-angle of the PCC voltage (φ). The ability of the PLL in tracking the phase angle during transients depends on its control settings and the severity of the distortion of the PCC voltage waveform. Other models of PLL and synchronization techniques are presented in [97-99].

The PLL is locked after the transformer, as shown in Figure 5.1(a), and generates a ramp signal locked in phase to the input voltage [98, 100]. Thus, for a properly operating PLL, the angle θ should closely track the phase angle φ of the VSC's ac busbar. The dynamically changing reference from a PLL therefore influences actual firings in control circuits and plays an important role in the dynamic performance of the system.

Figure 5.2 shows a schematic diagram of the developed phasor model of the VSC-based HVDC transmission system. As shown reference real and reactive power orders (P and Q) are used to generate reference values for the magnitude (E_m) and phase difference, also called firing angle (α) of the ac output voltage of the voltage-source converter. Note that the reference angle α is specified relative to the phase angle at the PCC. The controller that generates the VSC output voltage command based on the given real and reactive power commands may be chosen from any of the previously described control schemes, such as direct or decoupled controllers [1, 7, 64].

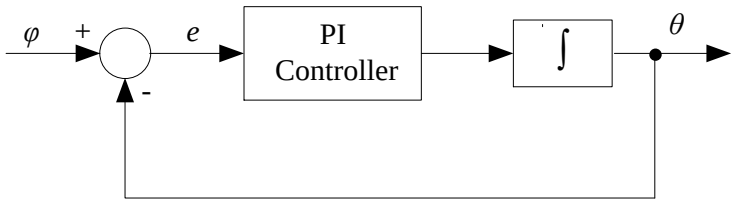

(a) PLL Model

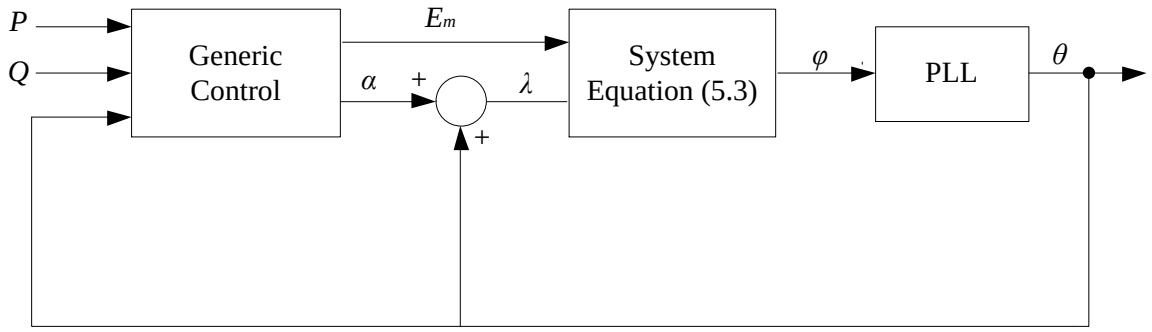

(b) Complete System Model

Figure 5.2:. PLL and complete system model

The VSC voltage generated by the control system is then used in the system equations block (see Figure 5.2) to generate the PCC angle φ based on (5.3). A PLL model is then used to dynamically track this angle and to produce a reference phase angle (θ) for the actual generation of the VSC output voltage.

5.2.2 Verification of the Phasor-Based Model

An electromagnetic transient simulation model of a VSC-HVDC system is developed (employing the PSCAD/EMTDC simulator), which models the VSC transmission system in full detail, including the semiconductor switches, the PLL and the detailed converter controls. This model is valid over a large frequency range that covers fundamental frequency behaviour, harmonics and switching transients, i.e., approx 0 to 10 kHz [101]. The accuracy of the simplified phasor-based model is then verified against this highly accurate transient model. The parameters of the network used in both models are shown in Table 5.1.

Table 5.1: System Parameters

Parameter	Value
E_s	1.01 pu
E_m	1.0 pu
X_t	15%
SCR	2.0

Figure 5.3(a) shows the variations of the resulting phase angles at the terminals of the VSC (λ) and the PCC (θ), by ordering a 7° change of the ordered α (from 0° to 7°). It is evident that both angles reach the 7° difference in steady state confirming the requested order. The PLL error signals (e in Figure 5.2(a)) obtained from the simplified phasor model and the fully detailed EMT model are shown in Figure 5.3(b). The two traces are essentially in complete agreement, except for the higher frequency switching related

ripple evident in the detailed model. The error tends to zero after a short period of transient oscillations. Any change in the ordered α will change the power flow through the line and will naturally affect the magnitude of the voltage at the PCC. Figure 5.3(c) shows the variations of this voltage for the ordered α obtained using the two models. Again, the results show essentially identical transient and steady state voltage dips. The above tests therefore provide confidence in the validity of the phasor model developed. This model is next used to determine limitations on the power transfer capability of VSC-HVDC systems.

5.3 Operating Limitations of the VSC-HVDC System

At first glance, it may seem that the phase angle α and modulation index of the VSC should be arbitrarily controllable. However, power balance considerations discussed in this section show that there is a limit imposed by the network impedance on the maximum possible value for α.

The following analysis is based on the premise that power flow between the converter and the PCC must equal the power flow between PCC and the terminating ac system plus any power loss.

5.3.1 Phase Angle Limits

Consider a simplified case where the transformer and the terminating ac system impedance are both represented using purely inductive elements of X_t and X, respectively.

The fundamental frequency real power transmitted between the VSC and the PCC (P_1) and between the PCC and the ac network (P_2) are given as follows (see Figure 5.1.b).

$$P_1 = \frac{E_m E_B}{X_T} \sin(\lambda - \varphi) = \frac{E_m E_B}{X_T} \sin(\alpha) \tag{5.4}$$

$$P_2 = \frac{E_B E_s}{X} \sin(\varphi) \tag{5.5}$$

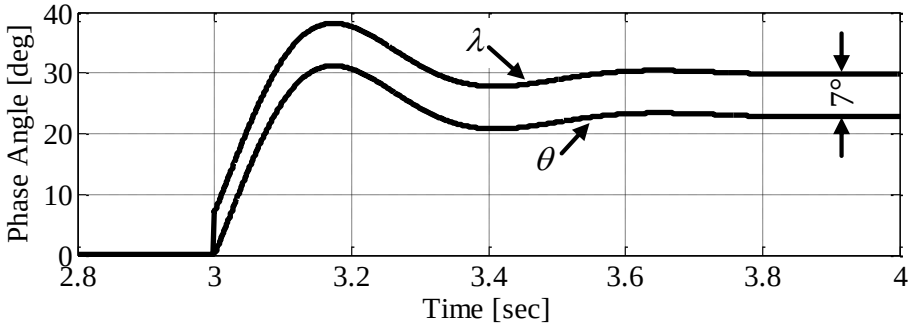

(a) Variation of the phase angles at the terminals of the VSC(λ) and the PCC(θ)

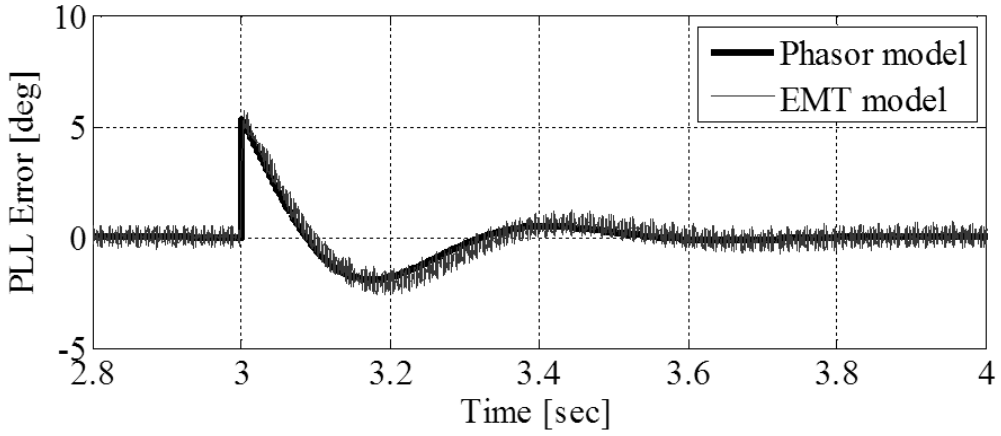

(b) PLL error

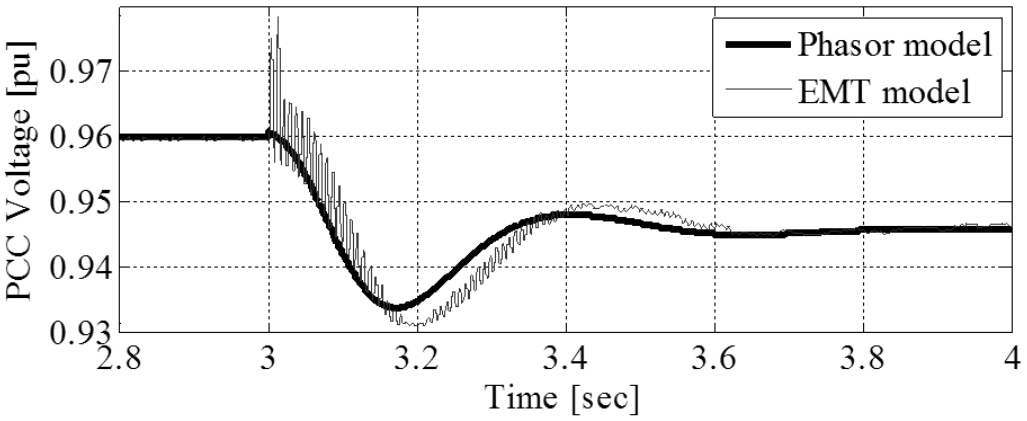

(c) Variation of the voltage magnitude at the PCC

Figure 5.3:. Verification of the phasor model

Power balance at the PCC requires that $P_1 = P_2$; therefore,

$$\frac{E_m E_B}{X_T}\sin(\alpha) = \frac{E_m E_B}{X}\sin(\varphi) \tag{5.6}$$

or

$$\sin(\alpha) = \frac{X_T}{X}\frac{E_s}{E_m}\sin(\varphi) \tag{5.7}$$

This expression can be used to determine the two boundary limitations on the relative phase shift of the VSC output voltage and the phase angle at the PCC, as follows. It should be noted that $\sin(\alpha)$ and $\sin(\varphi)$ must always be less than or equal to unity. This fact results in the following limits on the angles φ and α.

Case 1: If $\frac{X_T}{X}\frac{E_s}{E_n} < 1.0$ then equation (5.7) demands that:

$$\varphi_{\max} = \frac{\pi}{2} \text{ and hence } \alpha_{\max} = \sin^{-1}\left(\frac{X_T}{X}\frac{E_s}{E_m}\right) \tag{5.8}$$

Case 2: For $\frac{X_T}{X}\frac{E_s}{E_n}>1.0$:

$$\alpha_{\max}=\frac{\pi}{2} \text{ and hence } \varphi_{\max}=\sin^{-1}\left(\frac{X}{X_T}\frac{E_m}{E_s}\right) \tag{5.9}$$

These are operating limits on the possible angles and do not necessarily correspond to maximum power transfer limits, as will be shown later.

Given that in a normal power system, the voltages are typically close to 1.0 pu, the major determinant of α_{max} is the ratio of the transformer leakage reactance to the reactance of the ac network. Unless the ac network has an extremely high SCR (small X), the quantity $(X_T/X)\cdot(E_s/E_m)$ is less than unity and the limits in case 1 above apply.

For a more realistic case when the ac network impedance is represented as $\mathbf{Z}=Z\angle\beta$, the expression for the maximum phase shift α (as in (9)) will be as follows.

$$\varphi_{\max}=\frac{\pi}{2} \text{ and } \qquad \alpha_{\max}=\sin^{-1}\left(\frac{E_s X_T}{E_m Z}\right)-\beta+\beta_T \tag{5.10}$$

where β_T is given in (5.2) and is the phase angle of the total impedance ($\mathbf{Z}+jX_T$).

The limits imposed on the phase angles will affect and limit the real and reactive power transfer capability between the converter and the terminating ac system.

5.3.2 Simulation Results

Two models of a VSC-based transmission system are constructed. A strong ac system with a short-circuit ratio (SCR) of $5\angle75°$ and a relatively weak ac system with an SCR of $2\angle75°$ are considered. Table 5.2 shows the maximum firing angles possible derived using (5.10) above. A detailed transient model of each system is developed in the

PSCAD/EMTDC transient simulator and is used to validate the results obtained with the phasor-based model of the system as described above.

Table 5.2 : AC System Model Parameters

System type	System parameters	Max. phase shift (α)[1]
Weak system	SCR=2∠75° i.e., R=0.132 pu, X=0.493 pu	20.6°
Strong system	SCR=5∠75° i.e., R=0.053 pu, X=0.197 pu	54.3°

[1] using (5.10)

Figure 5.4 shows the dynamic response of the PCC voltage for step changes in the phase angle α for the strong ac termination. Figure 5.4(a) demonstrates the case where the new α order (of 50°) is just less than α_{max} (= 54.3°) and Figure 5.4(b) is for the case where the new α order (of 55°) is slightly larger than α_{max}. Figure 5.4(a) shows that requesting an α order less than α_{max} results in a stable operating point, whereas requesting $\alpha>\alpha_{max}$ results in an unstable operating point. This simulation supports the analytical results for α_{max} derived in equation (5.10); i.e., α_{max} is indeed the maximum possible firing angle.

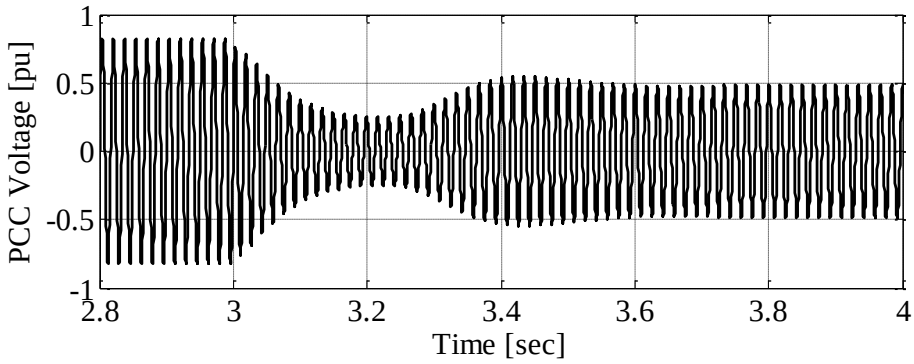

(a) Stable operation

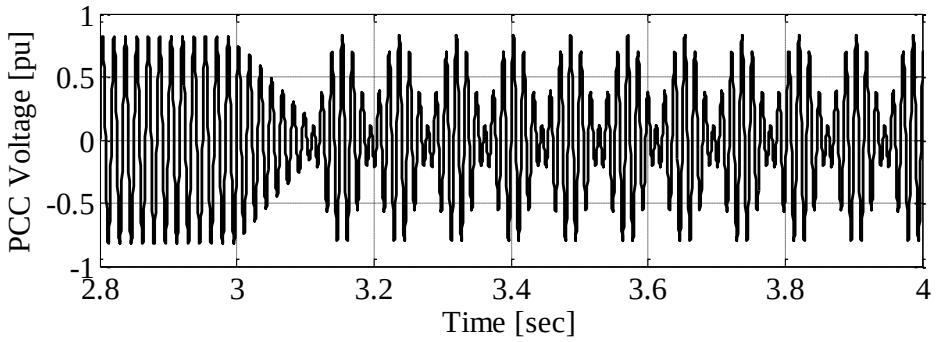

(b) Unstable operation

Figure 5.4: Dynamic response of the PCC voltage (SCR = 5.0)

In practice, most VSC-HVDC converters are controlled so as to keep the PCC at a constant voltage. For a constant PCC voltage of 1.0 pu, the angle λ (as shown in Figure 5.1) between the VSC output and the infinite bus is varied from 0° to 180°. The corresponding plots of the real power versus the firing angle α are obtained for the weak and strong systems and are shown in Figure 5.5(a) and Figure 5.5(b), respectively. The solid black segment corresponds to the range where PCC voltage control (regulated to 1.0 pu) is possible. However, due to the voltage rating of the VSC, its valve-side ac voltage E_m has a maximum limit. Once this limit is reached, operation switches to another control mode in which the PCC voltage is uncontrolled for the remaining range of λ which leads that the PCC voltage drops. The colored segments in the graphs of Figure 5.5(a) and Figure 5.5(b) are drawn for E_m limits ranging from 1.0 to 1.2 pu, and peel off from the power curve for constant PCC voltage. The figures show that the real power curves have a nose point at $\alpha=\alpha_{max}$. It appears that the same value of α gives two possible values of P, for example points A and B shown for the green curve for α=15°. These correspond to different values of λ. It will be shown later that the dotted portions of the P characteristics

after attainment of the nose point are non-feasible, as the operation is unstable with the PLL locked to the PCC voltage.

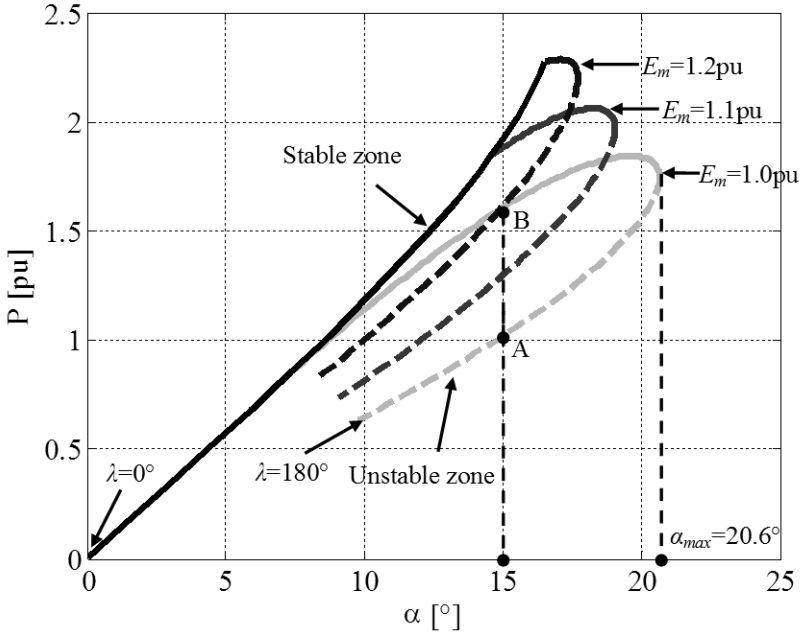

(a) Weak ac system

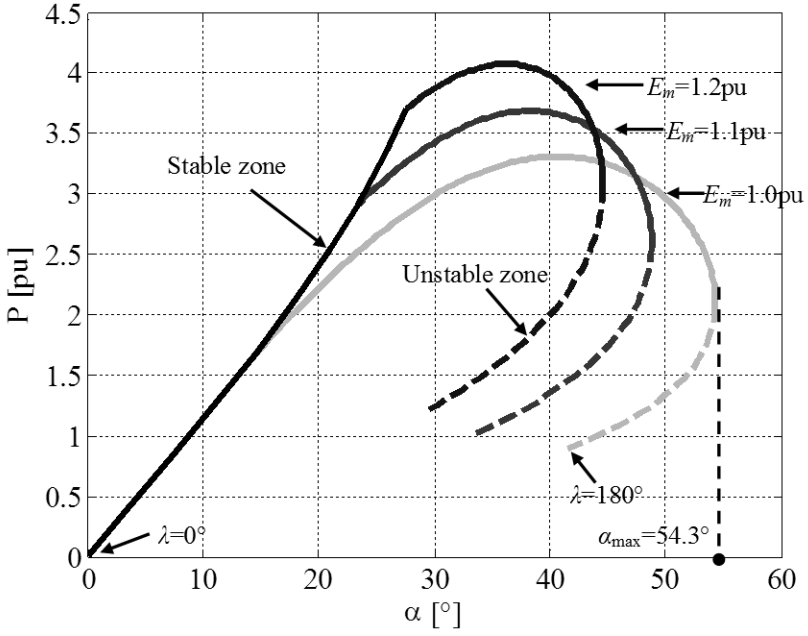

(b) Strong ac system

Figure 5.5: Real and reactive power performance

The variations of λ with α corresponding to the three E_m limits as in Figure 5.5(a) for the weak system are shown in Figure 5.6 (for the weak system). A test is performed to differentiate between the stable and unstable segments of the real power curves shown in Fig. 5(a), which also correspond to λ values to the left and right, respectively, of the peak in Figure 5.6. In the range t = [1,2) s, the system is forced to operate at point A. This is achieved by locking the PLL to the infinite bus (see Figure 5.1), and firing the IGBTs with the corresponding phase shift of λ=162° as indicated in Figure 5.6. This gives a value of firing angle α=15°, with respect to the PCC. It should be noted, that such operation is not realistic, as the PLL is usually locked to the PCC voltage waveform. The simulation is merely conducted to confirm the analytical solution for α and λ of Figure 5.6. For $t \geq 2$s, the PLL's point of phase locked is moved from the infinite bus to the PCC, as is the case in actual practice. A firing angle α=15° is ordered. If the λ=162° operating point (point A) were stable, the system would have remained in this condition, as α =15° is still the valid solution corresponding to operating point A. However, as shown in simulation results of Figure 5.7, the system immediately moves to operating point B, where from Figure 5.6, λ=71.4°. This supports the earlier statement that points such as A on the dotted sections of the *P*-α characteristic are unstable, and points such as B on the solid section are stable.

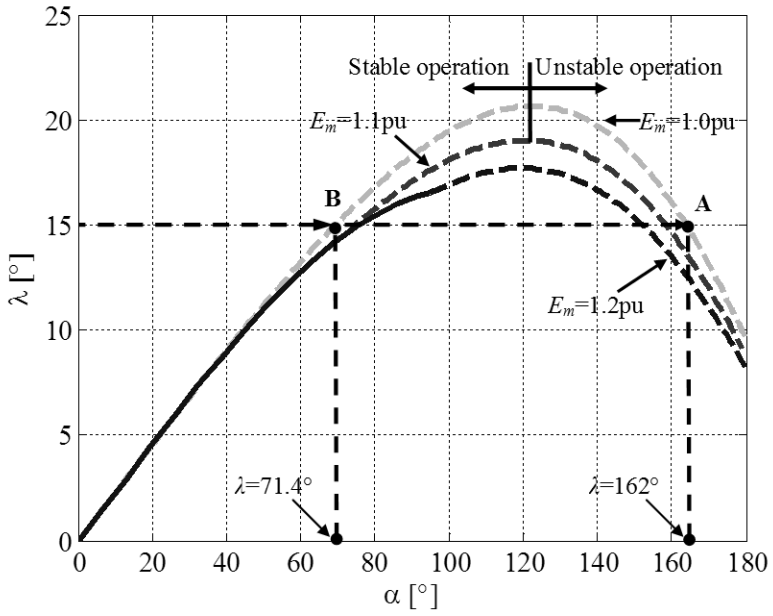

Figure 5.6: Variation of phase shift angle versus VSC voltage angle

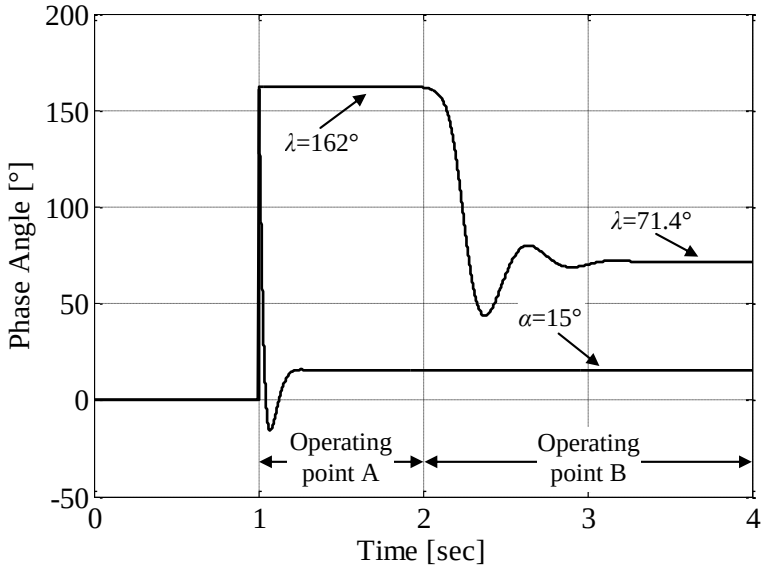

Figure 5.7: Phase angle variation

The corresponding plots of the reactive power versus the firing angle α are obtained for the weak and strong systems and are shown in Figure 5.8(a) and Figure 5.8(b), respectively. The curves follow a relatively similar trend to the real power curve in terms of nose point at α_{max} as well as stable and unstable portions of the curves.

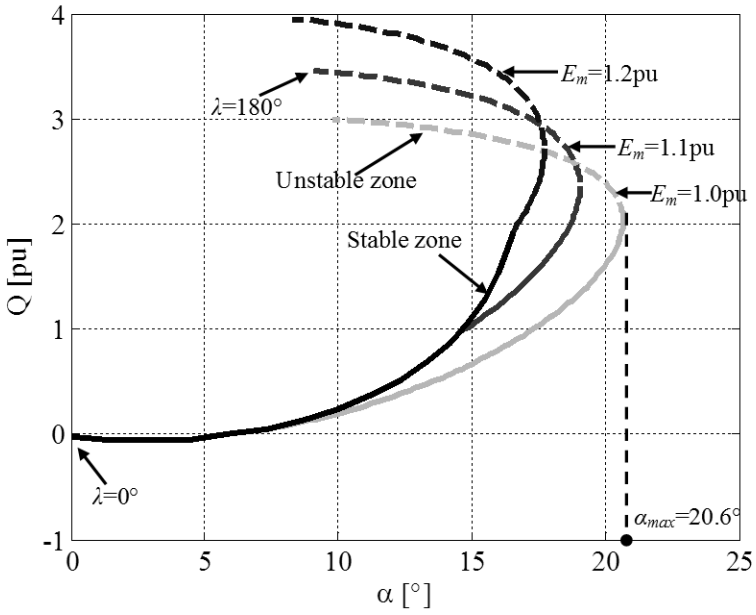

(a) Weak AC system

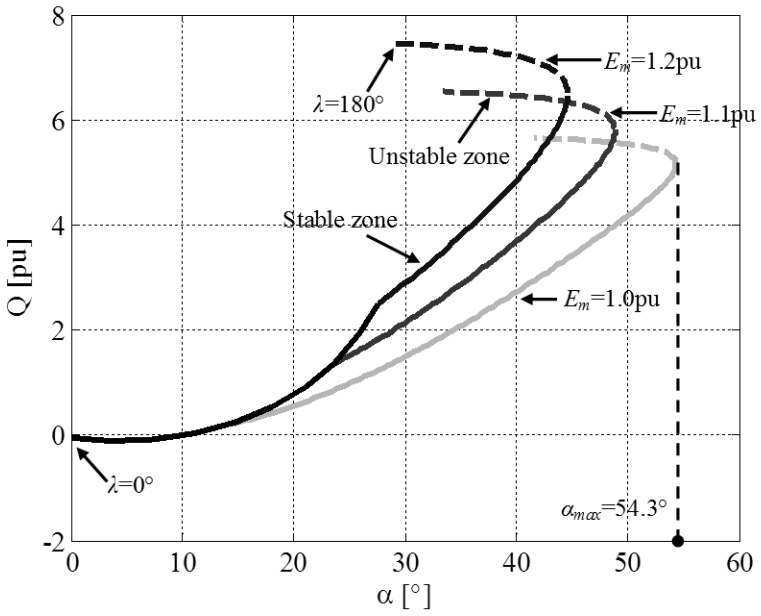

(b) Strong AC system

Figure 5.8: Real and reactive power performance

Figure 5.9(a) and Figure 5.9(b) investigate in depth the variation of the PCC voltage E_B versus λ. It is shown that for the strong system, E_B drops to a lower value (0.38pu) than the strong system case (0.73pu) in case of E_m=1.0pu reflecting a general behaviour for different E_m values. Moreover, E_B is kept controlled at a constant value for a larger range of λ in case of weak AC system before the voltage starts dropping down.

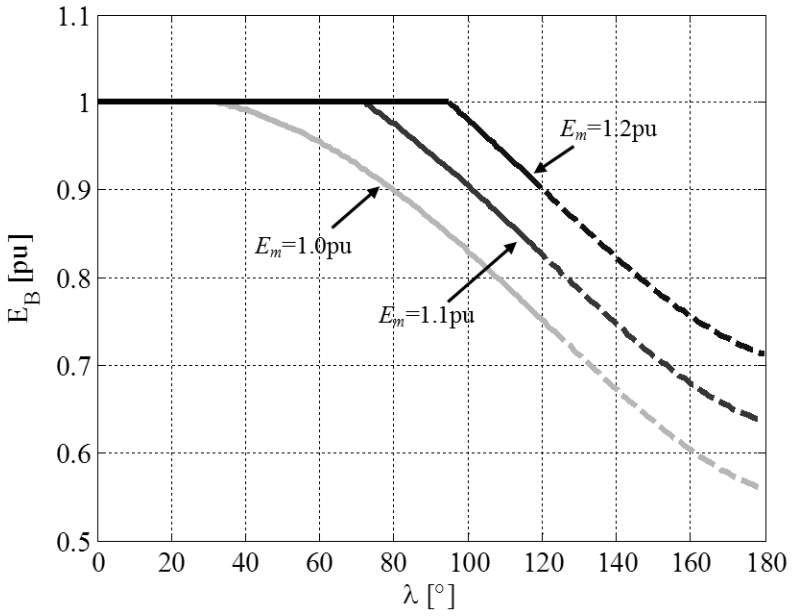

(a) Weak AC system

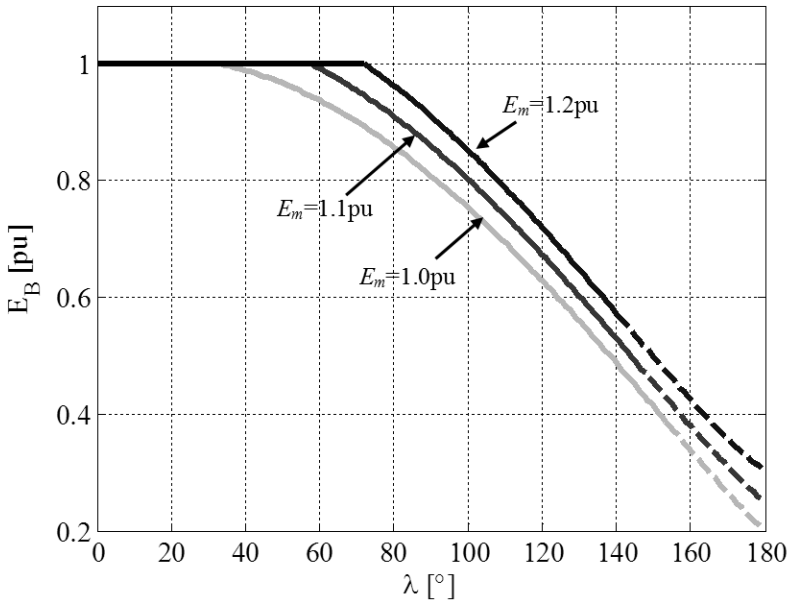

(b) Strong AC system

Figure 5.9: Real and reactive power performance.

5.4 Parametric Analysis of Operating Limits

The operating limits as previously shown are affected by the strength (SCR) of the terminating AC system and the leakage reactance of the VSC's converter transformer. This section discusses the variation of the firing angle limit α_{max} with respect to the magnitude and phase of the SCR and transformer leakage reactance. The limit on the maximum available power (MAP) out of the VSC is also examined.

In LCC-HVDC, the effective short circuit ratio (ESCR) normally characterizes the system strength, and includes the effect of the ac filters on the ac network's thevenin impedance [102]. However for VSC-HVDC, these are negligibly small, and hence the SCR is used in the parametric plots to follow.

5.4.1 Parametric Variation of Firing Angle and Power Transfer Limit with SCR

In this test, the system strength (SCR) is varied, and its impact on the maximum firing angle and the maximum power is investigated. Figure 5.10 shows the maximum phase shift angle α_{max} as a function of the short-circuit ratio of the terminating ac system. The graphs are plotted for three different values of network impedance angle β (see Fig. 1) ranging from 65° to 85°. It is seen that the maximum phase shift increases in step with the SCR.

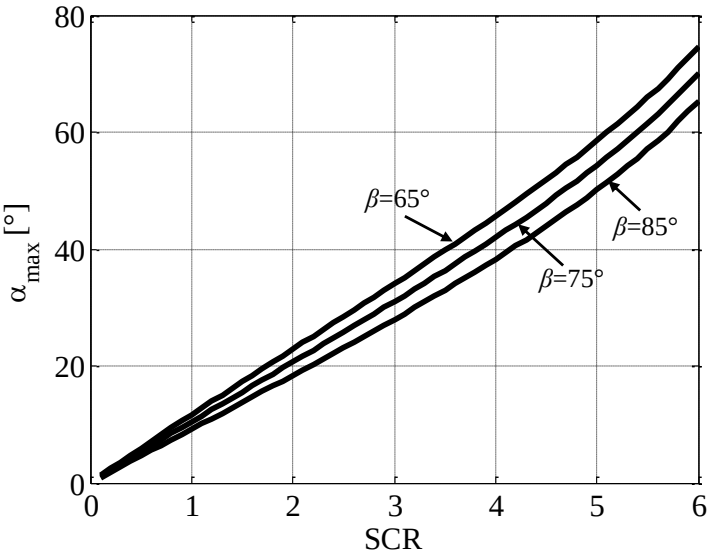

Figure 5.10: Variation of the α_{max} with the AC system strength

One of the important measures is the maximum power P_{max} that can be transmitted through the dc line. Figure 5.11 shows the variation of the maximum power limit P_{max} for different ac system strengths (i.e. different SCR values). The results show that the limit to the transferrable power increases as the system becomes stronger. This trend is similar to that for conventional LCC-HVDC [102], but the P_{max} for the VSC-HVDC is much larger than that for the LCC-HVDC at a given SCR value. Also, the lower practical limit on the SCR for LCC-HVDC systems is about 2.5 (effective short circuit ratio ESCR ~ 2) [102]. In comparison, the VSC-HVDC can operate with much lower SCR as seen in Figure 5.11.

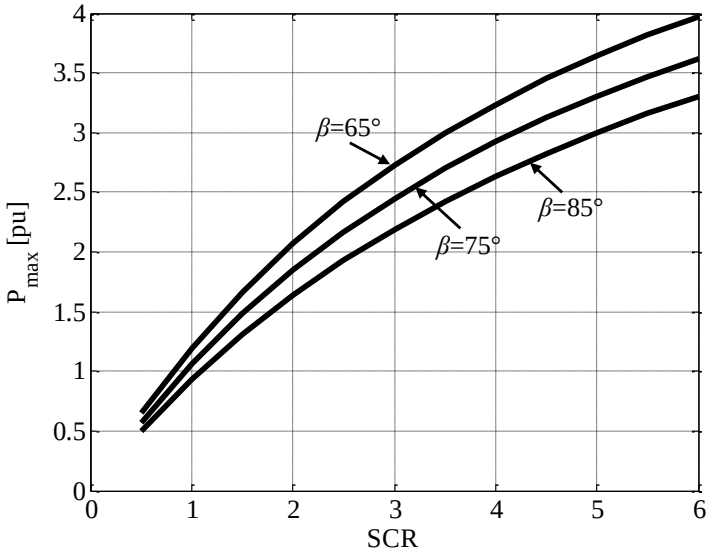

Figure 5.11: Maximum real power flow limits vs the AC system SCR

5.4.2 Sensitivity to Transformer Leakage Reactance

One of the design considerations for VSC-HVDC is the selection of the leakage impedance value for the converter transformer due to its essential role in ac output current control of the VSC [1]. The size of the impedance affects the scheme dynamic behaviour, the harmonic contents of the converter ac current as well as the limitations deduced from transient conditions analysis and fault scenarios [1]. This section investigates how the transformer impedance affects the operating limits of the VSC-HVDC.

The variations of the maximum firing angle (α_{max}) versus the transformer leakage reactance (X_t) for three SCR values of 1.0 (weak system), 3.0 and 5.0 (very strong system) are shown in Figure 5.12. The leakage reactance is varied between 11% and 19%. With SCR = 1.0 the sensitivity of α_{max} to changes in X_t is minimal. There is a higher

sensitivity for larger short-circuit ratios. This implies that stronger ac systems are more sensitive to the changes in X_t.

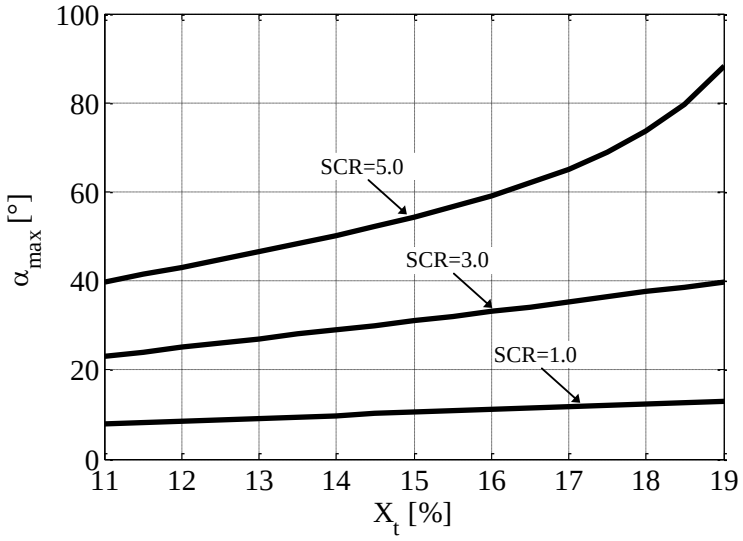

Figure 5.12: Variation of α_{max} vs. the transformer leakage inductance

The X_t value also affects the transferred maximum real power P_{max} through the line. Figure 5.13 shows P_{max} for different X_t values (from 11% to 19%). The maximum real power decreases with the increase of the value of X_t. Moreover, P_{max} tends to be more sensitive to the variations of X_t for stronger systems.

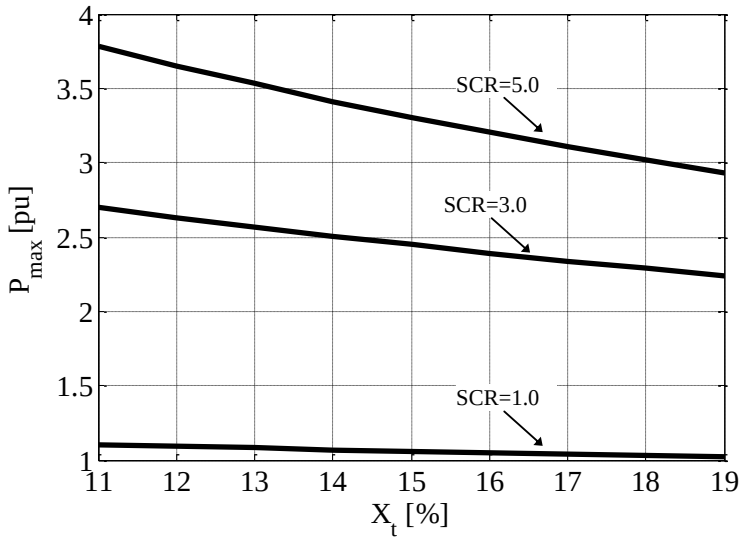

Figure 5.13: Maximum Real power flow limits vs the leakage transformer

5.5 Summary

This chapter analyzed the stable operating limits of VSC-HVDC transmission systems. A phasor based quasi-steady state of the converter system was proposed that includes representations of the system strength and the phase-locked loop based firing control system. The developed model was validated using electromagnetic transient simulation. The limits on the maximum available power were calculated using the developed model and the stable zone of operation is also specified, which took into consideration the maximum voltage rating of the VSC. Ultimately, the variation of SCR and transformer reactance was presented to specify their effects on the VSC-HVDC operating limits.

Chapter 6: VSC Modelling and Performance

6.1 Introduction

This chapter presents a proposed model for three level VSC used in back to back VSC-HVDC transmission scheme. The three level VSC is modelled using dependent current and voltage sources. The model presented herein has the ability to present the full spectrum as well as the fundamental voltage behaviour of the SPWM technique. Decoupled control strategy is implemented in the simulation model in order to control the VSC. Validation of the model is performed during steady state and transient operation conditions. Model behaviour under symmetrical and unsymmetrical fault conditions is also presented. The beneficial use of the model in terms of simulation time is demonstrated as well. Simulation results are obtained using an electromagnetic transient simulation program (PSCAD/EMTDC).

6.2 Modelling of the VSC

The modelling of the three level VSC is a challenging issue, as mentioned in Chapter 1. Due to factors such as power systems' expansion a larger presence of fast-acting controllers using VSCs, either in the form of VSC based HVDC transmission or in forms of FACTS devices, is expected. Simplicity as well as accuracy is expected from a VSC model in order to suitably represent them in studies where a large number of such devices

are used. However, a trade-off between both of them is required to be able to achieve the required accuracy with a non-complicated model.

The model developed herein for the three-level VSC relies on a dependent current source component in representing the VSC and a dependent voltage source to represent the voltage-synthesis behaviour of the VSC. The proposed model provides two important options, the first is to simulate the VSC in sinusoidal PWM control mode and the second is to simulate the fundamental component of the VSC voltage only. Both these models will feature substantially reduced simulation burden compared with the original model that employs models for the switching elements.

Figure 6.1 presents one end of the back to back system, which includes the AC source, converter transformer, VSC and the DC link capacitors. The VSC is modelled as the previously described three-level diode clamped converter shown in Figure 6.2. Figure 6.3 represents the proposed simplified model that replaces the VSC and relies on the dynamic average model methodology to represent the VSC [24-26, 28].

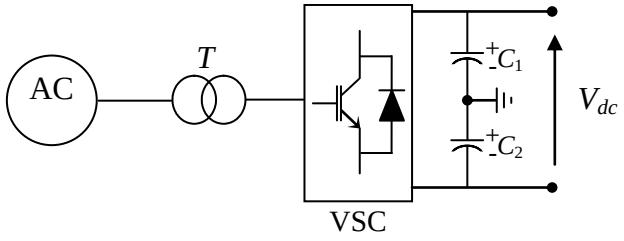

Figure 6.1: One end of the back to back system

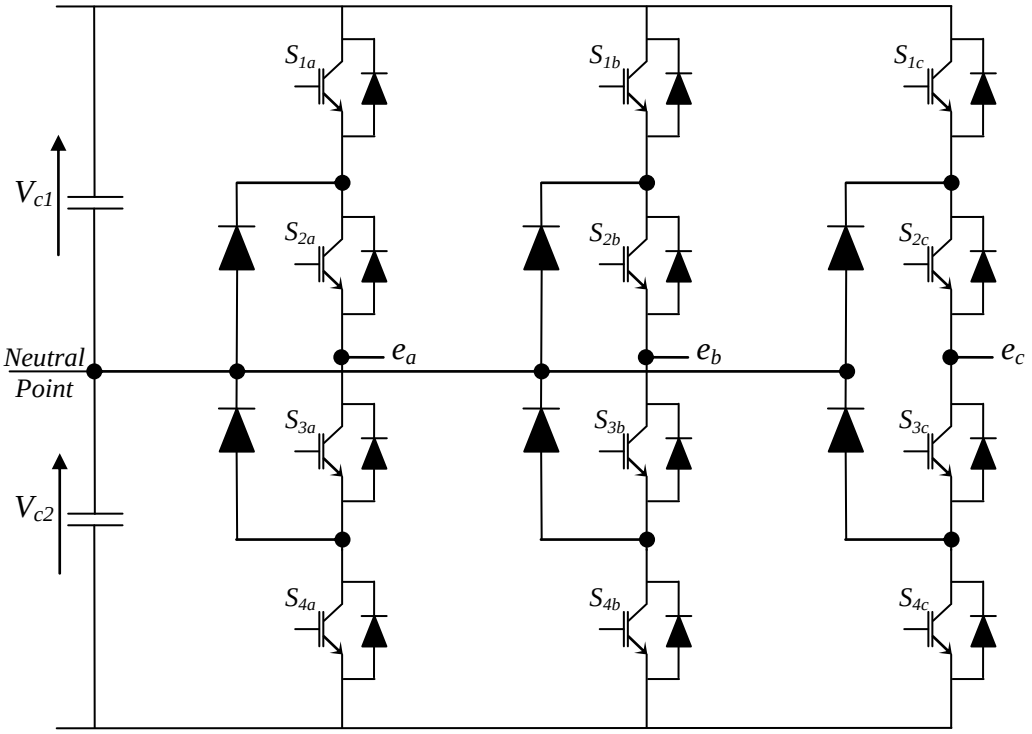

Figure 6.2: Three-level diode clamped converter

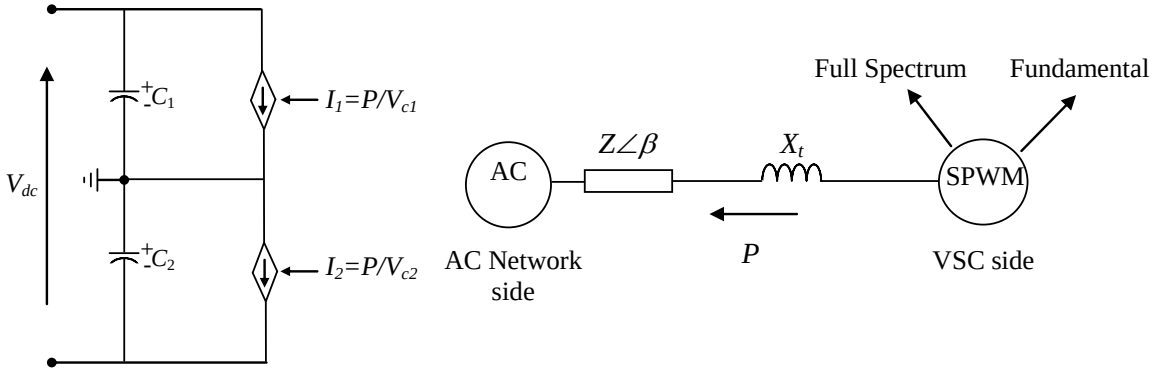

Figure 6.3: Model of the VSC

The sinusoidal PWM used to control the VSC is realised by comparing a high-frequency triangular carrier signal with a low frequency sinusoidal reference. The intersections of

the two signals determine the switching instants of the IGBT valves, as described in details in Chapter 3. During one period of the triangular carrier signal, the low frequency sinusoidal reference waveform can be assumed to have a nearly constant value**.** In the dynamic average modeling, the output waveform is represented only using its dynamic average value, which is calculated during each switching interval and varies depending on the local value of the reference waveform.

The VSC is modeled as controlled voltage source with magnitude of V_c on the ac side and a controlled current source with magnitude of I_{dc} on the dc side. The dynamic average value model uses three-phase dependent voltage sources with their average line to neutral values are expressed as follows [24, 25, 27, 103]

$$V_{ca} = \frac{1}{2} d_a V_{dc} \tag{6.1}$$

$$V_{cb} = \frac{1}{2} d_b V_{dc} \tag{6.2}$$

$$V_{cc} = \frac{1}{2} d_c V_{dc} \tag{6.3}$$

where V_{dc} is the dc link voltage; d_a, d_b and d_c are the modulation indices of each of the three phases. For the case of balanced three-phase systems, the modulation indices should have the same magnitude and be shifted by 120º. The values of the modulation indices are obtained from the decoupled control system and are calculated as follows.

$$d_a = m\cos(\omega t + \delta) \tag{6.4}$$

$$d_b = m\cos(\omega t + \delta - 120°) \tag{6.5}$$

$$d_c = m\cos(\omega t + \delta + 120°) \tag{6.6}$$

where m is the modulation index and δ is the phase shift angle of the VSC output voltage. Both m and δ represent the outputs of the decoupled control, as presented in Chapter 3.

An independent current source is used to model the VSC to account for the dynamic variations of the dc voltage caused by sudden changes in the requested power order. Then, neglecting the converter losses and using the power balance between the ac and dc sides of the VSC. The current source value is presented as:

$$I_1 = \frac{P}{V_c} \tag{6.7}$$

where P is the real power and V_c is the converter dc side capacitor voltage.

The dependent voltage source signal used in the model is a result of the voltage output of the SPWM signal based on comparison between the reference sinusoidal modulating waveform and the carrier signal. The fundamental component represent of this SPWM signal represent the control signal in case of using the second option of the proposed model. The current source control signal is a result of the real power transmitted between the AC source and the dependent voltage source and the DC link voltage.

The model is tested in the back to back VSC-HVDC system with specifications presented in Chapter 4. The AC system ESCR for both sending and receiving end is set at 2.0 representing a weak terminating AC terminal.

6.3 Model Validation

Validation of the model is done through two steps:

I. Validation for steady state and start-up performance

II. Validation in case of fault conditions

The validation is performed for the detailed circuit including all the switching versus the full spectrum of the SPWM voltage and versus a model that only considers the fundamental component of the VSC voltage.

6.3.1 Validation for steady state and start up performance

The VSC-HVDC back to back system shown in Figure 6.4 is used in the simulation case, the converter controller is decoupled control based methodology presented in Chapter 3. The simulation results presented herein are based on comparing the detailed VSC model including the valves switching with the proposed model (full spectrum and fundamental) at the receiving end where the real and reactive power are controlled. This is achieved through two operating conditions: starting performance and step response (change in system operating conditions).

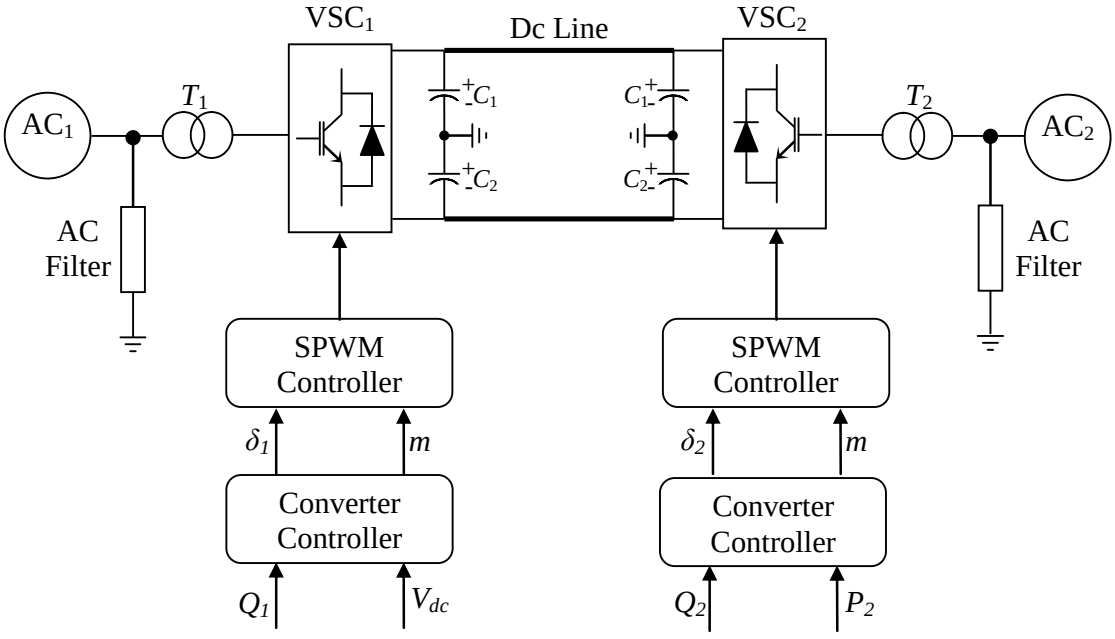

Figure 6.4: Block diagram of the implemented VSC transmission scheme

6.3.1.1 System start-up performance

In this section, the proposed model (full spectrum and fundamental) is validated against the detailed three level VSC for startup condition. The real power is set at 0.5pu and the reactive power is set at 0.3pu. Figure 6.5.(a) and Figure 6.5(b) present the real and reactive power during the startup condition. Figure 6.6 demonstrates the phase A current during steady state operation. It is noted that the SPWM based model including the full spectrum represents an accurate matching to the detailed three level VSC during the startup period. The fundamental based model shows an acceptable response assuming the level of simplicity inherent in that model. The high frequency oscillation that is joining the detailed model performances for both figures is a result of the high frequency switching of the VSC valves. The three models follow the pre-set reference value during the steady state operation.

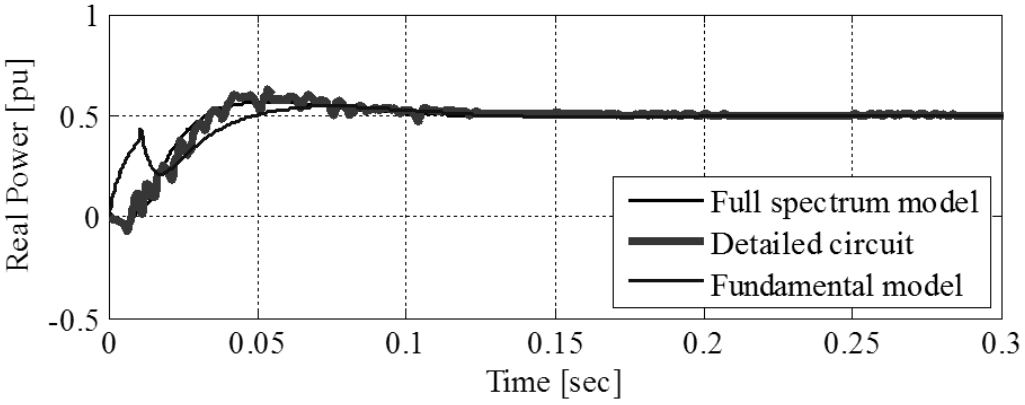

(a) Real power

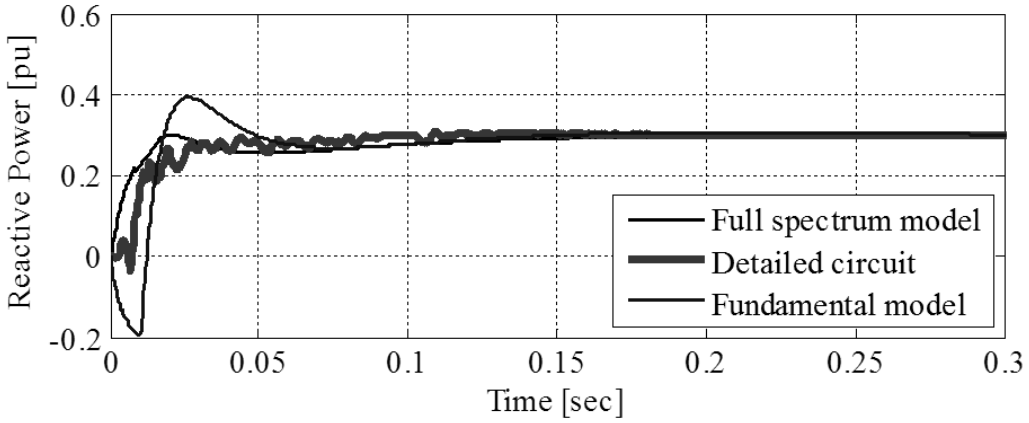

(b) Reactive power

Figure 6.5: System start up at P=0.5pu and Q=0.3pu

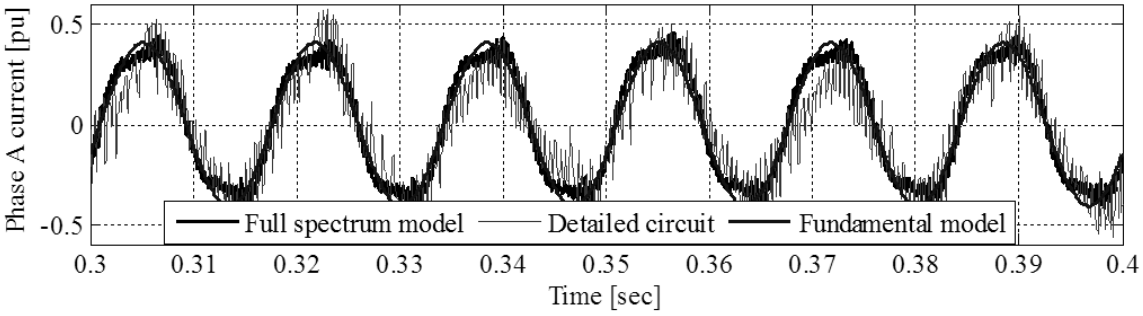

Figure 6.6: Phase A current during steady state operation

6.3.1.2 Decoupling and change in operating condition performance

The validity of the proposed model is tested in case of decoupling response at the system's receiving end while changing the real power order from 0.5pu to 0.8pu and keeping the reactive power order at 0.3pu, as shown in Figure 6.7. The real and reactive power responses show similarity in the three models response keeping in consideration the high frequency ripples in the detailed model due the switching of the valves.

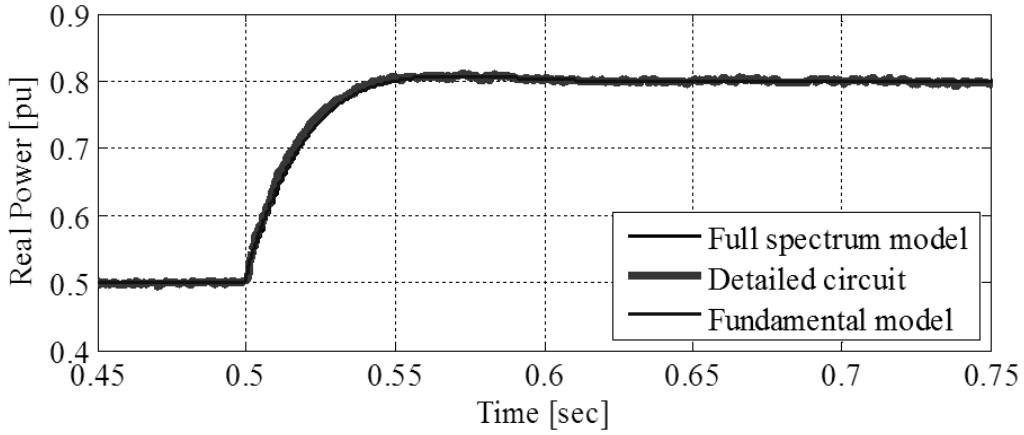

(a) **Real power**

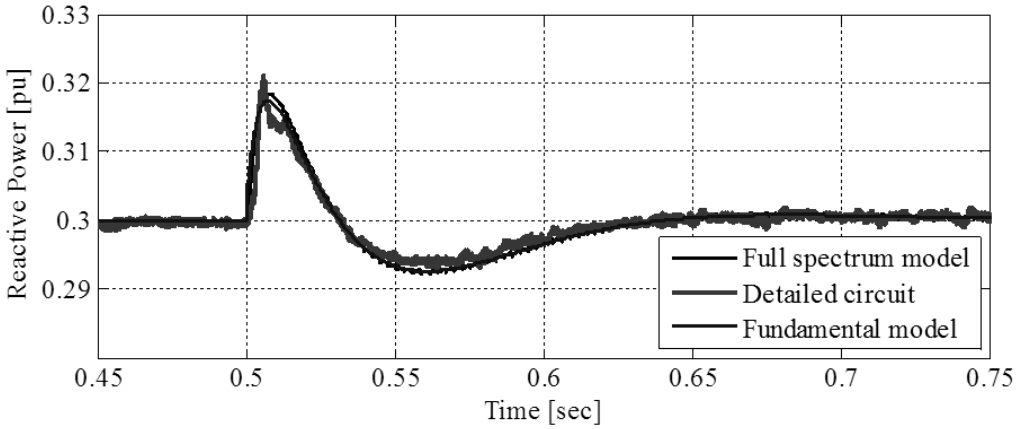

(b) Reactive power

Figure 6.7: Increase of real power order from 0.5pu to 0.8pu

6.3.2 Validation in case of fault conditions

The model's behaviour during symmetrical and asymmetrical fault conditions, both for the full spectrum and fundamental component based model, extends the validity of the proposed model to a more trustful level. Single phase to ground fault and three phases to ground fault are created on the AC source side of the converter transformer. The starting

conditions are implemented under a real power of 0.5 pu and reactive power order of 0.3pu. The faults are applied at 0.5sec for 0.05sec (3 cycles).

6.3.2.1 Single phase to ground fault

This scenario is used to simulate one of the most common faults in power systems, assuming that phase A of the AC voltage at receiving end is affected by a single phase to ground fault. During the fault (from 0.5sec to 0.55sec), the three models show similar response for real and reactive power as shown in Figure 6.8(a) and Figure 6.8(b) in terms of number of oscillations as well as magnitude of oscillations. When the fault is removed, the real and reactive power stabilizes within 0.1sec and 0.05 sec, respectively. The proposed models (full spectrum and fundamental) show a similar response to the detailed three-level VSC model in terms of magnitude of overshoot and the trend of response.

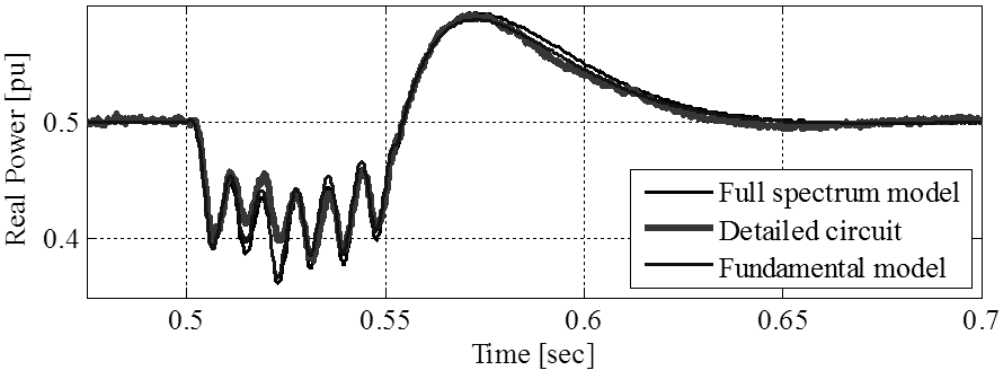

(a) Real power

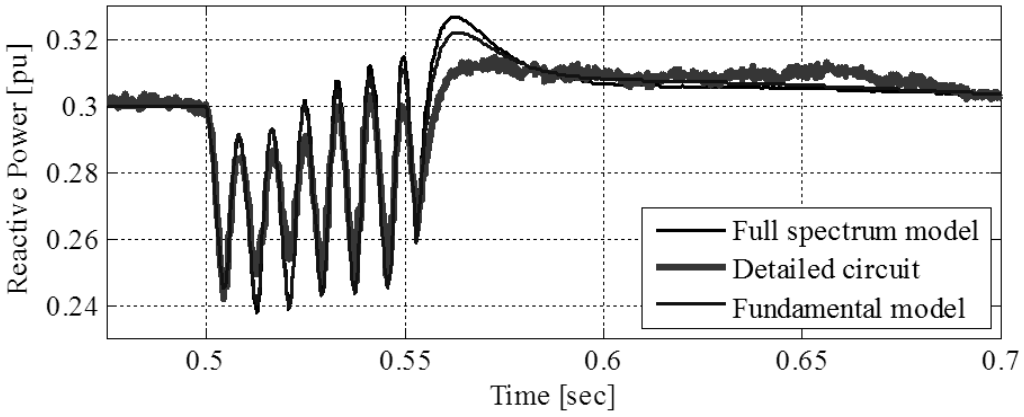

(b) Reactive power

Figure 6.8: Single phase to ground fault at phase A

6.3.2.2 Three phase to ground fault

This scenario is used to simulate a less common but severe fault in power systems, assuming that phases at receiving end are affected by a solid three phase to ground fault. During the fault (from 0.5sec to 0.55sec), the three models show identical response for real power and reactive power as shown in Figure 6.9(a) and Figure 6.9(b). The SPWM based model shows a slightly more accurate response in comparison to the fundamental based model in terms magnitude and trend of the response as shown in the figures. When the fault is removed, the real power and reactive power stabilize within 0.1sec and 0.15, respectively.

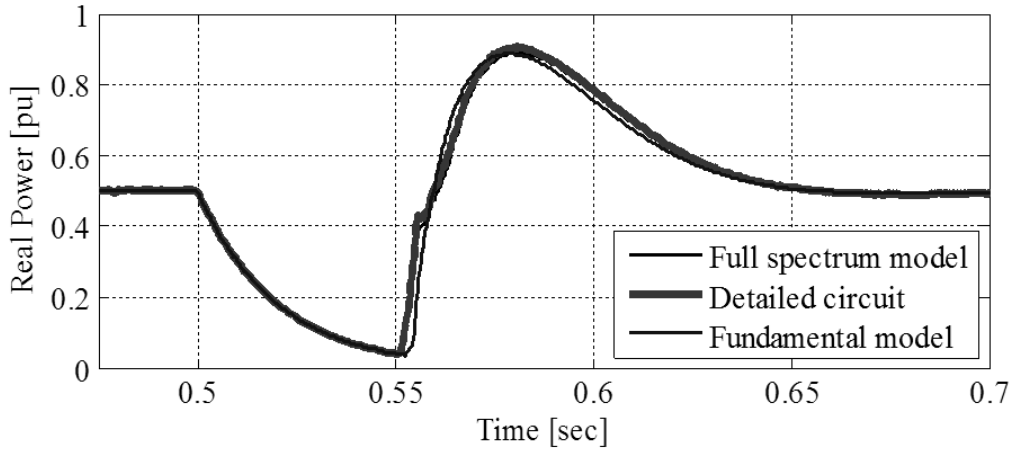

(a) Real power

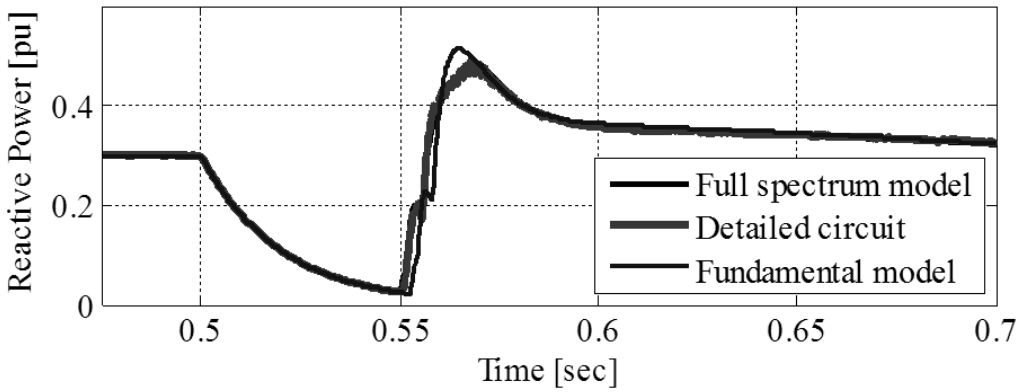

(b) Reactive power

Figure 6.9: Three phase to ground fault response

6.4 Speed of the Simulation

As it was mentioned earlier in the chapter both the accuracy and the simplicity are measures that define the effectiveness of any model. After demonstrating in the previous section the accuracy of the model in terms of steady state and fault response, this section will represent its computational simplicity by means of simulation time. In order to

achieve that objective both the full spectrum proposed model and the detailed three level VSC model are simulated for a duration of 1.0 sec under different solution time steps as shown in Figure 6.10. The solution time is reduced by 50% when the SPWM model is used and 54% when the fundamental model is used in case of solution time step of 5µsec. In case of larger time steps (40µsec and above), the solution time is reduced by around 60% when the SPWM model is used and 70% when the fundamental model. These results confirm the simplicity of the model not only in terms of circuit components but also from the simulation time point-of-view.

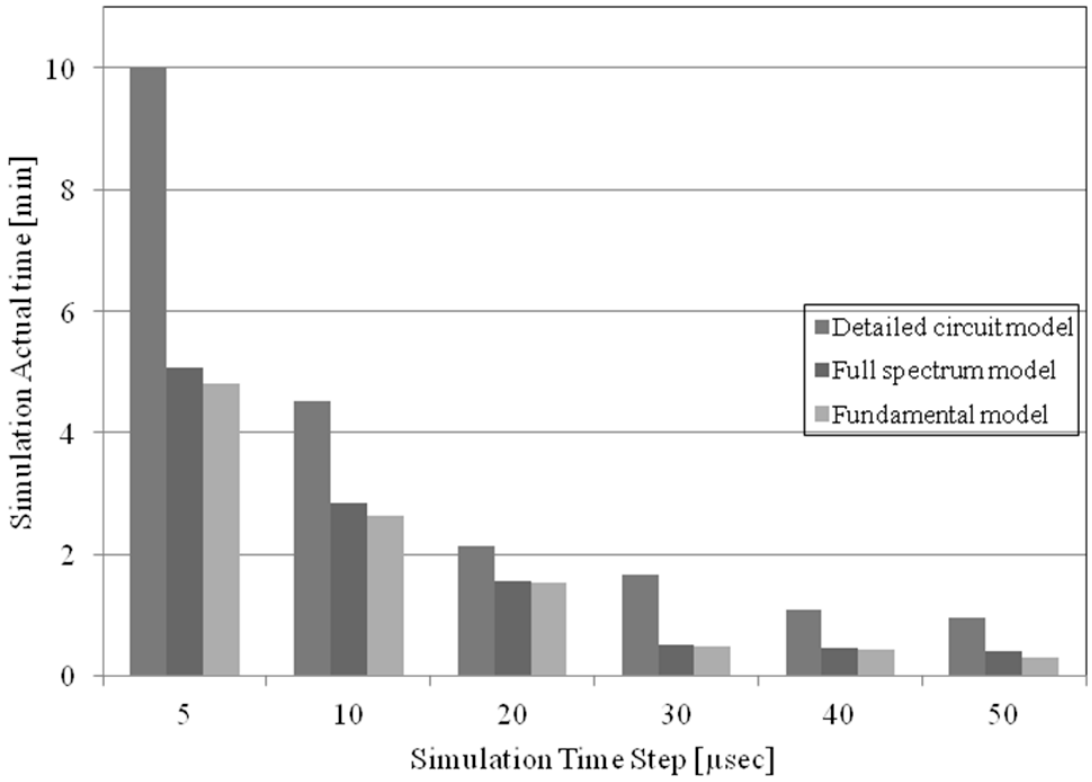

Figure 6.10: Comparison between the proposed model (full spectrum and fundamental) and the detailed circuit in terms of simulation speed

6.5 Summary

This chapter presented a model for the VSC based on the dynamic average model concept. The proposed model offered the possibility to generate the full spectrum and the fundamental behaviour of the VSC voltage. The model was validated against the detailed circuit model of the VSC using the PSCAD/EMTDC during steady state and fault conditions. The new feature resulting from the inclusion of SPWM harmonics in the average model leads to more accuracy in the dynamic behaviour of the system. The proposed model showed a significant reduction in term of simulation time and considerable matching in terms of dynamic performance.

Chapter 7: Conclusions and Future Work

7.1 Conclusions

This thesis was concerned with investigating and specifying stable operating limits of VSC-HVDC transmission systems; the development of a simplified VSC model based on dynamic average methodology was also proposed. An extensive simulation and analysis of a back to back VSC transmission system emphasizing on the control modes and the control topologies of such systems was also presented.

The main configurations of HVDC systems and the role of their building blocks have were presented and thoroughly discussed in the surveyed literature. The two-level and three-level diode-clamped VSCs with their associated PWM were implemented in two simulation cases, one supplying a passive load and the other supplying an active load.

In this thesis, simplified mathematical models and extensive effort on digital time domain simulation with PSCAD/EMTDC program was chosen as the means to address the various control modes available for VSC-HVDC transmission system in addition to the practical management between these control modes to take advantage of the two degrees of freedom offered at each end. Emphasis was focused upon control topologies and a comparison between direct and decoupled control was performed. The decoupled control technique showed greater superiority over the direct control from the point of view of current control. In the decoupled control, the current is limited to a value that is pre-

selected by the designer reflecting the rated current of the converter valves enabling an extra protection of the valves. A hybrid control method was implemented in case of passive receiving end with the intention of achieving the advantages of both direct and decoupled controls on one hand, and on the other hand reducing their drawbacks. Moreover, the simplex optimization was discussed and optimization procedure was also introduced for the back to back VSC transmission system.

The performance and simulation curves for active and passive systems were depicted. The decoupled control showed a superior performance, not only from the current control point of view, but also from the dynamic performance and steady state response approach over the direct control method. The proposed hybrid control, in case of passive load, showed adequate performance in both two level VSC and three level VSC. Moreover, optimization role was significant in adjusting and refining controllers' gains resulting in better steady state performance; leading to less overshoot and decrease of the settling time for various step changes of the controlled parameters.

The main contribution of the thesis is the ability to specify accurately the stable operating limits of VSC-HVDC under different SCR ratios that was presented in Chapter 5. The stable operating limits were deduced through mathematical analysis. The ratio of the transformer leakage reactance to the AC network reactance was shown to have a major impact on the operating limits of the VSC-HVDC system. A phasor based quasi-steady state model of the converter system that included representations of the system strength and the phase-locked loop based firing control system was initially developed to analyze

the operating limits. The model validation was performed using the electromagnetic transient simulation program PSCAD/EMTDC and showed accurate matching with the detailed model. The limits on the maximum available power were calculated, which took into account the maximum voltage rating of the VSC. It was found that the weaker the AC network strength, the smaller the maximum transferrable power. Also with the weaker the AC network, the maximum power limit is less sensitive to transformer leakage reactance variations.

The analysis showed that VSC-HVDC converters can operate into much weaker networks than is possible with LCC-HVDC. Also for a given SCR, the VSC-HVDC system has a significantly larger maximum available power in comparison with LCC-HVDC. Although the EMT simulations are carried out using a three level VSC converter, the results are generally applicable to any type of converter.

Another contribution was the inclusion of SPWM harmonics in the dynamic average-value model of the VSC presented in Chapter six. The proposed model was introduced in order to satisfy both the accuracy in dynamic performance as well as the reduction of the simulation time for the particular operating conditions. The developed model has the ability to generate both the fundamental component and full spectrum of the VSC voltage. Moreover, the inclusion of SPWM harmonics has proven to gives more accuracy to the dynamic behaviour of the system. A significant reduction in simulation time has been achieved. The proposed model' dynamic performance has been validated for both

steady state and fault conditions. The model validation showed good agreement between the proposed model and the actual detailed circuit representing the VSC.

7.2 Suggestions for Future Work

The work undertaken in this report paved the way for more thorough improvements in the performance and operating characteristics of VSC transmission systems. Several suggestions for future works may be proposed from this point to open the path for further research. These include:

- Using the proposed VSC model in the studies that are currently undertaken in Manitoba Hydro for Bipole III.
- Implementing a multiterminal DC transmission system (MTDC) using the proposed model of the VSC and studying the operating limits of the scheme.
- Modifying the proposed VSC model to be implemented for the modular multi-level VSC.
- Investigating waveform synthesis (pulse-width modulations) methods for lowering the switching rate of the converter valves while maintaining its improved harmonic spectrum: as one of the major drawbacks in VSC transmission systems that causes a limitation in its ratings is the switching losses. The research work can be directed towards assessment of various pulse-shaping methods to allow quantitative analysis of their relative merits.

Appendix A: AC Filter Design

This AC filter has been presented in Chapter 2 in terms of functionality and operation requirement. This appendix presents the mathematical modeling of the filter circuit and the filter performance and effect on the VSC-HVDC circuit.

A.1 Mathematical Modeling of the Filter Circuit

The modeled VSC system uses a SPWM with N=33. This number of pulses introduces the 31st and the 33rd harmonics and their multiples. In order to remove these harmonics a high pass filter with the circuit presented in Figure A.1, is designed with the following parameters:

- Cut off-frequency: 31×60 =1860Hz.
- Filter reactive power: Q_{fil} =10MVAR.
- Quality factor: Q = 10.

The following analysis describes the state space modelling of the AC filter circuit. The inductance is assumed to have an internal resistance of value R_F and an inductance of L_F. The filter capacitance has a value of C_F.

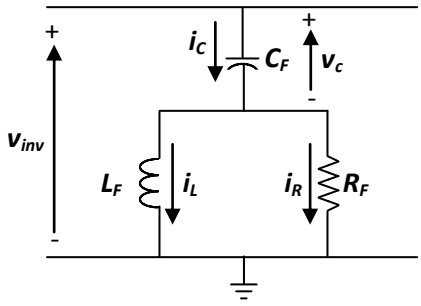

Figure A.1 High pass filter circuit

From Figure A.1 it can be can deduced that

$$v_{in} = L_F \frac{di_L}{dt} + v_c \tag{A.1}$$

Then,

$$\frac{di_L}{dt} = -\frac{1}{L_F} v_c + \frac{1}{L_F} v_{in} \tag{A.2}$$

And,

$$i_c = i_L + i_R = C_F \frac{dv_c}{dt} \tag{A.3}$$

$$i_c = i_L + \frac{(v_{in} - v_c)}{R} = C_F \frac{dv_c}{dt} \tag{A.4}$$

Then,

$$\frac{dv_c}{dt} = \frac{1}{C_F} i_L - \frac{1}{R_F C_F} v_c + \frac{1}{R_F C_F} v_{in} \tag{A.5}$$

Transforming to the matrix state equation,

$$\dot{\mathbf{x}} = \mathbf{A}\ \mathbf{x} + \mathbf{B}\ \mathbf{u} \tag{A.6}$$

$$\mathbf{y} = \mathbf{C}\ \mathbf{x} \tag{A.7}$$

Where,

$$\dot{\mathbf{x}} = \begin{bmatrix} \frac{di_L}{dt} & \frac{dv_c}{dt} \end{bmatrix}^T \tag{A.8}$$

$$\mathbf{x} = \begin{bmatrix} i_L & v_c \end{bmatrix}^T \tag{A.9}$$

$$\mathbf{u} = v_{inv} \tag{A.10}$$

$$y = i_c \tag{A.11}$$

$$\mathbf{A} = \begin{bmatrix} 0 & -\frac{1}{L_F} \\ \frac{1}{C_F} & -\frac{1}{R_F C_F} \end{bmatrix} \tag{A.12}$$

$$\mathbf{B} = \begin{bmatrix} \frac{1}{L_F} \\ \frac{1}{R_F C_F} \end{bmatrix} \tag{A.13}$$

$$\mathbf{C} = \begin{bmatrix} 1 & -\frac{1}{R_F} \end{bmatrix} \tag{A.14}$$

$$D = \begin{bmatrix} \frac{1}{R_F} \end{bmatrix} \tag{A.15}$$

The s-domain transfer function of the switch may be obtained from the following relation:

$$G(s) = C\left(sI - A\right)^{-1} B + D \tag{A.16}$$

Substituting from the above equations, it can be seen that the output to input transfer function in the s-domain is given by the equation:

$$G(s) = \frac{R_F L_F C_F s^2 + L_F s + R_F}{L_F C_F s^2 + R_F C_F s} \tag{A.17}$$

Then the filter electrical paramaters (R_F, L_F and C_F) can be calculated using the following equations:

$$C_F = \frac{Q_{fil}}{\omega V_{AC}{}^2} \quad \text{(A.18)}$$

$$L_F = \frac{1}{\omega_{cut-off}^2 c} \quad \text{(A.19)}$$

$$R_F = \frac{\omega_{cut-off} L}{Q} \quad \text{(A.20)}$$

Where $\omega_{cut\text{-}off}$ is the tuned or cut-off frequency and ω is the fundamental frequency.

A.2 Filter Performance in the Frequency Domain

In the frequency domain, the Bode Plot of the filter characteristics is presented in Figure A.2 for different values of reactive power and Figure A.3 represents the characteristics for different values of quality factor.

It can be seen that changing, either increasing or decreasing; the filter reactive power has no effect on the filter bandwidth. However decreasing the quality factor results in increasing the bandwidth for the same cut off frequency. On the other hand, increasing the filter reactive power results to a decrease in the filter impedance for the same cut off frequency.

A.3 Effect of Filter in AC Current Waveforms

Figure A.4 shows the harmonic voltage spectrum before and after applying the high pass filter. This in effect implies the smoothing of the waveform and the further reduction in

the THD content of the output voltage and hence current signals in order to enable their conformity to the standards.

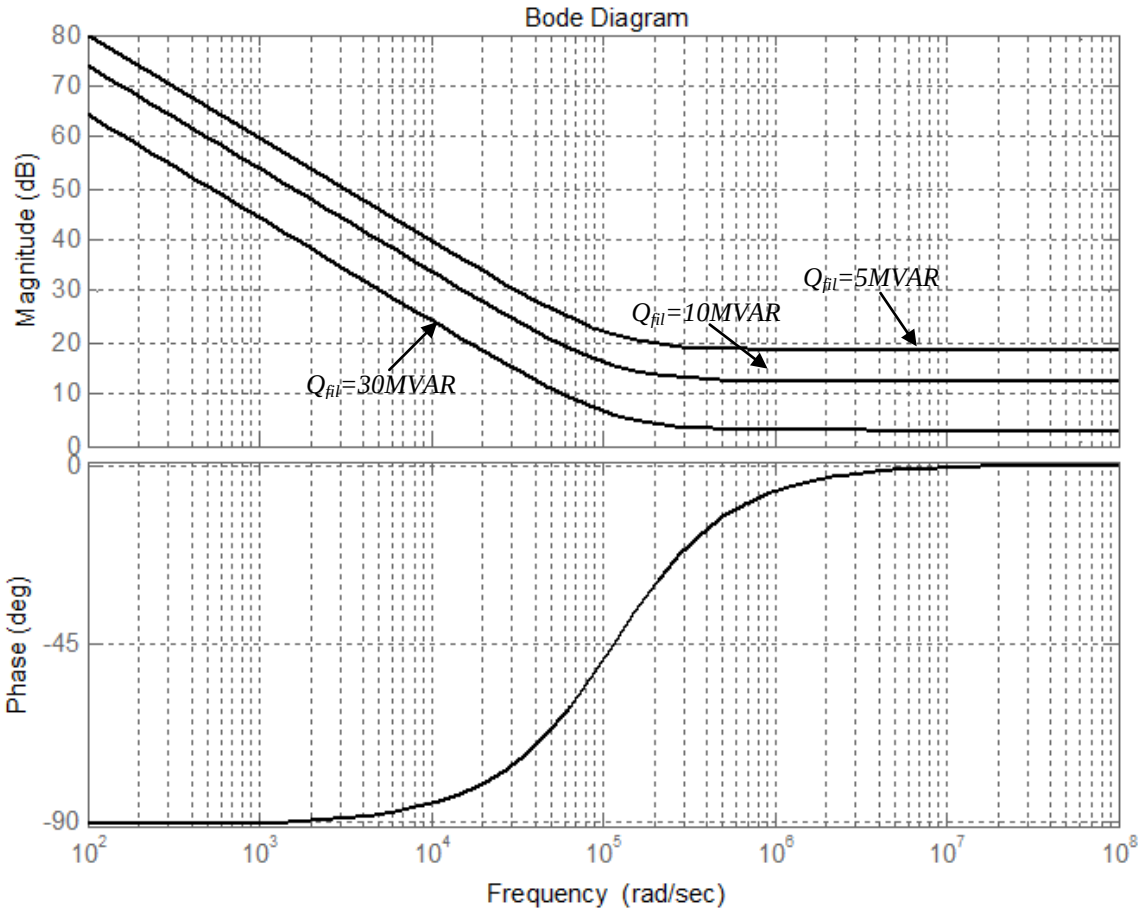

Figure A.2 Bode plot of the AC filter characteristics at different reactive power values

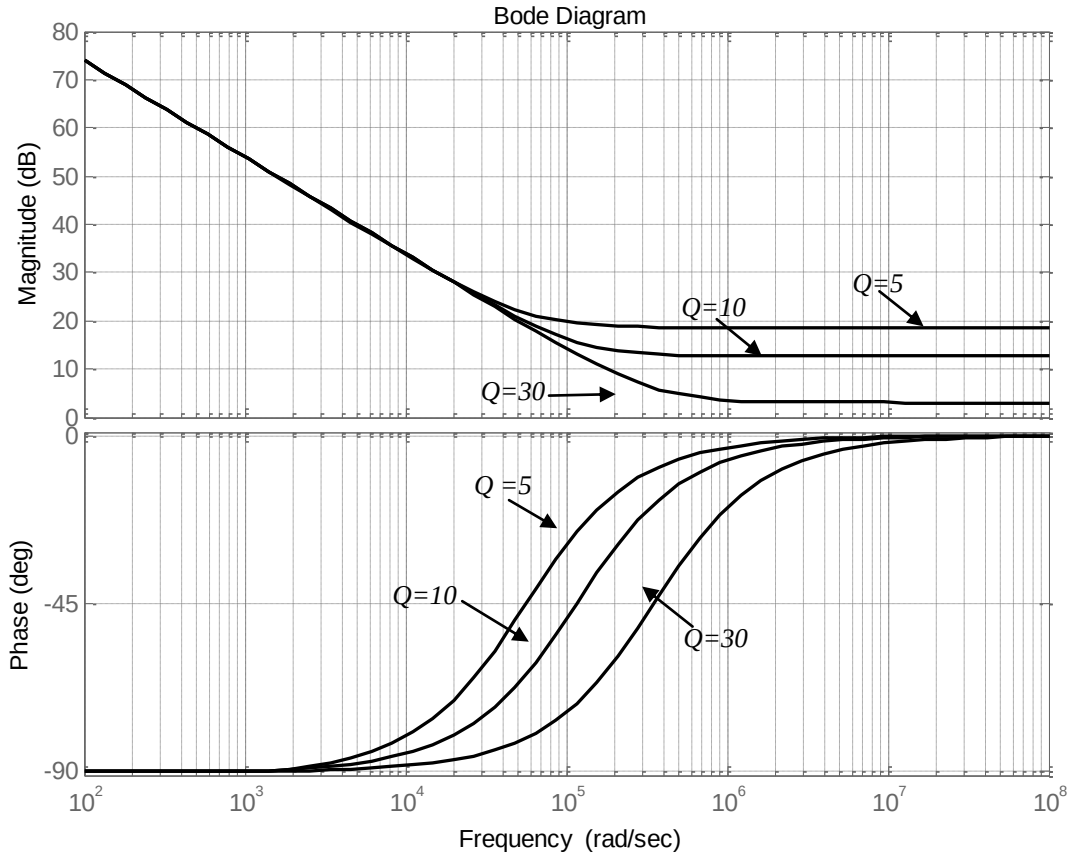

Figure A.3: Bode plot of the AC filter characteristics at different quality factor values

Figure A.4: Effect of filter on the harmonic current spectrum

Appendix B: Optimization Algorithm

The Optimization concept has been presented in Chapter 4 in terms of operation requirements. This appendix presents details about the optimization technique used as well as the algorithm implemented.

B.1 Simplex Optimization Method

The simplex optimization technique is chosen among various nonlinear optimization algorithms as it is considered as one of the fastest optimization technique in terms of reaching the optimal solution compared to other optimization techniques. Simplex method is one of the very robust direct optimization methods, that can be subdivided into two broad categories: methods using the first derivative information such as the conjugate gradient, variable metric methods and methods that do not rely on the computation of the first derivative, such as the direction-set and the simplex method [104]. This geometry-based method is due to Nelder & Mead [104], and is suitable for cases where the number of variables ranges from 10 to 20; which makes it a preferred choice for the VSC-HVDC transmission model presented herein. The main concept beyond the simplex optimization technique is based on the successive re-shaping and minimizing of a simplex object in n-dimensional space, where the simplex object is comprised of n+1 vertices for n dimensions [86, 105, 106]. For example a line segment on a line, a triangle on a plane, a tetrahedron in three-dimensional space and so forth.

B.2 Optimization Algorithm

The optimization algorithm implemented herein, starts with the design of the objective function which is considered as the most challenging step in the optimization procedure. The objective function design depends on the designer creativity and intention. The creativity part is present in designing a simple objective function to avoid the complexity in modeling and implementation. The intention or the objective side is defined by the designer such as minimizing the DC link capacitors voltage ripple magnitude, reducing current ripple, minimizing overshoot magnitude or reducing settling time.

After the proper design of the objective function, the optimization algorithm starts by an arbitrary point chosen by the designer and proceeds in a stepwise fashion towards the maxima or minima of the designated objective function by successive improvements, relying mainly on the history terms to calculate the next step. The simplex algorithm stops when the step towards the maxima or minima is smaller than a preset tolerance value determined by the designer. Otherwise, the simulation will start again with new values for the gains, as shown in Figure B.1.

For a VSC-HVDC transmission system, the operating point can change based on the network and users operating conditions i.e. change of direction and amount of power flow at different peak load hours. These result in modifying the values of the control signal specified by the control system; whether it is direct, decoupled or hybrid control. The optimum performance of the controlled parameters cannot be reached in this case. To overcome this problem, different operating conditions are specified for a single run of the optimization procedure with the intention of covering the expected range of changes of operating conditions. This solution leads to optimize the controlled parameters for

different operating conditions with a great advantage in avoiding running separate optimization procedures for each of the expected range of operating conditions and consequently saving time and resources.

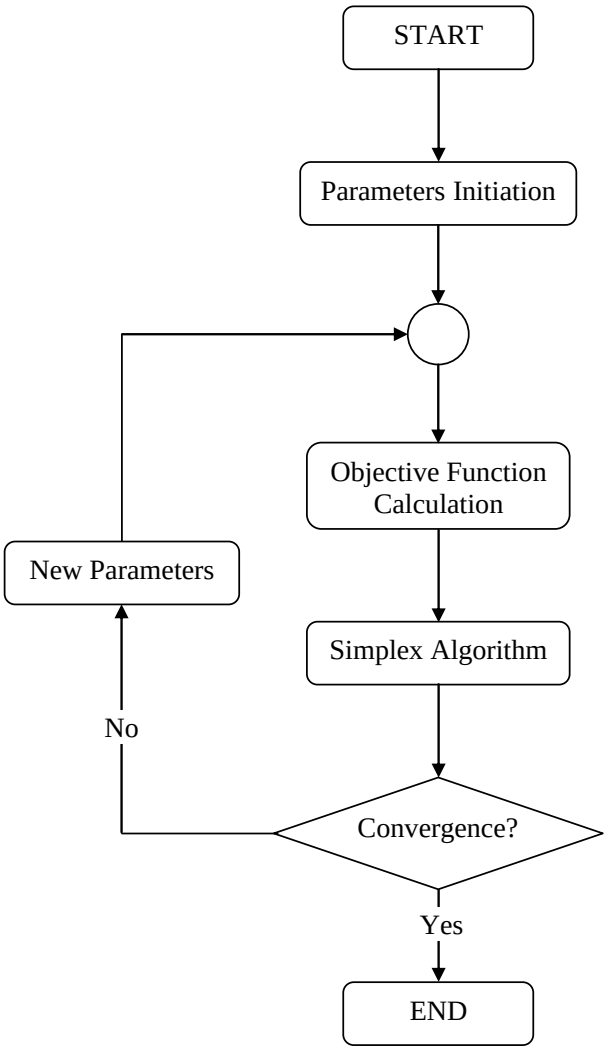

Figure B.1: Flow Chart of the Optimization Process

B.3 Optimization Procedures

Implementation of the simulation-based optimization involves (i) simulation of the network for a given set of controller parameters (as prescribed by the optimization algorithm), (ii) evaluation of the respective objective function(s) using the simulated waveforms, and (iii) generation of a new set of controller parameters (by the optimization algorithm) for use in the subsequent simulation. This cycle of interaction between the simulation platform (PSCAD/EMTDC in this case) and the optimization algorithm continues until a set of parameters is obtained for which the performance of the control system is in an acceptable conformity with the desired objectives. The optimization procedure of the back-to-back scheme and can be subdivided into two separate main steps:

Step 1: Optimization of the inner and outer loop controller gains.

Step 2: Optimization of the capacitor balancing gains in case of three level VSC.

Step 1:

This case consists of 16 PI-controller gains distributed equally between the sending and receiving end. The optimization is performed through two parallel procedures for both the sending and receiving ends control parameters. This step is demonstrated in more details in the following sections.

Step 2:

This case consists of two PI gains representing the capacitor voltages balancing controller gains; in case of three level VSC. The objective function used in this case:

$$O.F.=\int\left(\left(1-\frac{V_{c1}}{V_{cref}}\right)^2+\left(1-\frac{V_{c2}}{V_{cref}}\right)^2\right)dt \qquad \text{(B.1)}$$

The simulation results of the sending end converter are shown in Figure B.2. From these results, it is noticed that after using the optimization, the capacitor voltage ripples are within a lower band resulting in better performance of the overall system and increasing the voltage balance of the DC link capacitors.

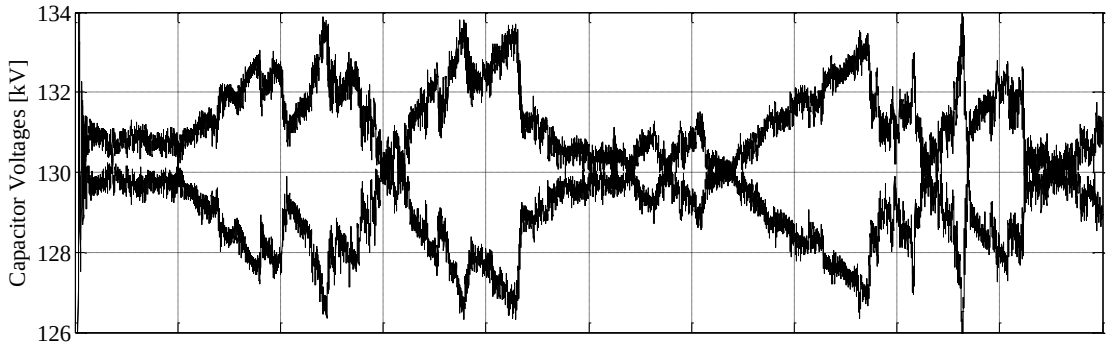

(a) Unoptimized gains

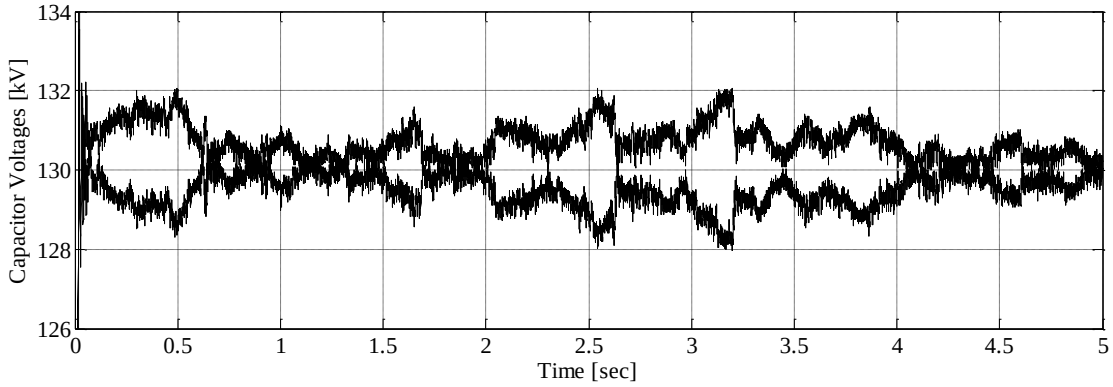

(b) Optimized gains

Figure B.2: Effect of gains optimization on the capacitor voltage balancing

References

[1] "VSC Transmission," CIGRE WG B4-37April 2005.

[2] D. A. Woodford, "HVDC Transmission," in *Manitoba HVDC Research Center*, ed, March 1998.

[3] K. Meah and S. Ula, "Comparative Evaluation of HVDC and HVAC Transmission Systems," in *IEEE Power Engineering Society General Meeting*, 2007, pp. 1-5.

[4] J. Setreus and L. Bertling, "Introduction to HVDC Technology for Reliable Electrical Power Systems," in *Proceedings of the 10th International Conference on Probabilistic Methods Applied to Power Systems (PMAPS)*, 2008, pp. 1-8.

[5] W. Long and S. Nilsson, "HVDC transmission: yesterday and today," *IEEE Power and Energy Magazine*, vol. 5, pp. 22-31, 2007.

[6] B. R. Andersen, L. Xu, P. J. Horton, and P. Cartwright, "Topologies for VSC transmission," *IEE Power Engineering Journal*, vol. 16, pp. 142-150, 2002.

[7] F. Schettler, H. Huang, and N. Christl, "HVDC transmission systems using voltage sourced converters design and applications," in *IEEE Power Engineering Society Summer Meeting*, 2000, pp. 715-720 vol. 2.

[8] K. Eriksson, "Operational experience of HVDC Light," in *Seventh International Conference on AC-DC Power Transmission(Conf. Publ. No. 485)*, 2001, pp. 205-210.

[9] N. S. Dhaliwal, L. D. Recksiedler, and D. T. Y. Tang, "Operating experiences of the Nelson River HVDC system," in *Proceedings IEEE Transmission and Distribution Conference*, 1996, pp. 174-180.

[10] R. A. Valiquette, "HVDC life extension for Nelson River HVDC system," in *IEEE Power Engineering Society Winter Meeting*, 2002, pp. 1059-1062 vol.2.

[11] H. Konishi, C. Takahashi, H. Kishibe, and H. Sato, "A consideration of stable operating power limits in VSC-HVDC systems," in *Seventh International Conference on AC-DC Power Transmission (Conf. Publ. No. 485)*, 2001, pp. 102-106.

[12] Z. Lidong and H. P. Nee, "Multivariable feedback design of VSC-HVDC connected to weak ac systems," in *IEEE Bucharest PowerTech*, 2009, pp. 1-8.

[13] A. Farag, M. Durrant, H. Werner, and K. Abbott, "Robust control of a VSC HVDC terminal attached to a weak AC system," in *Proceedings of 2003 IEEE Conference on Control Applications*, 2003, pp. 173-177 vol.1.

[14] M. Durrant, H. Werner, and K. Abbott, "Model of a VSC HVDC terminal attached to a weak AC system," in *IEEE Conference on Control Applications*, 2003, pp. 178-182 vol.1.

[15] L. Harnefors, M. Bongiorno, and S. Lundberg, "Input-Admittance Calculation and Shaping for Controlled Voltage-Source Converters," *IEEE Transactions on Industrial Electronics*, vol. 54, pp. 3323-3334, 2007.

[16] D. Jovcic, L. A. Lamont, and L. Xu, "VSC transmission model for analytical studies," in *IEEEPower Engineering Society General Meeting*, 2003.

[17] Z. Lidong, L. Harnefors, and H. P. Nee, "Power-Synchronization Control of Grid-Connected Voltage-Source Converters," *IEEE Transactions on Power Systems*, vol. 25, pp. 809-820, 2010.

[18] Z. Lidong, L. Harnefors, and H. P. Nee, "Interconnection of Two Very Weak AC Systems by VSC-HVDC Links Using Power-Synchronization Control," *IEEE Transactions on Power Systems*, vol. 26, pp. 344-355, 2011.

[19] Z. Lidong, L. Harnefors, and H. P. Nee, "Modeling and Control of VSC-HVDC Links Connected to Island Systems," *IEEE Transactions on Power Systems*, vol. 26, pp. 783-793, 2011.

[20] K. R. Padiyar and N. Prabhu, "Modelling, control design and analysis of VSC based HVDC transmission systems," in *International Conference on Power System Technology (PowerCon)*, 2004, pp. 774-779 Vol.1.

[21] L. A. Lamont and D. Jovcic, "Multivariable interaction indicators for VSC transmission controller design," in *IEEE Power Engineering Society General Meeting*, 2006, p. 6 pp.

[22] L. A. Lamont, D. Jovcic, and K. Abbott, "Fast direct voltage controller for VSC transmission," in *39th International Universities Power Engineering Conference (UPEC)*, 2004, pp. 1135-1139 vol. 2.

[23] S. Cole and R. Belmans, "Modelling of VSC HVDC using coupled current injectors," in *IEEE Power and Energy Society General Meeting*, 2008, pp. 1-8.

[24] S. Chiniforoosh, J. Jatskevich, A. Yazdani, V. Sood, V. Dinavahi, J. A. Martinez, and A. Ramirez, "Definitions and Applications of Dynamic Average Models for Analysis of Power Systems," *IEEE Transactions on Power Delivery*, vol. 25, pp. 2655-2669, 2010.

[25] A. Yazdani and R. Iravani, "Dynamic model and control of the NPC-based back-to-back HVDC system," *IEEE Transactions on Power Delivery,* vol. 21, pp. 414-424, 2006.

[26] Y. Wang, S.-Z. Zhao, C. Huangfu, and J.-J. Ruan, "Dynamic Model and Control of Voltage Source Converter Based HVDC," in *Asia-Pacific Power and Energy Engineering Conference (APPEEC)*, 2009, pp. 1-5.

[27] H. Ouquelle, L. A. Dessaint, and S. Casoria, "An average value model-based design of a deadbeat controller for VSC-HVDC transmission link," in *IEEE Power & Energy Society General Meeting*, 2009, pp. 1-6.

[28] S. Cole, J. Beerten, and R. Belmans, "Generalized Dynamic VSC MTDC Model for Power System Stability Studies," *IEEE Transactions on Power Systems,* vol. 25, pp. 1655-1662, 2010.

[29] M. P. Bahrman, "HVDC transmission overview," in *IEEE/PES Transmission and Distribution Conference and Exposition*, 2008, pp. 1-7.

[30] L. Carlsson, G. Flisberg, and L. Weimers, "Recent Evolution in Classic HVDC," in *The 4th International Conference on Power Transmission & Distribution*, Changsha, China, 2003.

[31] C. C. Davidson, R. M. Preedy, J. Cao, C. Zhou, and J. Fu, "Ultra-high power thyristor valves for HVDC in developing countries," in *9th IET International Conference on AC and DC Power Transmission*, 2010, pp. 1-5.

[32] B. R. Andersen, "HVDC transmission-opportunities and challenges," in *The 8th IEE International Conference on AC and DC Power Transmission, ACDC 2006. ,* 2006, pp. 24-29.

[33] V. G. Agelidis, G. D. Demetriades, and N. Flourentzou, "Recent Advances in High-Voltage Direct-Current Power Transmission Systems," in *IEEE International Conference on Industrial Technology (ICIT)*, 2006, pp. 206-213.

[34] T. Bauer, H. P. Lips, G. Thiele, T. Tylutki, and M. Uder, "Operational tests on HVDC thyristor modules in a synthetic test circuit for the Sylmar East Restoration Project," *IEEE Transactions on Power Delivery,* vol. 12, pp. 1151-1158, 1997.

[35] B. L. Sheng, E. Jansson, A. Blomberg, H. O. Bjarme, and D. Windmar, "A new synthetic test circuit for the operational tests of HVDC thyristor modules," in *Sixteenth Annual IEEE Applied Power Electronics Conference and Exposition (APEC)*, 2001, pp. 1242-1246 vol.2.

[36] T. Xie, T. Guang-fu, Z. Kun-peng, and G. Chong, "A New Operational Tests Circuit for Testing +/-660kV UHVDC Thyristor Valves," in *International Conference on Electrical and Control Engineering (ICECE)*, 2010, pp. 3177-3180.

[37] L. Hu and R. Yacamini, "Harmonic transfer through converters and HVDC links," *IEEE Transactions on Power Electronics,* vol. 7, pp. 514-525, 1992.

[38] R. Yacamini and J. W. Resende, "Harmonic generation by HVDC schemes involving converters and static VAr compensators," *IEE Proceedings Generation, Transmission and Distribution,* vol. 143, pp. 66-74, 1996.

[39] J. Arrillaga, G. Woods, and R. M. Duke, "Thyristor-controlled in-phase boosting for h.v. d.c. convertors," *IEE Proceedings Generation, Transmission and Distribution,* vol. 127, pp. 221-227, 1980.

[40] D. O'Kelly, "Voltage control for an HVDC convertor," *IEE Proceedings Generation, Transmission and Distribution,* vol. 131, p. 5, 1984.

[41] H. K. Tyll and F. Schettler, "Power system problems solved by FACTS devices," in *IEEE/PES Power Systems Conference and Exposition (PSCE)*, 2009, pp. 1-5.

[42] Y. You, E. F. Fuchs, D. Lin, and P. R. Barnes, "Reactive power demand of transformers with DC bias," *IEEE Industry Applications Magazine,* vol. 2, pp. 45-52, 1996.

[43] J. A. C. Forrest, "Harmonic load losses in HVDC converter transformers," *IEEE Transactions on Power Delivery,* vol. 6, pp. 153-157, 1991.

[44] L. Hu and R. Yacamini, "Harmonic transfer through converters and HVDC links," *IEEE Transactions on Power Electronics,* vol. 7, pp. 514-525, 1992.

[45] J. Reeve and J. A. Baron, "Harmonic DC Line Voltages Arising from HVDC Power Conversion," *IEEE Transactions on Power Apparatus and Systems,* vol. PAS-89, pp. 1619-1624, 1970.

[46] J. Reeve and J. A. Baron, "Harmonic Interaction Between HVDC Converters and ac Power Systems," *IEEE Transactions on Power Apparatus and Systems,* vol. PAS-90, pp. 2785-2793, 1971.

[47] "IEEE Guide for the Analysis and Definition of DC-Side Harmonic Performance of HVDC Transmission Systems," *IEEE Std 1124-2003,* pp. 1-68, 2003.

[48] C. Wong, N. Mohan, S. E. Wright, and K. N. Mortensen, "Feasibility Study of AC- and DC-side Active Filters for HVDC Converter Terminals," *IEEE Power Engineering Review,* vol. 9, pp. 50-50, 1989.

[49] Z. Wenyan, A. J. Isaksson, and A. Ekstrom, "Analysis on the control principle of the active DC filter in the Lindome converter station of the Konti-Skan HVDC link," *IEEE Transactions on Power Systems,* vol. 13, pp. 374-381, 1998.

[50] H. Pang, Z. Wang, and J. Chen, "Study on the Control of Shunt Active DC Filter for HVDC Systems," *IEEE Transactions on Power Delivery*, vol. 23, pp. 396-401, 2008.

[51] W. Hualei and M. A. Redfern, "The advantages and disadvantages of using HVDC to interconnect AC networks," in *45th International Universities Power Engineering Conference (UPEC)*, 2010, pp. 1-5.

[52] E. M. Yap, M. Al-Dabbagh, S. K. Kapuduwage, T. O. Maung, and N. Talebi, "HVDC and FACTS for improved power delivery through long transmission lines," in *IEEE Power Engineering Society Inaugural Conference and Exposition in Africa*, 2005, pp. 299-304.

[53] K. P. Basu, "Stability enhancement of power system by controlling HVDC power flow through the same AC transmission line," in *IEEE Symposium on Industrial Electronics & Applications (ISIEA)*, 2009, pp. 663-668.

[54] M. P. Bahrman, J. G. Johansson, and B. A. Nilsson, "Voltage source converter transmission technologies: the right fit for the application," in *IEEE Power Engineering Society General Meeting,*, 2003, p. 1847 Vol. 3.

[55] G. Reed, R. Pape, and M. Takeda, "Advantages of voltage sourced converter (VSC) based design concepts for FACTS and HVDC-link applications," in *IEEE Power Engineering Society General Meeting*, 2003, p. 1821 Vol. 3.

[56] N. Flourentzou, V. G. Agelidis, and G. D. Demetriades, "VSC-Based HVDC Power Transmission Systems: An Overview," *IEEE Transactions on Power Electronics,*, vol. 24, pp. 592-602, 2009.

[57] D. Guanjun, T. Guangfu, H. Zhiyuan, and D. Ming, "New technologies of voltage source converter (VSC) for HVDC transmission system based on VSC," in *IEEE Power and Energy Society General Meeting - Conversion and Delivery of Electrical Energy in the 21st Century*, 2008, pp. 1-8.

[58] V. F. Lescale, "Modern HVDC: state of the art and development trends," in *International Conference on Power System Technology (POWERCON '98)*, 1998, pp. 446-450 vol.1.

[59] M. P. Kazmierkowski and L. Malesani, "Current control techniques for three-phase voltage-source PWM converters: a survey," *IEEE Transactions on Industrial Electronics*, vol. 45, pp. 691-703, 1998.

[60] A. Lindberg and T. Larsson, "Pwm And Control Of Three Level Voltage Source Converters In An Hvdc Back-to-back Station," in *Sixth International Conference on AC and DC Power Transmission*, 1996, pp. 297-302.

[61] A. M. Abbas and P. W. Lehn, "PWM based VSC-HVDC systems: A review," in *IEEE Power & Energy Society General Meeting*, 2009, pp. 1-9.

[62] M. Jeroense, "HVDC, the next generation of transmission highlights with focus on extruded cable systems," in *International Symposium on Electrical Insulating Materials (ISEIM)*, 2008, pp. 10-15.

[63] M. M. Zakaria Moustafa and S. Filizadeh, "Electromagnetic Transient Simulation of a Back-to-Back Voltage Source Converter Based Transmission Scheme," in *Canadian Conference on Electrical and Computer Engineering (CCECE)*, 2007, pp. 1570-1573.

[64] M. M. Zakaria Moustafa and S. Filizadeh, "Simulation of a VSC transmission scheme supplying a passive load," in *34th Annual Conference of IEEE Industrial Electronics (IECON 2008), 2008.* . 2008, pp. 942-946.

[65] L. Weimers, "HVDC Light: A New Technology for a Better Environment," *IEEE Power Engineering Review*, vol. 18, pp. 19-20, 1998.

[66] G. Schmidt, B. Fiegl, and S. Kolbeck, "HVDC transmission and the environment," *Power Engineering Journal*, vol. 10, pp. 204-210, 1996.

[67] L. A. Koshcheev, "Environmental characteristic of HVDC overhead transmission lines," in *Third Workshop on Power Grid Interconnnection in Northeast Asia, Vladivostok ,Rusia*, Sept. 30-Oct 3, 2003.

[68] L. Zilberti, E. Pons, O. Bottauscio, M. Chiampi, and M. Pastorelli, "Evaluation of the Electromagnetic Environment Around Underground HVDC Lines," *IEEE Transactions on Power Delivery*, vol. 25, pp. 3085-3094, 2010.

[69] http://www.abb.com/hvdc.

[70] S. Kouro, M. Malinowski, K. Gopakumar, J. Pou, L. G. Franquelo, W. Bin, J. Rodriguez, Pe, x, M. A. rez, and J. I. Leon, "Recent Advances and Industrial Applications of Multilevel Converters," *IEEE Transactions on Industrial Electronics*, vol. 57, pp. 2553-2580, 2010.

[71] J. Rodriguez, L. Jih-Sheng, and P. Fang Zheng, "Multilevel inverters: a survey of topologies, controls, and applications," *IEEE Transactions on Industrial Electronics,*, vol. 49, pp. 724-738, 2002.

[72] M. Malinowski, K. Gopakumar, J. Rodriguez, Pe, x, and M. A. rez, "A Survey on Cascaded Multilevel Inverters," *IEEE Transactions on Industrial Electronics*, vol. 57, pp. 2197-2206, 2010.

[73] M. H. Rashid, *Power Electronics: Circuits, Devices and Applications*, Third ed.: Prentice Hall, 2004.

[74] D. Soto and T. C. Green, "A comparison of high-power converter topologies for the implementation of FACTS controllers," *IEEE Transactions on Industrial Electronics*, vol. 49, pp. 1072-1080, 2002.

[75] L. Jih-Sheng and P. Fang Zheng, "Multilevel converters-a new breed of power converters," *IEEE Transactions on Industry Applications,* vol. 32, pp. 509-517, 1996.

[76] N. Hingorani and L. Gyugyi, *Concepts and Technology of Flexible AC Transmission Systems*: IEEE Press, 1999.

[77] M. Glinka and R. Marquardt, "A new AC/AC multilevel converter family," *IEEE Transactions on Industrial Electronics,,* vol. 52, pp. 662-669, 2005.

[78] M. Glinka and R. Marquardt, "A new AC/AC multilevel converter family," *IEEE Transactions on Industrial Electronics,* vol. 52, pp. 662-669, 2005.

[79] M. Hagiwara and H. Akagi, "PWM control and experiment of modular multilevel converters," in *IEEE Power Electronics Specialists Conference (PESC)*, 2008, pp. 154-161.

[80] A. Lesnicar and R. Marquardt, "An innovative modular multilevel converter topology suitable for a wide power range," in *IEEE Bologna Power Tech Conference Proceedings*, 2003.

[81] L. Malesani and P. Tomasin, "PWM current control techniques of voltage source converters-a survey," in *International Conference on Industrial Electronics, Control, and Instrumentation (IECON '93)*, 1993, pp. 670-675 vol.2.

[82] S. C. Bansal and U. M. Rao, "Evaluation of p.w.m. inverter schemes," *Proceedings of the Institution of Electrical Engineers,* vol. 125, pp. 328-334, 1978.

[83] J. Holtz, "Pulsewidth modulation-a survey," *IEEE Transactions on Industrial Electronics*, vol. 39, pp. 410-420, 1992.

[84] B. Andersen and C. Barker, "A new era in HVDC?," *IEE Review,* vol. 46, pp. 33-39, 2000.

[85] D. Van Hertem, J. Verboomen, R. Belmans, and W. L. Kling, "Power flow controlling devices: an overview of their working principles and their application range," in *International Conference on Future Power Systems*, 2005.

[86] Z. Chengyong, L. Xiangdong, and L. Guangkai, "Parameters Optimization of VSC-HVDC Control System Based on Simplex Algorithm," in *IEEE Power Engineering Society General Meeting*, 2007, pp. 1-7.

[87] R. Song, C. Zheng, R. Li, and X. Zhou, "VSCs based HVDC and its control strategy," in *IEEE/PES Transmission and Distribution Conference and Exhibition: Asia and Pacific,* 2005, pp. 1-6.

[88] P. N. Enjeti, P. D. Ziogas, and M. Ehsani, "Unbalanced PWM converter analysis and corrective measures," in *IEEE Industry Applications Society Annual Meeting*, 1989, pp. 861-870 vol.1.

[89] Z. Jing, C. Hairong, P. Wulue, and W. Chao, "VSC-HVDC Control under Unbalanced Supply Conditions," in *IEEE Power Engineering Society General Meeting*, 2007, pp. 1-6.

[90] N. Celanovic and D. Boroyevich, "A comprehensive study of neutral-point voltage balancing problem in three-level neutral-point-clamped voltage source PWM inverters," *IEEE Transactions on Power Electronics,* vol. 15, pp. 242-249, 2000.

[91] C. Newton and M. Sumner, "Neutral point control for multi-level inverters: theory, design and operational limitations," in *IEEE Industry Applications Conference Thirty-Second IAS Annual Meeting (IAS)* 1997, pp. 1336-1343 vol.2.

[92] R. M. Tallam, R. Naik, and T. A. Nondahl, "A carrier-based PWM scheme for neutral-point voltage balancing in three-level inverters," *IEEE Transactions on Industry Applications,* vol. 41, pp. 1734-1743, 2005.

[93] A. von Jouanne, S. Dai, and H. Zhang, "A multilevel inverter approach providing DC-link balancing, ride-through enhancement, and common-mode voltage elimination," *IEEE Transactions on Industrial Electronics,* vol. 49, pp. 739-745, 2002.

[94] C. Schauder and H. Mehta, "Vector analysis and control of advanced static VAr compensators," *IEE Proceedings Generation, Transmission and Distribution,* vol. 140, pp. 299-306, 1993.

[95] https://pscad.com/.

[96] A. von Jouanne, S. Dai, and H. Zhang, "A multilevel inverter approach providing DC-link balancing, ride-through enhancement, and common-mode voltage elimination," *IEEE Transactions on Industrial Electronics,*, vol. 49, pp. 739-745, 2002.

[97] H. Guan-Chyun and J. C. Hung, "Phase-locked loop techniques. A survey," *IEEE Transactions on Industrial Electronics,* vol. 43, pp. 609-615, 1996.

[98] D. Jovcic, "Phase locked loop system for FACTS," *IEEE Transactions on Power Systems,* vol. 18, pp. 1116-1124, 2003.

[99] M. Boyra and J. L. Thomas, "A review on synchronization methods for grid-connected three-phase VSC under unbalanced and distorted conditions," in *Proceedings of the 14th European Conference on Power Electronics and Applications (EPE 2011),*, 2011, pp. 1-10.

[100] A. Gole, V. K. Sood, and L. Mootoosamy, "Validation and analysis of a grid control system using D-Q-Z transformation for static compensator systems," in *Can. Conf. Elect. Comput. Eng*, Montreal, QC, Canada, 1989, pp. 745 -748.

[101] A. Gole, J. A. Martinez-Velasco, and A. J. F. Keri, "Modeling and Analysis of System Transients Using Digital Programs," *IEEE PES Special Publication,* 1999.

[102] "IEEE Guide for Planning DC Links Terminating at AC Locations Having Low Short-Circuit Capacities," *IEEE Std 1204-1997,* p. i, 1997.

[103] P. C. Krause, O. Wasynczuk, S. D. Sudhoff, and I. P. E. Society, *Analysis of electric machinery and drive systems*: IEEE press, 2002.

[104] J. A. Nelder and R. Mead, "A Simplex-Method for Function Minimization," *Computer Journal,* vol. 7, pp. 308-313, 1965.

[105] S. D. Round and R. M. Duke, "Real-time optimization of an active filter's performance," *IEEE Transactions on Industrial Electronics,* vol. 41, pp. 278-284, 1994.

[106] A. M. Gole, S. Filizadeh, R. W. Menzies, and P. L. Wilson, "Optimization-enabled electromagnetic transient simulation," *IEEE Transactions on Power Delivery,* vol. 20, pp. 512-518, 2005.